Order Number 9124502

Theory and applications of scattering and inverse scattering problems

Wang, Yi-Ming, Ph.D.

University of Illinois at Urbana-Champaign, 1991

U·M·I
300 N. Zeeb Rd.
Ann Arbor, MI 48106

THEORY AND APPLICATIONS OF SCATTERING AND INVERSE SCATTERING PROBLEMS

BY

YI-MING WANG

B.Sc., Beijing University, 1982
M.S., University of Illinois, 1988

THESIS

Submitted in partial fulfillment of the requirements
for the degree of Doctor of Philosophy in Electrical Engineering
in the Graduate College of the
University of Illinois at Urbana-Champaign, 1991

Urbana, Illinois

UNIVERSITY OF ILLINOIS AT URBANA-CHAMPAIGN

THE GRADUATE COLLEGE

DECEMBER 1990

WE HEREBY RECOMMEND THAT THE THESIS BY

YI-MING WANG

ENTITLED THEORY AND APPLICATIONS OF

SCATTERING AND INVERSE SCATTERING PROBLEMS

BE ACCEPTED IN PARTIAL FULFILLMENT OF THE REQUIREMENTS FOR

THE DEGREE OF DOCTOR OF PHILOSOPHY

W. C. Chew

Director of Thesis Research

Timothy R. Field

Head of Department

Committee on Final Examination†

W. C. Chew

Chairperson

Paul E. Mayes

J. T. F

K. C. Yu

† Required for doctor's degree but not for master's

O-517

THEORY AND APPLICATIONS OF DIRECT AND INVERSE SCATTERING PROBLEMS

Yi-Ming Wang, Ph.D.
Department of Electrical and Computer Engineering
University of Illinois at Urbana-Champaign,1991

Two algorithms based on the recursive operator algorithm are proposed to solve for the scattered field from an arbitrarily shaped, inhomogeneous scatterer. By discretizing the object into N subobjects, the scattering solution of an arbitrarily shaped inhomogeneous scatterer can be formulated as a scattering solution of an N-scatterer problem, each of whose scattered fields is approximated by M harmonics. Using the translation formulas, a recursive approach is developed which enables us to derive an $n+1$-scatterer solution from an n-scatterer solution. Therefore, knowing the isolated transition matrices for all subscatterers, the total transition matrices for an N-scatterer problem can be obtained recursively. The computation time of such an algorithm is proportional to N^2M^2P, where P is the number of harmonics used in the translation formulas. Furthermore, by introducing an aggregate transition matrix to the recursive scheme, a fast algorithm, whose computational complexity is linear in N, is developed. The algorithm has been used to solve for the scattering solution of a 10λ diameter, two-dimensional dielectric scatterer with about 12,000 unknowns, taking 32 sec on a CRAY-2 supercomputer.

In order to solve the electromagnetic inverse scattering problem beyond the Born approximation, two iterative algorithms are developed. They are the Born iterative method and the distorted Born iterative method. Numerical simulations are performed in several cases in which the conditions for the

Born approximation are not satisfied. The results show that in both low and high frequency cases, good reconstructions of the permittivity distribution are obtained. Meanwhile, the simulations reveal that each method has its advantages. The distorted Born iterative method shows a faster convergence rate compared to that for the Born iterative method, while the Born iterative method is more robust to noise contamination compared to that for the distorted Born iterative method.

A boosting procedure which helps to retrieve the maximum amount of information content is proposed to solve the limited angle inverse scattering problem. Using the boosting procedure in the limited angle inverse scattering problem, good reconstructions are achieved for both well-to-well tomography and subsurface detection.

By applying the fast recursive algorithm to the solution of the direct scattering part of the iterative schemes and the conjugate gradient method to the solution of the inversion part of the iterative schemes, the computational complexity of the Born iterative method and the distorted Born iterative method is further reduced from N^3 to N^2.

DEDICATION

TO

MY PARENTS

AND

MY WIFE

ACKNOWLEDGEMENTS

I wish to express my deepest gratitude to my advisor, Professor W. C. Chew, for his patient guidance, encouragement and support. His wisdom in providing an environment in which research may be efficiently pursued is deeply appreciated.

I would also like to thank my committee members, Professors Y. T. Lo, P. E. Mayes, and K. C. Yeh, for their many constructive criticisms and comments. Many thanks are also due to Professor W. D. O'Brien for his helpful discussions and suggestions.

I would also like to acknowledge all of my colleagues in the Electromagnetics Laboratory for many enlighting discussions. In particular, I would like to thank Dr. C. H. Chan, Ms. M. Moghaddam, Mr. L. Gurel, and Mr. M. Nasir.

I wish to express my profound gratitude to my wife for her constant love and encouragement. I am also grateful to my family, especially my parents, for their unwavering encouragement and support.

TABLE OF CONTENTS

LIST OF PRINCIPAL SYMBOLS

k_0	Wave number in free space
k_i	Wave number in the scatterer i
$J_n(x)$	n-th order Bessel function
$H_n^{(1)}(x)$	n-th order Hankel function of the first kind
$\psi^t(k_0, \mathbf{r}_i)$	Basis harmonics in the coordinate system i, outgoing wave harmonics
$\Re g\psi^t(k_0, \mathbf{r}_i)$	Regular part of $\psi^t(k_0, \mathbf{r}_i)$, standing wave harmonics
$\overline{\alpha}_{ji}$	Translation matrix which translates the outgoing wave harmonics in the coordinate system i into the standing wave harmonics in the coordinate system j
$\overline{\beta}_{ji}$	Translation matrix which translates the outgoing wave harmonics in the coordinate system i into the outgoing wave harmonics in the coordinate system j
$\overline{\mathbf{T}}$	Transition matrix which relates the scattered field to the incident field
$\overline{\overline{\mathbf{W}}}$	Transmission matrix which relates the field inside the scatterer to the incident field
$\overline{\mathbf{T}}_{i(1)}$	Isolated scatterer transition matrix for the scatterer i
$\overline{\overline{\mathbf{W}}}_{i(1)}$	Isolated scatterer transmission matrix for the scatterer i
$\overline{\mathbf{T}}_{i(n)}$	n-scatterer transition matrix for the scatterer i
$\overline{\tau}$	Aggregate transition matrix
$\overline{\tau}_{(n)}$	n-scatterer aggregate transition matrix
$\widetilde{\overline{\tau}}_{i(N)}$	Complementary partial aggregate transition matrix

CHAPTER 1

INTRODUCTION

Electromagnetic scattering from an inhomogeneous scatterer is one of the most frequently encountered problems in computational electromagnetics. The major interest in computational electromagnetics is to find an efficient and effective way to solve such a problem. Traditionally, there are two numerical methods available for the solution of the scattering problem. They are the method of moments and the finite element method (FEM). Because of the automatic satisfaction of the radiation condition in the method of moments, its implementation is relatively easier than that of the finite element method. However, the computational complexity of the method of moments is N^3. For the finite element method, since the region to be considered is unbounded in the scattering problem, we have to truncate it somewhere outside of the scatterer. To satisfy the radiation condition at this truncated boundary, several techniques have been developed, such as the unimoment method and the absorbing boundary condition method. The implementation of these techniques will result in increasing the bandwidth of the matrix generated by the finite element method.

In Chapter 2 of this thesis, an alternative efficient method for the solution of the electromagnetic scattering problem is developed by using the recursive operator algorithms. This method is adopted from a recursive algorithm for the solution of a multiple scattering problem. It provides us with a concise and efficient method to solve a general electromagnetic scattering problem.

In the recursive operator algorithm, as in the method of moments, the object is first discretized by about 10-12 points per wavelength for accurate solutions. Then, we consider each mesh in the object as an individual subscatterer in an N-scatterer problem. Knowing the isolated transition matrix $\overline{\mathbf{T}}_{i(1)}$ for each subscatterer, the solution to N scatterers is constructed by using the translation formulas. First, an N^2 algorithm is developed by expressing the final solution in terms of the total transition matrices $\overline{\mathbf{T}}_{i(N)} \cdot \boldsymbol{\beta}_{i0}$, $i = 1, 2, \ldots, N$, where $\overline{\mathbf{T}}_{i(N)} \cdot \boldsymbol{\beta}_{i0}$ gives the scattering amplitude from the scatterer i when N scatterers are present. In the N^2 algorithm, at the $(n+1)$-th recursion step, the number of float-point operations is $O(n)$, because the interactions between the $(n+1)$-th scatterer and the previous n scatterers have to be accounted for. Consequently, after N recursions, the number of floating-point operations required is $O(N^2)$. Then, after introducing the aggregate $\boldsymbol{\tau}$ matrix, a fast recursive algorithm, whose computational complexity is linear in N in the low frequency limit, is developed. In the aggregate $\boldsymbol{\tau}$ matrix algorithm, at the $(n+1)$-th recursive step, only the two-scatterer problem has to be solved: one scatterer is the sum of the previous n scatterers, characterized by an n-th aggregate $\boldsymbol{\tau}_{(n)}$ matrix; the other is the scatterer $(n+1)$, characterized by $\overline{\mathbf{T}}_{n+1(1)}$. Therefore, the computational effort at each recursion step will be independent of the ordinal number of the recursion. As a result, this leads to an $O(N)$ algorithm after N recursions.

In inverse scattering problems, we attempt to infer the property of the scatterer from the measured scattered field outside of the scatterer. This type of problem arises in a variety of applications such as medical imaging, geophysical exploration, remote sensing, nondestructive evaluation, and radar target recognition. Generally, the measurement data and the object

are related in a nonlinear fashion. In one dimension, the Gel'fand-Levitan method and the Marchenko method have been proposed to solve such a nonlinear inverse problem. However, in higher dimensions, a numerical method is usually required to solve the nonlinear inverse scattering problem. In Chapter 3 of this thesis, two iterative algorithms are developed to solve the higher dimensional nonlinear inverse scattering problem. They are the Born iterative method and the distorted Born iterative method. Both of the algorithms have been implemented in the two-dimensional cases. The effectiveness of these algorithms is verified by the numerical simulations conducted in Section 2.3.

In the limited angle inverse scattering problem, the locations of the receivers and transmitters are restricted in some regions which cannot completely surround the object. The limited angle measurement data results in the reduction of the information content contained in the measurements. This leads to further aggravation of the ill-conditioning of the problem rendering its solution more difficult. To overcome the above difficulty, a boosting procedure, which will help us to retrieve the maximum amount of information for an arbitrarily predefined experiment setup, is proposed, based on a physical viewpoint in Section 4.2. The importance of the boosting procedure is confirmed by the numerical simulations.

One problem faced by the nonlinear inverse scattering algorithms discussed in Chapter 3 of this thesis is the intensive computation time involved. To reduce the computational complexity of the algorithms, we have applied the fast algorithm developed in Chapter 2 of this thesis to the solution of the direct scattering part of the iterative inverse scattering algorithms and the conjugate gradient method to the solution of the inverse scattering part of

the iterative inverse scattering algorithms. This reduces the overall computational complexity of the algorithms from N^3 to N^2. The result is reported in Section 4.3.

Finally, in Chapter 5, the conclusions and some future work related to the topic of this thesis are presented.

CHAPTER 2

RECURSIVE OPERATOR ALGORITHMS FOR THE SOLUTION OF SCATTERING PROBLEMS

2.1 Introduction

The solution of the electromagnetic scattering problem from an arbitrarily shaped homogeneous scatterer has been formulated in terms of the transition matrix by Waterman [1,2,3] in 1965. Meanwhile, the solution of multiple scattering by spheres and cylinders has been of great interest for years because of its importance in a variety of applications [4-8]. Since then, scores of researchers have sought to improve and extend the methods to solve for more general scattering problems with less constraint on applications [9–15]. Among those, Peterson and Ström [9,10] in 1973 extended the method to the solution of an arbitrary number of scatterers with arbitrary cross section by applying the translation formulas to the spherical (and cylindrical) wave solution of the Helmholtz equation. The total $\mathbf{T}$ matrix was represented in terms of the individual $\mathbf{T}$ matrices and the translation matrices by introducing two auxiliary matrices in the iterative procedure. Because the auxiliary matrices were obtained by solving an $(N-1)$-th linear system equation, which requires $(N-1)^3$ floating-point operations, the overall computational complexity of the method is at least N^3. In order to reduce the computational complexity, Chew developed a recursive procedure which has an N^2 computational complexity for long wavelength limits. The method is accomplished by introducing the intermediate transition matrices $\overline{\mathbf{T}}_{i(n)}$ for each scatterer in the n-th iteration step. The physics interpretation of the $\overline{\mathbf{T}}_{i(n)}$ is that it gives the scattering amplitude from the i-th scatterer when n scatterers are present.

Another scattering problem which has been of great interest for years is the scattering solution from an arbitrary inhomogeneous medium. The solution of the problem is essential for many applications such as radar detection, geophysical exploration in a complex environment, and nondestructive evaluation. For many years, the solution of the problem depended mainly on two numerical techniques: the method of moments (MOM) and the finite element method (FEM). In the method of moments [16,17,18], since the radiation condition is automatically satisfied, the implementation of it is easier than that of FEM. The subdomain method where the scatterer is divided into N subobjects as in the case of finite element analysis is popular because of its versatility. The rule-of-thumb is to discretize the object by about 10-12 points per wavelength for accurate solutions. Using such a method, the scattering problem can be cast into a problem involving N linear algebraic equations. The solution of such a set of linear algebraic equations by Gauss' elimination yields an algorithm whose computation time scales as $N^3/3$. Hence, the method of moments cannot be easily applied to large scatterers as the computation time scales too rapidly with N.

The conjugate gradient method has been used to reduce the algorithmic complexity yielding an iterative algorithm with complexity $O(N^2P)$ where P is the number of steps in the iteration. However, the number of steps P required depends on the condition number of the matrix equation. For ill-conditioned matrices, the method may not converge [19]. The fast Fourier transform method has also been used to exploit the convolutional nature of the scattering integral equation yielding a conjugate-gradient type algorithm with complexity $O(PN\log_2 N)$ [19,20,21]. However, conjugate gradient methods have the disadvantage of providing a solution for only one incident wave at a time. The algorithm has to be restarted for each new incident wave.

To deal with the radiation condition in the use of the finite element method, several techniques have been developed, such as the unimoment method and the absorbing boundary condition method. The implementation of these methods will result in increasing the bandwidth of the matrix generated by the finite element method. Some of these techniques are still the topics of current research, e.g., the absorbing boundary conditions.

Using a recursive operator algorithm [14,15], now modified for wave scattering problems, we shall illustrate two recursive algorithms for the solution of such a problem [22,23,24]. One is an N^2M^2P algorithm; the other is an NMP^2 algorithm, where M is the number of harmonics for each subobject and P is the number of harmonics used for the translation formulas [14,15,22–24].

In these methods, a large inhomogeneous object is decomposed into many subobjects as in the method of moments when subdomain basis functions are used. Then a recursive operator algorithm is developed which accounts for multiple scattering between the scatterers. Knowing the scattering solution for every isolated scatterer, the solution to N scatterers is constructed recursively.

2.2 One Scatterer Solution

In order to illustrate the physical meaning of the transition matrix $\overline{\mathbf{T}}$ and the transmission matrix $\overline{\mathbf{W}}$, we shall start from a simple two-dimensional scattering problem. Shown in Figure 2.1 is the geometry of the problem. The scatterer is a homogeneous circular cylinder with a radius a. The relative permittivities of the scatterer and the background medium are ϵ_r and 1, respectively. The scatterer is illuminated by an incident field from the positive x-axis with the electric field vector perpendicular to the xy-plane. The

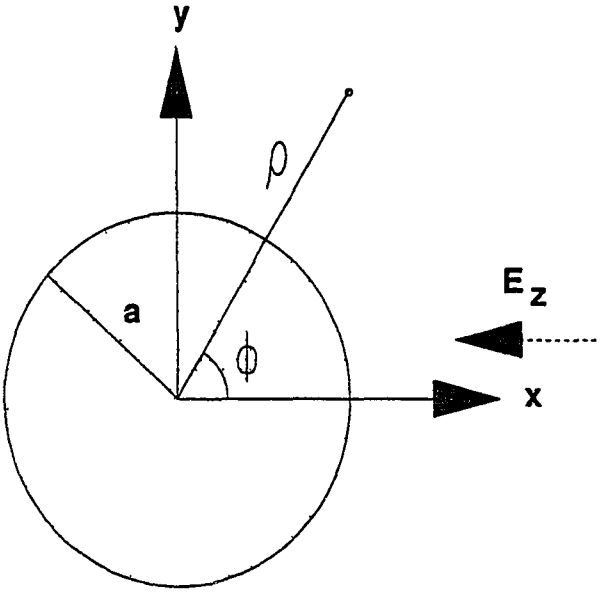

Figure 2.1. A homogeneous dielectric circular cylinder illuminated by a plane wave from the positive x-axis with the electric field vector perpendicular to the xy-plane.

center of the cylinder coincides with the origin of the coordinate system. In the following derivation, the time dependence $e^{i\omega t}$ is suppressed. The plane incident field is

$$E_z^i = E_0 e^{-jk_0 x} = E_0 e^{-ik_0 \rho \cos\phi}. \tag{2.2.1}$$

From the relation of [25,26,27]

$$e^{-ik_0 \rho \cos\phi} = \sum_{n=-\infty}^{+\infty} i^{-n} J_n(k_0\rho) e^{jn\phi}, \tag{2.2.2}$$

we have

$$E_z^i = E_0 \sum_{n=-\infty}^{+\infty} i^{-n} J_n(k_0\rho) e^{jn\phi}. \tag{2.2.3}$$

The total field outside of the cylinder is considered as a sum of the incident and scattered fields, that is,

$$E_z^{(1)} = E_z^i + E_z^s.$$

To represent the outgoing-traveling wave, the scattered field is of the form

$$E_z^s = E_0 \sum_{n=-\infty}^{+\infty} i^{-n} t_n H_n^{(1)}(k_0\rho) e^{jn\phi}$$

and the total field outside of the cylinder is given by

$$E_z^{(1)} = E_0 \sum_{n=-\infty}^{+\infty} i^{-n} [J_n(k_0\rho) + t_n H_n^{(1)}(k_0\rho)] e^{in\phi}, \quad \rho > a. \tag{2.2.4}$$

The field inside of the cylinder can be represented as

$$E_z^{(2)} = E_0 \sum_{n=-\infty}^{+\infty} i^{-n} w_n J_n(k\rho) e^{in\phi}, \quad \rho < a, \tag{2.2.5}$$

where

$$k = k_0\sqrt{\epsilon_r}.$$

The two boundary conditions are

$$E_z^{(1)} = E_z^{(2)}, \quad H_\phi^{(1)} = H_\phi^{(2)}, \quad \text{at} \quad \rho = a. \tag{2.2.6}$$

From the field equations

$$H_\phi = \frac{1}{i\omega\mu}(\nabla \times \mathbf{E})_\phi$$

$$= \frac{i}{\omega\mu}E_z,$$

the second boundary condition becomes

$$\frac{\partial E_z^{(1)}}{\partial \rho}|_{\rho=a} = \frac{\partial E_z^{(2)}}{\partial \rho}|_{\rho=a}, \tag{2.2.7}$$

since $\mu_1 = \mu_2 = \mu_0$ in the problem. Matching the boundary conditions at $\rho = a$, we have

$$E_0 \sum_{n=-\infty}^{+\infty} i^{-n}[J_n(k_0a) + t_nH_n^{(1)}(k_0a)]e^{jn\phi} = E_0 \sum_{n=-\infty}^{+\infty} i^{-n}w_nJ_n(ka)e^{jn\phi}, \tag{2.2.8}$$

$$E_0 \sum_{n=-\infty}^{+\infty} i^{-n}k_0[J_n{}'(k_0a) + t_nH_n^{(1)\prime}(k_0a)]e^{jn\phi} = E_0 \sum_{n=-\infty}^{+\infty} i^{-n}kw_nJ_n'(ka)e^{jn\phi}. \tag{2.2.9}$$

Because $e^{in\phi}$, $n = -\infty, \ldots, -2, -1, 0, 1, 2, \ldots, +\infty$, form an orthogonal set, we have

$$J_n(k_0a) + t_nH_n^{(1)}(k_0a) = w_nJ_n(ka), \tag{2.2.10}$$

$$J_n'(k_0a) + t_nH_n^{(1)\prime}(k_0a) = w_n\sqrt{\epsilon_r}J_n'(ka). \tag{2.2.11}$$

Solving the above for t_n and w_n, we obtain

$$t_n = [J_n'(k_0a)H_n^{(1)}(k_0a) - J_n(k_0a)H_n^{(1)\prime}(k_0a)]/D_n, \tag{2.2.12}$$

$$w_n = [J_n(ka)J_n'(k_0a) - J_n'(ka)J_n(k_0a)]/D_n, \tag{2.2.13}$$

where

$$D_n = \sqrt{\epsilon_r}J_n'(ka)H_n^{(1)}(k_0a) - J_n(ka)H_n^{(1)\prime}(k_0a). \tag{2.2.14}$$

Now, we define the basis column vectors $\psi(k_0, \boldsymbol{\rho})$, $\Re g\psi(k_0, \boldsymbol{\rho})$, and $\Re g\psi(k, \boldsymbol{\rho})$ as

$$\psi(k_0, \boldsymbol{\rho})_m = H_m^{(1)}(k_0\rho)e^{jm\phi}, \tag{2.2.15}$$

$$\Re g\psi(k_0, \boldsymbol{\rho})_m = J_m(k_0\rho)e^{jm\phi}, \tag{2.2.16}$$

$$\Re g\psi(k, \boldsymbol{\rho})_m = J_m(k\rho)e^{jm\phi}. \tag{2.2.17}$$

Under the above notations, Equation (2.2.3) becomes

$$E_z^i(\boldsymbol{\rho}) = \Re g\psi^t(k_0, \boldsymbol{\rho}) \cdot \mathbf{a}, \tag{2.2.18}$$

where the supersript t on $\Re g\psi$ stands for "the transpose of," and $\mathbf{a}$ is a column vector whose components are expansion coefficients of the incident field in the basis vector $\Re g\psi(k_0, \boldsymbol{\rho})$, which are

$$a_m = i^{-m}E_0, \quad m = -\infty, \ldots, -2, -1, 0, 1, 2, \ldots, \infty.$$

Substituting the solutions (2.2.12) and (2.2.13) into Equations (2.2.4) and (2.2.5) and using the vector notation, we obtain

$$E_z^{(1)} = \Re g\psi^t(k_0, \boldsymbol{\rho}) \cdot \mathbf{a} + \psi^t(k_0, \boldsymbol{\rho}) \cdot \overline{\mathbf{T}} \cdot \mathbf{a}, \quad \rho > a, \tag{2.2.19}$$

$$E_z^{(2)} = \Re g\psi^t(k, \boldsymbol{\rho}) \cdot \overline{\mathbf{W}} \cdot \mathbf{a}. \quad \rho < a, \tag{2.2.20}$$

where $\overline{\mathbf{T}}$ and $\overline{\mathbf{W}}$ are the transition matrix and the transmission matrix, respectively. Comparing Equations (2.2.19) and (2.2.20) with Equations (2.2.4) and (2.2.5), we can see that

$$T_{mn} = \begin{cases} t_n, \text{if } m = n \\ 0, \text{if } m \neq n, \end{cases} \tag{2.2.21}$$

$$W_{mn} = \begin{cases} w_n, \text{if } m = n \\ 0, \text{if } m \neq n. \end{cases} \tag{2.2.22}$$

The transition matrix $\overline{\mathbf{T}}$ relates the amplitude of the scattered field to the amplitude of the incident field, while the transmission matrix $\overline{\mathbf{W}}$ relates the amplitude of the internal field to the amplitude of the incident field. In the example, both the transition matrix and the transmission matrix are diagonal matrices and are obtained analytically. In general, this may not be true. The matrices may not be diagonal and may have to be obtained by using the numerical method, such as the extended boundary condition method [28]. Nevertheless, once the transition matrix $\overline{\mathbf{T}}$ and the transmission matrix $\overline{\mathbf{W}}$ are obtained, the solution of the problem can always be written in the form of Equations (2.2.19) and (2.2.20).

When the subobjects are a fraction of a wavelength, their shapes can be approximated by circular cylinders without much loss of accuracy. Hence, the $\overline{\mathbf{T}}$-matrices of every such isolated scatterer can be easily found.

Once the $\overline{\mathbf{T}}$ matrices for every isolated scatterer are found, they can be used easily to construct the solution of scattering by many scatterers. When more than one scatterer are present, multiple scattering exists between the scatterers. The solution to such a problem can be found recursively by using the translational addition theorem for spherical harmonics or cylindrical harmonics [9,10,14,15,22–24,28].

In the following sections, we shall derive two recursive algorithms for the solution of the N-scatterer problem given the isolated transition matrix $\overline{\mathbf{T}}_{i(1)}$ and transmission matrix $\overline{\mathbf{W}}_{i(1)}$ for each scatterer.

2.3 N^2 Recursive Algorithm

In order to gain a physical insight into the recursive operator method introduced in the following sections, we shall consider first the solution of a two-scatterer problem.

2.3.1 Two-scatterer solution

For a two-scatterer problem, three coordinate systems are introduced. One is a global coordinate system. The others are two local coordinate systems located at the centers of two scatterers, respectively (Figure 2.2). Suppose that the incident field can be represented in terms of the standing harmonic waves related to the global coordinate system as

$$\phi_{inc}(\mathbf{r}) = \Re g\psi^t(k_0, \mathbf{r}_0) \cdot \mathbf{a}, \tag{2.3.1}$$

where $\psi^t(k_0, \mathbf{r}_0)$ is the outgoing harmonics expressed in the global coordinate system, $\Re g$ stands for "the regular part of," and $\mathbf{a}$ is a column vector whose components are the expansion coefficients of the incident wave in terms of the $\Re g\psi$. Similarly, the total field in the presence of two scatterers can be expressed as

$$\phi(\mathbf{r}) = \Re g\psi^t(k_0, \mathbf{r}_0) \cdot \mathbf{a} + \psi^t(k_0, \mathbf{r}_1) \cdot \mathbf{f}_1 + \psi^t(k_0, \mathbf{r}_2) \cdot \mathbf{f}_2, \tag{2.3.2}$$

where $\mathbf{f}_1$ and $\mathbf{f}_2$ are the unknowns to be determined. The scattered fields from each scatterer, which are the last two terms in the above equation, are written in terms of the outgoing harmonics expressed in the local coordinate

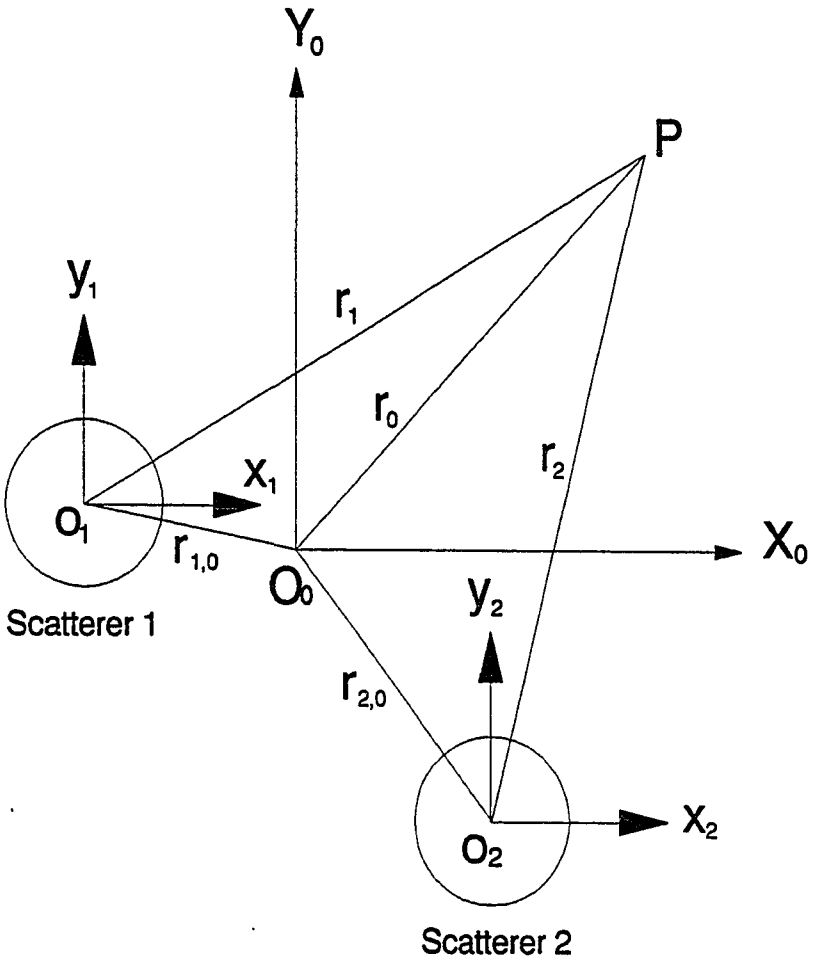

Figure 2.2. Coordinate systems of a two-scatterer problem. O_0 is the origin of the global coordinate system. O_1 and O_2 are the origins of the local coordinate systems related to the first and the second scatterers, respectively.

systems of the scatterers. In order to find $\mathbf{f}_1$ and $\mathbf{f}_2$, the following translation formulas, which relate the harmonic functions at two different locations, are needed [9,10,28,29,36]:

$$\psi^t(k_0, \mathbf{r}_i) = \Re g\psi^t(k_0, \mathbf{r}_j) \cdot \overline{\boldsymbol{\alpha}}_{ji}, \qquad |\mathbf{r}_j| < d_{i,j}, \tag{2.3.3a}$$

$$\psi^t(k_0, \mathbf{r}_i) = \psi^t(k_0, \mathbf{r}_j) \cdot \overline{\boldsymbol{\beta}}_{ji}, \qquad |\mathbf{r}_j| > d_{i,j}, \tag{2.3.3b}$$

$$\Re g\psi^t(k_0, \mathbf{r}_i) = \Re g\psi^t(k_0, \mathbf{r}_j) \cdot \overline{\boldsymbol{\beta}}_{ji}, \qquad \forall |\mathbf{r}_j|, \tag{2.3.3c}$$

where $d_{i,j}$ is the distance between O_i and O_j, the origins of the i and j coordinate systems. Using these formulas, we can readily express the harmonic expansion of the field of one coordinate system in terms of another coordinate system. The explicit expressions of $\overline{\boldsymbol{\alpha}}_{ij}$ and $\overline{\boldsymbol{\beta}}_{ij}$ for cylindrical harmonics are given in Appendix A.

Using (2.3.3a) and (2.3.3b), the total field outside the scatterers can be expressed in terms of the local coordinate system of the first scatterer

$$\phi(\mathbf{r}) = \Re g\psi^t(k_0, \mathbf{r}_1) \cdot \overline{\boldsymbol{\beta}}_{10} \cdot \mathbf{a} + \psi^t(k_0, \mathbf{r}_1) \cdot \mathbf{f}_1 + \psi^t(k_0, \mathbf{r}_1) \cdot \overline{\boldsymbol{\alpha}}_{12} \cdot \mathbf{f}_2. \tag{2.3.4}$$

Notice that Equation (2.3.4) is valid only when $\mathbf{r}_1 < d_{1,2}$ in order to apply (2.3.3a). In the above equation, the first and third terms can be considered as the incident field impinging upon scatterer 1. Meanwhile, the second term is the scattered field from scatterer 1. Here, the isolated $\overline{\mathbf{T}}$ matrices, $\overline{\mathbf{T}}_{1(1)}$ and $\overline{\mathbf{T}}_{2(1)}$, for scatterers 1 and 2 are known, where parenthesized 1 indicates that they are the one scatterer $\overline{\mathbf{T}}$ matrices. Remember that the isolated $\overline{\mathbf{T}}$ matrix is obtained by matching boundary conditions on the surface of the scatterer, and it relates the scattered field to the total incident field. Therefore, we can relate $\mathbf{f}_1$ to $\mathbf{a}$ and $\mathbf{f}_2$ using the $\overline{\mathbf{T}}_{1(1)}$ matrix as

$$\mathbf{f}_1 = \overline{\mathbf{T}}_{1(1)} \cdot [\overline{\boldsymbol{\beta}}_{10} \cdot \mathbf{a} + \overline{\boldsymbol{\alpha}}_{12} \cdot \mathbf{f}_2]. \tag{2.3.5}$$

By the same token, for scatterer 2, we have

$$\mathbf{f}_2 = \overline{\mathbf{T}}_{2(1)} \cdot [\overline{\boldsymbol{\beta}}_{20} \cdot \mathbf{a} + \overline{\boldsymbol{\alpha}}_{21} \cdot \mathbf{f}_1]. \tag{2.3.6}$$

Solving Equations (2.3.5) and (2.3.6) for $\mathbf{f}_1$ and $\mathbf{f}_2$, we have

$$\mathbf{f}_1 = [\bar{\mathbf{I}} - \overline{\mathbf{T}}_{1(1)} \cdot \overline{\boldsymbol{\alpha}}_{12} \cdot \overline{\mathbf{T}}_{2(1)} \cdot \overline{\boldsymbol{\alpha}}_{21}]^{-1} \cdot \overline{\mathbf{T}}_{1(1)} \cdot [\overline{\boldsymbol{\beta}}_{10} + \overline{\boldsymbol{\alpha}}_{12} \cdot \overline{\mathbf{T}}_{2(1)} \cdot \overline{\boldsymbol{\beta}}_{20}] \cdot \mathbf{a}, \tag{2.3.7}$$

$$\mathbf{f}_2 = [\bar{\mathbf{I}} - \overline{\mathbf{T}}_{2(1)} \cdot \overline{\boldsymbol{\alpha}}_{21} \cdot \overline{\mathbf{T}}_{1(1)} \cdot \overline{\boldsymbol{\alpha}}_{12}]^{-1} \cdot \overline{\mathbf{T}}_{2(1)} \cdot [\overline{\boldsymbol{\beta}}_{20} + \overline{\boldsymbol{\alpha}}_{21} \cdot \overline{\mathbf{T}}_{1(1)} \cdot \overline{\boldsymbol{\beta}}_{10}] \cdot \mathbf{a}. \tag{2.3.8}$$

From (2.3.7) and (2.3.8), we can define the two-scatterer $\overline{\mathbf{T}}$ matrix as

$$\mathbf{f}_1 = \overline{\mathbf{T}}_{1(2)} \cdot \overline{\boldsymbol{\beta}}_{10} \cdot \mathbf{a}, \tag{2.3.9}$$

$$\mathbf{f}_2 = \overline{\mathbf{T}}_{2(2)} \cdot \overline{\boldsymbol{\beta}}_{20} \cdot \mathbf{a}. \tag{2.3.10}$$

In the above, the scattered field from each scatterer is related to the incident field via the two-scatterer $\overline{\mathbf{T}}$ matrices, $\overline{\mathbf{T}}_{i(2)}$, $i = 1, 2$, where the first subscript i of $\overline{\mathbf{T}}$ means that this is for scatterer i, and the second parenthesized subscript 2 means that this is a two-scatterer $\overline{\mathbf{T}}$ matrix. This notation will be used in the following derivations.

Comparing (2.3.9) and (2.3.10) with (2.3.7) and (2.3.8), we have

$$\overline{\mathbf{T}}_{1(2)} \cdot \overline{\boldsymbol{\beta}}_{10} = [\bar{\mathbf{I}} - \overline{\mathbf{T}}_{1(1)} \cdot \overline{\boldsymbol{\alpha}}_{12} \cdot \overline{\mathbf{T}}_{2(1)} \cdot \overline{\boldsymbol{\alpha}}_{21}]^{-1} \cdot \overline{\mathbf{T}}_{1(1)} \cdot [\overline{\boldsymbol{\beta}}_{10} + \overline{\boldsymbol{\alpha}}_{12} \cdot \overline{\mathbf{T}}_{2(1)} \cdot \overline{\boldsymbol{\beta}}_{20}], \tag{2.3.11}$$

$$\overline{\mathbf{T}}_{2(2)} \cdot \overline{\boldsymbol{\beta}}_{20} = [\bar{\mathbf{I}} - \overline{\mathbf{T}}_{2(1)} \cdot \overline{\boldsymbol{\alpha}}_{21} \cdot \overline{\mathbf{T}}_{1(1)} \cdot \overline{\boldsymbol{\alpha}}_{12}]^{-1} \cdot \overline{\mathbf{T}}_{2(1)} \cdot [\overline{\boldsymbol{\beta}}_{20} + \overline{\boldsymbol{\alpha}}_{21} \cdot \overline{\mathbf{T}}_{1(1)} \cdot \overline{\boldsymbol{\beta}}_{10}]. \tag{2.3.12}$$

From (2.3.11) and (2.3.12), we have

$$\overline{\mathbf{T}}_{1(2)} = [\bar{\mathbf{I}} - \overline{\mathbf{T}}_{1(1)} \cdot \overline{\boldsymbol{\alpha}}_{12} \cdot \overline{\mathbf{T}}_{2(1)} \cdot \overline{\boldsymbol{\alpha}}_{21}]^{-1} \cdot \overline{\mathbf{T}}_{1(1)} \cdot [\overline{\boldsymbol{\beta}}_{10} + \overline{\boldsymbol{\alpha}}_{12} \cdot \overline{\mathbf{T}}_{2(1)} \cdot \overline{\boldsymbol{\beta}}_{20}] \cdot \overline{\boldsymbol{\beta}}_{01}, \tag{2.3.13}$$

$$\overline{\mathbf{T}}_{2(2)} = [\bar{\mathbf{I}} - \overline{\mathbf{T}}_{2(1)} \cdot \overline{\boldsymbol{\alpha}}_{21} \cdot \overline{\mathbf{T}}_{1(1)} \cdot \overline{\boldsymbol{\alpha}}_{12}]^{-1} \cdot \overline{\mathbf{T}}_{2(1)} \cdot [\overline{\boldsymbol{\beta}}_{20} + \overline{\boldsymbol{\alpha}}_{21} \cdot \overline{\mathbf{T}}_{1(1)} \cdot \overline{\boldsymbol{\beta}}_{10}] \cdot \overline{\boldsymbol{\beta}}_{02}. \tag{2.3.14}$$

The relation $\overline{\beta}_{i0}^{-1} = \overline{\beta}_{0i}$ has been used in (2.3.13) and (2.3.14). In the above, $\overline{\mathbf{T}}_{i(2)} \cdot \overline{\beta}_{i0}$ relates the scattered field from the i-th scatterer to the incident field expressed in terms of the global coordinate system, while $\overline{\mathbf{T}}_{i(2)}$ relates the scattered field from the i-th scatterer to the incident field expressed in terms of the local coordinate system of the i-th scatterer in a two-scatterer problem.

Finally, the total field exterior to the scatterers can be written as

$$\phi(\mathbf{r}) = \Re g\psi^t(k_0, \mathbf{r}_0) \cdot \mathbf{a} + 5\psi^t(k_0, \mathbf{r}_1) \cdot \overline{\mathbf{T}}_{1(2)} \cdot \overline{\beta}_{10} \cdot \mathbf{a} + \psi^t(k_0, \mathbf{r}_2) \cdot \overline{\mathbf{T}}_{2(2)} \cdot \overline{\beta}_{20} \cdot \mathbf{a}. \tag{2.3.15}$$

2.3.2 Three-scatterer solution

Before we go to the general recursive formulas of the N-scatterer problem, we shall investigate, in this subsection, the three-scatterer problem more closely in order to clarify some confusion in the domain of validity of the recursive algorithms. Three different approaches are used to derive the three-scatterer $\overline{\mathbf{T}}$ matrices. First, $\overline{\mathbf{T}}_{i(2)}$, $i = 1, 2$, are used to derive the three-scatterer $\overline{\mathbf{T}}$ matrices. Then, $\overline{\mathbf{T}}_{i(2)} \cdot \overline{\beta}_{i0}$, $i = 1, 2$, are used in the derivation instead of $\overline{\mathbf{T}}_{i(2)}$, $i = 1, 2$. Finally, the three-scatterer $\overline{\mathbf{T}}$ matrices are directly derived from the isolated $\overline{\mathbf{T}}$ matrices of the three scatterers.

Following the same notations as in Equation (2.3.15), the total field of the three-scatterer problem can be written as

$$\begin{aligned}\phi(\mathbf{r}) = \Re g\psi^t(k_0, \mathbf{r}_0) \cdot \mathbf{a} + \psi^t(k_0, \mathbf{r}_1) \cdot \overline{\mathbf{T}}_{1(3)} \cdot \overline{\beta}_{10} \cdot \mathbf{a} \\ + \psi^t(k_0, \mathbf{r}_2) \cdot \overline{\mathbf{T}}_{2(3)} \cdot \overline{\beta}_{20} \cdot \mathbf{a} + \psi^t(k_0, \mathbf{r}_3) \cdot \overline{\mathbf{T}}_{3(3)} \cdot \overline{\beta}_{30} \cdot \mathbf{a}.\end{aligned} \tag{2.3.16}$$

Suppose that the third scatterer is located far enough from the circle embracing the first two scatterers, with the center of the circle at the origin of

the global coordinate system. Then, the third term on the right-hand side of (2.3.16), together with the original incident field, can be considered as the total incident field impinging upon the first two scatterers. From the definition of the two-scatterer $\overline{\mathbf{T}}$ matrices given in the last subsection, we have

$$\overline{\mathbf{T}}_{1(3)} \cdot \overline{\boldsymbol{\beta}}_{10} = \overline{\mathbf{T}}_{1(2)} \cdot [\overline{\boldsymbol{\beta}}_{10} + \overline{\boldsymbol{\alpha}}_{13} \cdot \overline{\mathbf{T}}_{3(3)} \cdot \overline{\boldsymbol{\beta}}_{30}], \tag{2.3.17}$$

$$\overline{\mathbf{T}}_{2(3)} \cdot \overline{\boldsymbol{\beta}}_{20} = \overline{\mathbf{T}}_{2(2)} \cdot [\overline{\boldsymbol{\beta}}_{20} + \overline{\boldsymbol{\alpha}}_{23} \cdot \overline{\mathbf{T}}_{3(3)} \cdot \overline{\boldsymbol{\beta}}_{30}]. \tag{2.3.18}$$

Notice that here we have used the words "far enough" to describe the required distance from the center of the third scatterer to the origin of the global coordinate system. The quantitative requirement will be given later.

Meanwhile, using Equations (2.3.3a) and (2.3.3b), the total field can also be expressed in terms of the local coordinate system of the third scatterer as

$$\begin{aligned}\phi(\mathbf{r}) = {} & \Re g\psi^t(k_0, \mathbf{r}_3) \cdot \overline{\boldsymbol{\beta}}_{30} \cdot \mathbf{a} + \Re g\psi^t(k_0, \mathbf{r}_3) \cdot \overline{\boldsymbol{\alpha}}_{31} \cdot \overline{\mathbf{T}}_{1(3)} \cdot \overline{\boldsymbol{\beta}}_{10} \cdot \mathbf{a} \\ & + \Re g\psi^t(k_0, \mathbf{r}_3) \cdot \overline{\boldsymbol{\alpha}}_{32} \cdot \overline{\mathbf{T}}_{2(3)} \cdot \overline{\boldsymbol{\beta}}_{20} \cdot \mathbf{a} + \psi^t(k_0, \mathbf{r}_3) \cdot \overline{\mathbf{T}}_{3(3)} \cdot \overline{\boldsymbol{\beta}}_{30} \cdot \mathbf{a}. \end{aligned} \tag{2.3.19}$$

The above is valid only when $|\mathbf{r}_3| < d_{1,3}$ and $|\mathbf{r}_3| < d_{2,3}$, where $d_{1,3}$ is the distance between O_1 and O_3, and $d_{2,3}$ is the distance between O_2 and O_3. If we consider the first three terms on the right-hand side of Equation (2.3.19) as the total incident field impinging upon the third scatterer, then the last term on the right-hand side of (2.3.19), the scattered field from the third scatterer, can be related to the total incident field in terms of the isolated $\overline{\mathbf{T}}_{3(1)}$ as

$$\overline{\mathbf{T}}_{3(3)} \cdot \overline{\boldsymbol{\beta}}_{30} = \overline{\mathbf{T}}_{3(1)} \cdot [\overline{\boldsymbol{\beta}}_{30} + \sum_{i=1}^{2} \overline{\boldsymbol{\alpha}}_{3i} \cdot \overline{\mathbf{T}}_{i(3)} \cdot \overline{\boldsymbol{\beta}}_{i0}]. \tag{2.3.20}$$

On substituting (2.3.17) and (2.3.18) into (2.3.20), we have

$$\overline{\mathbf{T}}_{3(3)} \cdot \overline{\boldsymbol{\beta}}_{30} = \overline{\mathbf{T}}_{3(1)} \cdot [\overline{\boldsymbol{\beta}}_{30} + \sum_{i=1}^{2} \overline{\boldsymbol{\alpha}}_{3i} \cdot \overline{\mathbf{T}}_{i(2)} \cdot \overline{\boldsymbol{\beta}}_{i0} + \sum_{i=1}^{2} \overline{\boldsymbol{\alpha}}_{3i} \cdot \overline{\mathbf{T}}_{i(2)} \cdot \overline{\boldsymbol{\alpha}}_{i3} \cdot \overline{\mathbf{T}}_{3(3)} \cdot \overline{\boldsymbol{\beta}}_{30}]. \tag{2.3.21}$$

Then solving the above equation for $\overline{\mathbf{T}}_{3(3)} \cdot \overline{\boldsymbol{\beta}}_{30}$, we obtain

$$\overline{\mathbf{T}}_{3(3)} \cdot \overline{\boldsymbol{\beta}}_{3,0} = \left[\overline{\mathbf{I}} - \overline{\mathbf{T}}_{3(1)} \cdot \sum_{i=1}^{2} \overline{\boldsymbol{\alpha}}_{3,i} \cdot \overline{\mathbf{T}}_{i(2)} \cdot \overline{\boldsymbol{\alpha}}_{i3}\right]^{-1} \cdot \overline{\mathbf{T}}_{3(1)} \cdot \left[\overline{\boldsymbol{\beta}}_{3,0} + \sum_{i=1}^{2} \overline{\boldsymbol{\alpha}}_{3,i} \cdot \overline{\mathbf{T}}_{i(2)} \cdot \overline{\boldsymbol{\beta}}_{i0}\right]. \tag{2.3.22}$$

Knowing $\overline{\mathbf{T}}_{3(3)} \cdot \overline{\boldsymbol{\beta}}_{30}$, the other two $\overline{\mathbf{T}}$ matrices are readily obtained by using (2.3.17) and (2.3.18). They are

$$\overline{\mathbf{T}}_{i(3)} \cdot \overline{\boldsymbol{\beta}}_{i0} = \overline{\mathbf{T}}_{i(2)} \cdot [\overline{\boldsymbol{\beta}}_{i0} + \overline{\boldsymbol{\alpha}}_{i3} \cdot \overline{\mathbf{T}}_{3(3)} \cdot \overline{\boldsymbol{\beta}}_{30}], \quad i = 1, 2. \tag{2.3.23}$$

Equations (2.3.22) and (2.3.23) together constitute the recursive formulas which enable us to derive $\overline{\mathbf{T}}_{i(3)}$, $i = 1, 2, 3$, from $\overline{\mathbf{T}}_{i(2)}$, $i = 1, 2$.

The above derivation uses $\overline{\mathbf{T}}_{i(2)}$, $i = 1, 2$, as the building blocks to derive the three-scatterer $\overline{\mathbf{T}}$ matrices. Following the same arguments, we also can use $\overline{\mathbf{T}}_{i(2)} \cdot \overline{\boldsymbol{\beta}}_{i0}$, $i = 1, 2$, as the building blocks in the derivation of the three-scatterer $\overline{\mathbf{T}}$ matrices. In this case, we still can consider the last term on the right-hand side of (2.3.16) together with the original incident field as the total incident field impinging upon the first two scatterers if the third scatterer satisfies the same condition as in the above derivation. Since $\overline{\mathbf{T}}_{i(2)} \cdot \overline{\boldsymbol{\beta}}_{i0}$,

$i = 1, 2$, relate the scattered field from each scatterer to the incident field expressed in the global coordinate system, we can express the last term of (2.3.16) in terms of the global coordinate system using (2.3.3a) and treat it as part of the incident field impinging on the first two scatterers. Then, following the same argument for (2.3.15) and (2.3.16), we have

$$\overline{\overline{\mathbf{T}}}_{1(3)} \cdot \overline{\beta}_{10} = \overline{\overline{\mathbf{T}}}_{1(2)} \cdot \overline{\beta}_{10} \cdot [\overline{\overline{\mathbf{I}}} + \overline{\alpha}_{03} \cdot \overline{\overline{\mathbf{T}}}_{3(3)} \cdot \overline{\beta}_{30}], \tag{2.3.24}$$

$$\overline{\overline{\mathbf{T}}}_{2(3)} \cdot \overline{\beta}_{20} = \overline{\overline{\mathbf{T}}}_{2(2)} \cdot \overline{\beta}_{20} \cdot [\overline{\overline{\mathbf{I}}} + \overline{\alpha}_{03} \cdot \overline{\overline{\mathbf{T}}}_{3(3)} \cdot \overline{\beta}_{30}]. \tag{2.3.25}$$

Following the same argument from (2.3.19) to (2.3.20), we have

$$\overline{\overline{\mathbf{T}}}_{3(3)} \cdot \overline{\beta}_{30} = \overline{\overline{\mathbf{T}}}_{3(1)} \cdot [\overline{\beta}_{30} + \sum_{i=1}^{2} \overline{\alpha}_{3i} \cdot \overline{\overline{\mathbf{T}}}_{i(3)} \cdot \overline{\beta}_{i0}]. \tag{2.3.26}$$

Substituting (2.3.24) and (2.3.25) into (2.3.26) and solving for $\overline{\overline{\mathbf{T}}}_{3(3)} \cdot \overline{\beta}_{30}$, we obtain

$$\overline{\overline{\mathbf{T}}}_{3(3)} \cdot \overline{\beta}_{3,0} = \left[\overline{\overline{\mathbf{I}}} - \overline{\overline{\mathbf{T}}}_{3(1)} \cdot \sum_{i=1}^{2} \overline{\alpha}_{3,i} \cdot \overline{\overline{\mathbf{T}}}_{i(2)} \cdot \overline{\beta}_{i0} \cdot \overline{\alpha}_{03}\right]^{-1} \cdot \overline{\overline{\mathbf{T}}}_{3(1)} \cdot \left[\overline{\beta}_{3,0} + \sum_{i=1}^{2} \overline{\alpha}_{3,i} \cdot \overline{\overline{\mathbf{T}}}_{i(2)} \cdot \overline{\beta}_{i0}\right]. \tag{2.3.27}$$

Equations (2.3.27), (2.3.24), and (2.3.25) together constitute the recursive formulas yielding $\overline{\overline{\mathbf{T}}}_{i(3)} \cdot \overline{\beta}_{i0}$, $i = 1, 2, 3$, from $\overline{\overline{\mathbf{T}}}_{i(2)} \cdot \overline{\beta}_{i0}$, $i = 1, 2$.

From the above formal derivations, it seems that the two recursive schemes are equivalent. However, the domains of validity of the two recursive schemes are different. In order to find the domain of validity of the two recursive formulas, next, we shall derive the three-scatterer $\overline{\overline{\mathbf{T}}}$ matrices directly from the isolated $\overline{\overline{\mathbf{T}}}$ matrices, $\overline{\overline{\mathbf{T}}}_{i(1)}$, $i = 1, 2, 3$.

From (2.3.16), we know that the total field of the three-scatterer problem can be written as

$$\begin{aligned}\phi(\mathbf{r}) =& \Re g\psi^t(k_0,\mathbf{r}_0)\cdot\mathbf{a}+\psi^t(k_0,\mathbf{r}_1)\cdot\overline{\mathbf{T}}_{1(3)}\cdot\overline{\boldsymbol{\beta}}_{10}\cdot\mathbf{a}\\ &+\psi^t(k_0,\mathbf{r}_2)\cdot\overline{\mathbf{T}}_{2(3)}\cdot\overline{\boldsymbol{\beta}}_{20}\cdot\mathbf{a}+\psi^t(k_0,\mathbf{r}_3)\cdot\overline{\mathbf{T}}_{3(3)}\cdot\overline{\boldsymbol{\beta}}_{30}\cdot\mathbf{a}.\end{aligned} \tag{2.3.28}$$

Using (2.3.3a) and (2.3.3b), we can also express the above equation in terms of the local coordinate system of the first scatterer as

$$\begin{aligned}\phi(\mathbf{r}) =& \Re g\psi^t(k_0,\mathbf{r}_1)\cdot\overline{\boldsymbol{\beta}}_{10}\cdot\mathbf{a}+\psi^t(k_0,\mathbf{r}_1)\cdot\overline{\mathbf{T}}_{1(3)}\cdot\overline{\boldsymbol{\beta}}_{10}\cdot\mathbf{a}\\ &+\Re g\psi^t(k_0,\mathbf{r}_1)\cdot\overline{\boldsymbol{\alpha}}_{12}\cdot\overline{\mathbf{T}}_{2(3)}\cdot\overline{\boldsymbol{\beta}}_{20}\cdot\mathbf{a}+\Re g\psi^t(k_0,\mathbf{r}_1)\cdot\overline{\boldsymbol{\alpha}}_{13}\cdot\overline{\mathbf{T}}_{3(3)}\cdot\overline{\boldsymbol{\beta}}_{30}\cdot\mathbf{a}.\end{aligned} \tag{2.3.29}$$

Equation (2.3.29) is valid if $|\mathbf{r}_1| < d_{1,2}$ and $|\mathbf{r}_1| < d_{1,3}$. If we consider the first and last two terms on the right-hand side of (2.3.29) as the total incident field impinging upon the first scatterer, we have

$$\overline{\mathbf{T}}_{1(3)}\cdot\overline{\boldsymbol{\beta}}_{10}=\overline{\mathbf{T}}_{1(1)}\cdot[\overline{\boldsymbol{\beta}}_{10}+\overline{\boldsymbol{\alpha}}_{12}\cdot\overline{\mathbf{T}}_{2(3)}\cdot\overline{\boldsymbol{\beta}}_{20}+\overline{\boldsymbol{\alpha}}_{13}\cdot\overline{\mathbf{T}}_{3(3)}\cdot\overline{\boldsymbol{\beta}}_{30}]. \tag{2.3.30}$$

Similarly, for scatterers 2 and 3, we have

$$\overline{\mathbf{T}}_{2(3)}\cdot\overline{\boldsymbol{\beta}}_{20}=\overline{\mathbf{T}}_{2(1)}\cdot[\overline{\boldsymbol{\beta}}_{20}+\overline{\boldsymbol{\alpha}}_{21}\cdot\overline{\mathbf{T}}_{1(3)}\cdot\overline{\boldsymbol{\beta}}_{10}+\overline{\boldsymbol{\alpha}}_{23}\cdot\overline{\mathbf{T}}_{3(3)}\cdot\overline{\boldsymbol{\beta}}_{30}], \tag{2.3.31}$$

$$\overline{\mathbf{T}}_{3(3)}\cdot\overline{\boldsymbol{\beta}}_{30}=\overline{\mathbf{T}}_{3(1)}\cdot[\overline{\boldsymbol{\beta}}_{30}+\overline{\boldsymbol{\alpha}}_{31}\cdot\overline{\mathbf{T}}_{1(3)}\cdot\overline{\boldsymbol{\beta}}_{10}+\overline{\boldsymbol{\alpha}}_{32}\cdot\overline{\mathbf{T}}_{2(3)}\cdot\overline{\boldsymbol{\beta}}_{20}]. \tag{2.3.32}$$

Substituting (2.3.31) into (2.3.30), we obtain

$$\begin{aligned}\overline{\mathbf{T}}_{1(3)}\cdot\overline{\boldsymbol{\beta}}_{10} =& \overline{\mathbf{T}}_{1(1)}\cdot\overline{\boldsymbol{\beta}}_{10}+\overline{\mathbf{T}}\cdot\overline{\boldsymbol{\alpha}}_{12}\cdot\overline{\mathbf{T}}_{2(1)}\cdot[\overline{\boldsymbol{\beta}}_{20}+\overline{\boldsymbol{\alpha}}_{21}\cdot\overline{\mathbf{T}}_{1(3)}\cdot\overline{\boldsymbol{\beta}}_{10}\\ &+\overline{\boldsymbol{\alpha}}_{23}\cdot\overline{\mathbf{T}}_{3(3)}\cdot\overline{\boldsymbol{\beta}}_{30}]+\overline{\mathbf{T}}_{1(1)}\cdot\overline{\boldsymbol{\alpha}}_{13}\cdot\overline{\mathbf{T}}_{3(3)}\cdot\overline{\boldsymbol{\beta}}_{30}.\end{aligned} \tag{2.3.33}$$

Rearranging (2.3.33), we have

$$\begin{aligned}[\overline{\mathbf{I}}-\overline{\mathbf{T}}_{1(1)}\cdot\overline{\boldsymbol{\alpha}}_{12}\cdot\overline{\mathbf{T}}_{2(1)}\cdot\overline{\boldsymbol{\alpha}}_{21}]\cdot\overline{\mathbf{T}}_{1(3)}\cdot\overline{\boldsymbol{\beta}}_{10} =& \overline{\mathbf{T}}_{1(1)}\cdot[\overline{\boldsymbol{\beta}}_{10}+\overline{\boldsymbol{\alpha}}_{12}\cdot\overline{\mathbf{T}}_{2(1)}\cdot\overline{\boldsymbol{\beta}}_{20}]\\ &+\overline{\mathbf{T}}_{1(1)}\cdot[\overline{\boldsymbol{\alpha}}_{13}+\overline{\boldsymbol{\alpha}}_{12}\cdot\overline{\mathbf{T}}_{2(1)}\cdot\overline{\boldsymbol{\alpha}}_{23}]\cdot\overline{\mathbf{T}}_{3(3)}\cdot\overline{\boldsymbol{\beta}}_{30}.\end{aligned} \tag{2.3.34}$$

Then we have

$$\overline{\mathbf{T}}_{1(3)} \cdot \overline{\boldsymbol{\beta}}_{10} = [\overline{\mathbf{I}} - \overline{\mathbf{T}}_{1(1)} \cdot \overline{\boldsymbol{\alpha}}_{12} \cdot \overline{\mathbf{T}}_{2(1)} \cdot \overline{\boldsymbol{\alpha}}_{21}]^{-1} \cdot \overline{\mathbf{T}}_{1(1)} \cdot [\overline{\boldsymbol{\beta}}_{10} + \overline{\boldsymbol{\alpha}}_{12} \cdot \overline{\mathbf{T}}_{2(1)} \cdot \overline{\boldsymbol{\beta}}_{20}]$$

$$+ \underbrace{[\overline{\mathbf{I}} - \overline{\mathbf{T}}_{1(1)} \cdot \overline{\boldsymbol{\alpha}}_{12} \cdot \overline{\mathbf{T}}_{2(1)} \cdot \overline{\boldsymbol{\alpha}}_{21}]^{-1} \cdot \overline{\mathbf{T}}_{1(1)} \cdot [\overline{\boldsymbol{\alpha}}_{13} + \overline{\boldsymbol{\alpha}}_{12} \cdot \overline{\mathbf{T}}_{2(1)} \cdot \overline{\boldsymbol{\alpha}}_{23}] \cdot \overline{\mathbf{T}}_{3(3)} \cdot \overline{\boldsymbol{\beta}}_{30}}_{(\mathrm{II})} \cdot \tag{2.3.35}$$

From (2.3.11), we can recognize that the first term on the right-hand side of (2.3.35) is $\overline{\mathbf{T}}_{1(2)} \cdot \overline{\boldsymbol{\beta}}_{10}$. For the last term of (2.3.33), if we suppose that the third scatterer is outside of the circle embracing the first two scatterers with the center at the origin of the global coordinate system, the following identities hold

$$\overline{\boldsymbol{\alpha}}_{13} = \overline{\boldsymbol{\beta}}_{10} \cdot \overline{\boldsymbol{\alpha}}_{03}, \tag{2.3.36}$$

$$\overline{\boldsymbol{\alpha}}_{23} = \overline{\boldsymbol{\beta}}_{20} \cdot \overline{\boldsymbol{\alpha}}_{03}, \tag{2.3.37}$$

if

$$|\mathbf{r}_{3,0}| > \max(|\mathbf{r}_{1,0}|, |\mathbf{r}_{2,0}|), \tag{2.3.38}$$

where $\mathbf{r}_{i,0}$ is the distance between the origin of the local coordinate system of the i-th scatterer and the origin of the global coordinate system. Now, we define $C_{0,i}$ as a region bounded by a circle centered at the origin of the global coordinate system with the radius of $d_{0,i}$, that is,

$$C_{0,i} \equiv \{\mathbf{r}_0 \,|\, |\mathbf{r}_0| < d_{0,i}\}. \tag{2.3.39}$$

Now, we define Ω' as a union of $C_{0,1}$ and $C_{0,2}$, that is,

$$\Omega' \equiv C_{0,1} \bigcup C_{0,2} \equiv \{\mathbf{r} | \mathbf{r} \in C_{0,1}, \text{ or } \mathbf{r} \in C_{0,2}\}. \tag{2.3.40}$$

Then (2.3.38) becomes

$$\mathbf{r}_{3,0} \notin \Omega'. \tag{2.3.41}$$

Applying (2.3.36) and (2.3.37) to the last term of (2.3.35), we have

$$\begin{aligned}(\mathrm{II}) &= [\bar{\mathrm{I}} - \overline{\mathrm{T}}_{1(1)} \cdot \overline{\alpha}_{12} \cdot \overline{\mathrm{T}}_{2(1)} \cdot \overline{\alpha}_{21}]^{-1} \\ &\quad \cdot \overline{\mathrm{T}}_{1(1)} \cdot [\overline{\beta}_{10} + \overline{\alpha}_{12} \cdot \overline{\mathrm{T}}_{2(1)} \cdot \overline{\beta}_{20}] \cdot \overline{\alpha}_{03} \cdot \overline{\mathrm{T}}_{3(3)} \cdot \overline{\beta}_{30} \\ &= \overline{\mathrm{T}}_{1(2)} \cdot \overline{\beta}_{10} \cdot \ \overline{\alpha}_{03} \cdot \overline{\mathrm{T}}_{3(3)} \cdot \overline{\beta}_{30}. \end{aligned} \tag{2.3.42}$$

Equation (2.3.11) has been used in (2.3.42). Using (2.3.42), (2.3.35) yields

$$\overline{\mathrm{T}}_{1(3)} \cdot \overline{\beta}_{10} = \overline{\mathrm{T}}_{1(2)} \cdot \overline{\beta}_{10} \cdot [\bar{\mathrm{I}} + \overline{\alpha}_{03} \cdot \overline{\mathrm{T}}_{3(3)} \cdot \overline{\beta}_{30}], \tag{2.3.43}$$

which is the same as (2.3.24). By the same token, we can also recover (2.3.25) by substituting (2.3.30) into (2.3.31). Meanwhile, (2.3.32) is the same as (2.3.26). Therefore, the recursive formulas (2.3.23), (2.3.24), and (2.3.25) are valid only if (2.3.41) is true.

However, in order to recover (2.3.17) from (2.3.35), we require that

$$(\mathrm{II}) = \overline{\mathrm{T}}_{1(2)} \cdot [\overline{\alpha}_{13} \cdot \overline{\mathrm{T}}_{3(3)} \cdot \overline{\beta}_{30}]. \tag{2.3.44}$$

Using the identity $\overline{\beta}_{ij} = \overline{\beta}_{i0} \cdot \overline{\beta}_{0j}$, Equation (2.3.13) becomes

$$\overline{\mathrm{T}}_{1(2)} = [\bar{\mathrm{I}} - \overline{\mathrm{T}}_{1(1)} \cdot \overline{\alpha}_{12} \cdot \overline{\mathrm{T}}_{2(1)} \cdot \overline{\alpha}_{21}]^{-1} \cdot \overline{\mathrm{T}}_{1(1)} \cdot [\bar{\mathrm{I}} + \overline{\alpha}_{12} \cdot \overline{\mathrm{T}}_{2(1)} \cdot \overline{\beta}_{21}]. \tag{2.3.45}$$

From Equations (2.3.45) and (2.3.35), we can see that in order to satisfy (2.3.44), the following identity has to hold

$$\overline{\alpha}_{23} = \overline{\beta}_{21} \cdot \overline{\alpha}_{13}. \tag{2.3.46}$$

From Appendix A, we know that (2.3.46) is true only when the following condition is satisfied:

$$d_{1,3} > d_{1,2}. \tag{2.3.47}$$

Now, we define $C_{1,2}$ as a region bounded by a circle centered at the origin of the local coordinate system of scatterer 1 with the radius of $d_{1,2}$. The first subscript means that the center of the circle is located at the origin of the local coordinate system of scatterer 1. The radius of the circle is $d_{1,2}$, the distance between the origins of the local coordinate systems of scatterers 1 and 2. With the above definition, Equation (2.3.47) means that scatterer 3 is outside of $C_{1,2}$.

By the same token, in order to recover Equation (2.3.18) from Equations (2.3.30) and (2.3.31), the following identity is required:

$$d_{2,3} > d_{1,2}. \tag{2.3.48}$$

Condition (2.3.48) means that scatterer 3 has to be outside of $C_{2,1}$. Meanwhile, Equation (2.3.32) is the same as Equation (2.3.20). Therefore, if the conditions (2.3.47) and (2.3.48) are satisfied, the recursive formulas (2.3.22) and (2.3.23) are valid. Now, we define Ω'' as a union of $C_{1,2}$ and $C_{2,1}$, that is,

$$\Omega'' = C_{1,2} \bigcup C_{2,1} \equiv \{\mathbf{r} | \mathbf{r} \in C_{1,2}, \text{or } \mathbf{r} \in C_{2,1}\}. \tag{2.3.49}$$

Using the definition of Ω'', the restraint conditions (2.3.47) and (2.3.48) become

$$\mathbf{r}_{3,0} \notin \Omega_2''. \tag{2.3.50}$$

Comparing condition (2.3.50) with condition (2.3.41) shows that condition (2.3.50) is much stronger than condition (2.3.41). Meanwhile, condition (2.3.41) is easier to check than condition (2.3.50) in the numerical implementations. Figure 2.3 shows the domains of $C_{1,2}$, $C_{2,1}$, Ω', and $C_{0,i}$, $i = 1, 2$, for two specific cases. In Figure 2.3(a), the origin of the global coordinate

system coincides with the origin of the local coordinate system of the scatterer 1. In Figure 2.3(b), the origin of the global coordinate system is located between O_1 and O_2. In both cases, Ω_2' defined by Equation (2.3.40) is a subset of Ω_2'' defined by Equation (2.3.49). The above results pertaining to the domain of validity shall be extended to more general N-scatterer problems in the next subsection.

2.3.3 N-scatterer solution—recursive solution

In the last subsection, the three-scatterer solution is constructed from the two-scatterer solution. Here, we shall derive the recursive formulas which allow us to obtain the $n+1$-scatterer solution from the n-scatterer solution. First, we derive a recursive scheme by using $\overline{\mathbf{T}}_{i(n)} \cdot \overline{\boldsymbol{\beta}}_{i0}$ as the building blocks. Similar to (2.3.16), the total field exterior to the n scatterers for an n-scatterer problem is of the form [14,15,22–24]

$$\phi(\mathbf{r}) = \Re g\psi^t(k_0, \mathbf{r}_0) \cdot \mathbf{a} + \sum_{i=1}^{n} \psi^t(k_0, \mathbf{r}_i) \cdot \overline{\mathbf{T}}_{i(n)} \cdot \overline{\boldsymbol{\beta}}_{i0} \cdot \mathbf{a}. \tag{2.3.51}$$

Suppose that the n-scatterer solution is known, that is, all of the $\overline{\mathbf{T}}_{i(n)} \cdot \overline{\boldsymbol{\beta}}_{i0}$, $i = 1, 2, \ldots, n$, are known. Remember that each $\overline{\mathbf{T}}_{i(n)} \cdot \overline{\boldsymbol{\beta}}_{i0}$ relates the scattered field from the i-th scatterer to the incident field expressed in terms of the global coordinate system.

Similarly, the $(n+1)$-scatterer solution has the form

$$\phi(\mathbf{r}) = \Re g\psi^t(k_0, \mathbf{r}_0) \cdot \mathbf{a} + \sum_{i=1}^{n+1} \psi^t(k_0, \mathbf{r}_i) \cdot \overline{\mathbf{T}}_{i(n+1)} \cdot \overline{\boldsymbol{\beta}}_{i0} \cdot \mathbf{a}. \tag{2.3.52}$$

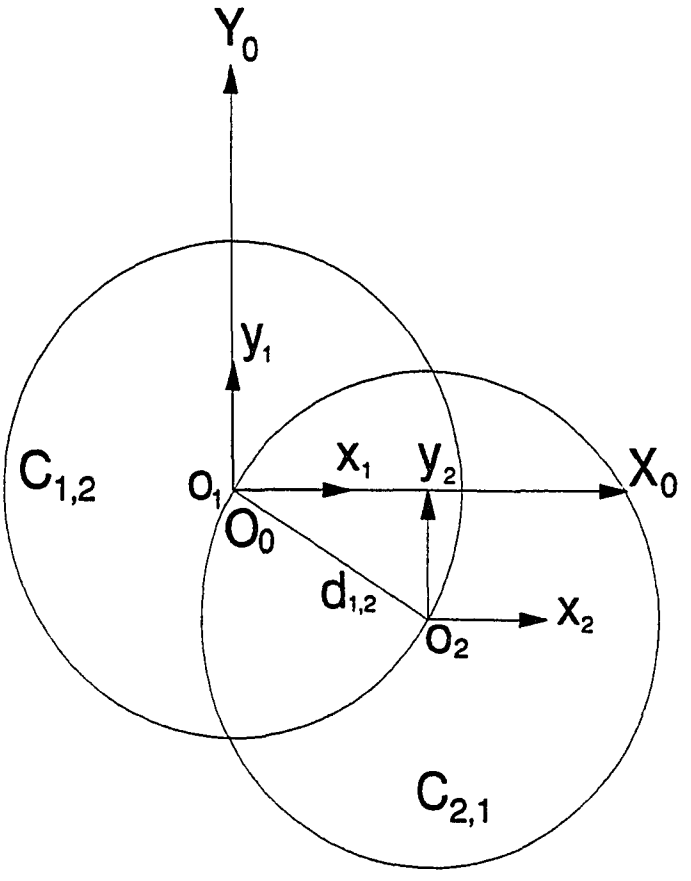

Figure 2.3(a). Domains of $C_{1,2}$, $C_{2,1}$, $C_{0,1}$, and $C_{0,2}$, when the origin of the global coordinates coincides with the origin of the local coordinates of the scatterer 1. Here, $C_{0,1}$ is empty and $C_{0,2} = C_{1,2}$.

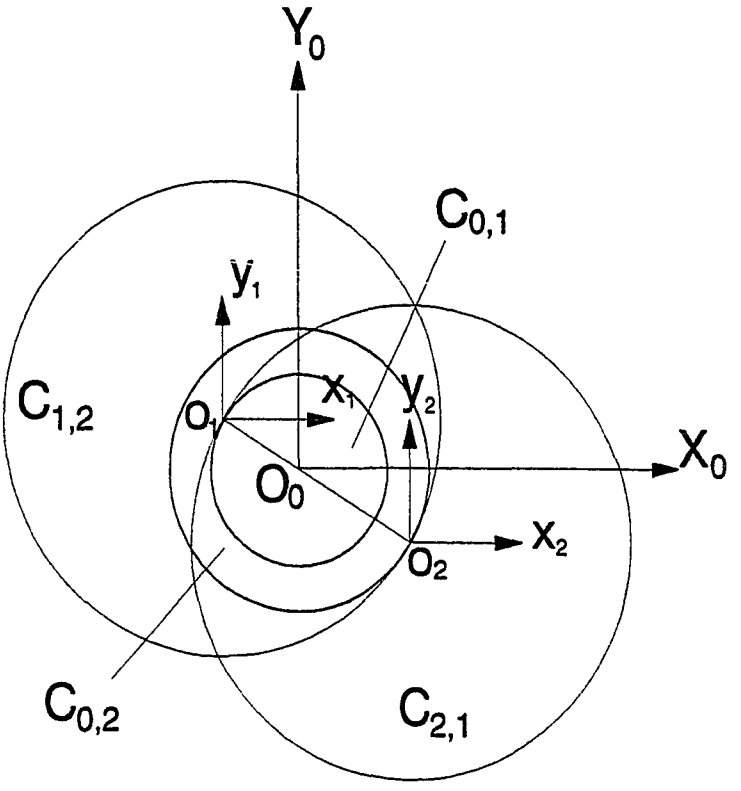

Figure 2.3(b). Domains of $C_{1,2}$, $C_{2,1}$, $C_{0,1}$, and $C_{0,2}$, when the origin of the global coordinates is located between O_1 and O_2, the origins of the coordinate systems related to the scatterers 1 and 2, respectively.

The above can be rewritten as

$$\phi(\mathbf{r}) = \Re g\psi^t(k_0, \mathbf{r}_0) \cdot \mathbf{a} + \sum_{i=1}^{n} \psi^t(k_0, \mathbf{r}_i) \cdot \overline{\mathbf{T}}_{i(n+1)} \cdot \overline{\boldsymbol{\beta}}_{i0} \cdot \mathbf{a} + \psi^t(k_0, \mathbf{r}_{n+1}) \cdot \overline{\mathbf{T}}_{n+1(n+1)} \cdot \overline{\boldsymbol{\beta}}_{n+1,0} \cdot \mathbf{a}. \tag{2.3.53}$$

The first and last terms in Equation (2.3.53) can be thought of as the total incident field impinging on the $i = 1, \ldots, n$ scatterers. Remember that the total field for an n-scatterer problem can be expressed in terms of Equation (2.3.51), only when the source of the scattering problem is outside of the circle embracing the n scatterers, that is, the source shall be outside of the Ω'_n, where

$$\Omega'_n \equiv \bigcup_{i=1}^{n} C_{0,i}. \tag{2.3.54}$$

Therefore, if

$$\mathbf{r}_{n+1,0} \notin \Omega'_n, \tag{2.3.55}$$

by using Equation (2.3.51), the scattered field amplitudes for the first n scatterer can be written as

$$\overline{\mathbf{T}}_{i(n+1)} \cdot \overline{\boldsymbol{\beta}}_{i0} \cdot \mathbf{a} = \overline{\mathbf{T}}_{i(n)} \cdot \overline{\boldsymbol{\beta}}_{i0} \cdot [\overline{\mathbf{I}} + \overline{\boldsymbol{\alpha}}_{0,n+1} \cdot \overline{\mathbf{T}}_{n+1(n+1)} \cdot \overline{\boldsymbol{\beta}}_{n+1,0}] \cdot \mathbf{a}, \quad i = 1, 2, \ldots, n, \tag{2.3.56}$$

where we have applied the translation formula (2.3.3a) to translating the last terms from the coordinate system of the i-th scatterer to the global coordinate system.

The scattered field amplitude from the $(n+1)$-th scatterer is due to the scattering of the incident field from the other n scatterers via the isolated-scatterer $\overline{\mathbf{T}}$ matrix. Hence, the scattered field amplitude due to the $(n+1)$-th

scatterer is related to the other field amplitudes as

$$\overline{\mathbf{T}}_{n+1(n+1)}\cdot\overline{\boldsymbol{\beta}}_{n+1,0}\cdot\mathbf{a}=\overline{\mathbf{T}}_{n+1(1)}\cdot\left[\overline{\boldsymbol{\beta}}_{n+1,0}+\sum_{i=1}^{n}\overline{\boldsymbol{\alpha}}_{n+1,i}\cdot\overline{\mathbf{T}}_{i(n+1)}\cdot\overline{\boldsymbol{\beta}}_{i0}\right]\cdot\mathbf{a}. \quad (2.3.57)$$

Using (2.3.56) in (2.3.57), we have

$$\overline{\mathbf{T}}_{n+1(n+1)}\cdot\overline{\boldsymbol{\beta}}_{n+1,0}=\overline{\mathbf{T}}_{n+1(1)}\cdot\left[\overline{\boldsymbol{\beta}}_{n+1,0}+\sum_{i=1}^{n}\overline{\boldsymbol{\alpha}}_{n+1,i}\cdot\overline{\mathbf{T}}_{i(n)}\cdot\overline{\boldsymbol{\beta}}_{i0}+\sum_{i=1}^{n}\overline{\boldsymbol{\alpha}}_{n+1,i}\cdot\overline{\mathbf{T}}_{i(n)}\cdot\overline{\boldsymbol{\beta}}_{i0}\cdot\overline{\boldsymbol{\alpha}}_{0,n+1}\cdot\overline{\mathbf{T}}_{n+1(n+1)}\cdot\overline{\boldsymbol{\beta}}_{n+1,0}\right]. \quad (2.3.58)$$

Solving this equation for $\overline{\mathbf{T}}_{n+1(n+1)}\cdot\overline{\boldsymbol{\beta}}_{n+1,0}$, we obtain

$$\overline{\mathbf{T}}_{n+1(n+1)}\cdot\overline{\boldsymbol{\beta}}_{n+1,0}=\left[\bar{\mathbf{I}}-\overline{\mathbf{T}}_{n+1(1)}\cdot\sum_{i=1}^{n}\overline{\boldsymbol{\alpha}}_{n+1,i}\cdot\overline{\mathbf{T}}_{i(n)}\cdot\overline{\boldsymbol{\beta}}_{i0}\cdot\overline{\boldsymbol{\alpha}}_{0,n+1}\right]^{-1}\cdot\overline{\mathbf{T}}_{n+1(1)}\cdot\left[\overline{\boldsymbol{\beta}}_{n+1,0}+\sum_{i=1}^{n}\overline{\boldsymbol{\alpha}}_{n+1,i}\cdot\overline{\mathbf{T}}_{i(n)}\cdot\overline{\boldsymbol{\beta}}_{i0}\right]. \quad (2.3.59)$$

From (2.3.56), we have

$$\overline{\mathbf{T}}_{i(n+1)}\cdot\overline{\boldsymbol{\beta}}_{i0}=\overline{\mathbf{T}}_{i(n)}\cdot\overline{\boldsymbol{\beta}}_{i0}\cdot[\bar{\mathbf{I}}+\overline{\boldsymbol{\alpha}}_{0,n+1}\cdot\overline{\mathbf{T}}_{n+1(n+1)}\cdot\overline{\boldsymbol{\beta}}_{n+1,0}],\quad i=1,2,\ldots,n. \quad (2.3.60)$$

Equations (2.3.59) and (2.3.60) together comprise the recursive relations that enable us to calculate the $\overline{\mathbf{T}}_{i(n+1)}\cdot\overline{\boldsymbol{\beta}}_{i0}$ matrices, $i=1,\ldots,n+1$, given the $\overline{\mathbf{T}}_{i(n)}\cdot\overline{\boldsymbol{\beta}}_{i0}$ matrices, $i=1,\ldots,n$. Hence, given the knowledge of the isolated-scatterer $\overline{\mathbf{T}}$ matrices, the N-scatterer solution is constructed recursively, starting from the one-scatterer solution. Once $\overline{\mathbf{T}}_{i(N)}\cdot\overline{\boldsymbol{\beta}}_{i0}$, $i=1,2,\ldots,N$,

are derived by using the recursive relations (2.3.59) and (2.3.60), the total field of the N-scatterer problem outside of the scatterers can be written as

$$\phi(\mathbf{r}) = \Re g\psi^t(k_0, \mathbf{r}_0) \cdot \mathbf{a} + \sum_{i=1}^{N} \psi^t(k_0, \mathbf{r}_i) \cdot \overline{\mathbf{T}}_{i(N)} \cdot \overline{\boldsymbol{\beta}}_{i0} \cdot \mathbf{a}. \tag{2.3.61}$$

The domain of validity for the recursive relations (2.3.59) and (2.3.60) is given by Equation (2.3.55), which is a general form of Equation (2.3.41) for a three-scatterer problem. Therefore, in order to apply the recursive relations (2.3.59) and (2.3.60), we need to chose a proper global coordinate system and to sort the N scatterers in this global coordinate system such that condition (2.3.55) is always true in every recursive step. This could be achieved by reordering the scatterers in the global coordinate system as

$$|\mathbf{r}_{1,0}| < |\mathbf{r}_{2,1}| < \cdots < |\mathbf{r}_{N,0}|. \tag{2.3.62}$$

The global coordinate system could be chosen in the following way. We view every scatterer as a unit mass point and choose the weight center of the N-mass point system as the origin of the global coordinate system. After ordering the scatterers according to (2.3.62) in the global coordinate system, condition (2.3.55) is always true for every recursive step. Consequently, the recursive relations (2.3.59) and (2.3.60) are eligible if (2.3.62) is true.

In the following, we shall derive a recursive scheme by using $\overline{\mathbf{T}}_{i(n)}$, $i = 1, 2, \ldots, n$, as the building blocks and investigate the domain of validity of this scheme. First, we assume that the n-scatterer solution is known, that is, the $\overline{\mathbf{T}}_{i(n)}$ matrices, $i = 1, 2, \ldots, n$, are given. We want to derive a recursive relation which enables us to obtain the $(n+1)$-scatterer solution from the n-scatterer solution.

From (2.3.52), the $(n+1)$-scatterer solution has the form

$$\phi(\mathbf{r}) = \Re g\psi^t(k_0, \mathbf{r}_0) \cdot \mathbf{a} + \sum_{i=1}^{n+1} \psi^t(k_0, \mathbf{r}_i) \cdot \overline{\mathbf{T}}_{i(n+1)} \cdot \overline{\boldsymbol{\beta}}_{i0} \cdot \mathbf{a}. \tag{2.3.63}$$

The above can be rewritten as

$$\begin{aligned}\phi(\mathbf{r}) = \Re g\psi^t(k_0, \mathbf{r}_0) \cdot \mathbf{a} + \sum_{i=1}^{n} \psi^t(k_0, \mathbf{r}_i) \cdot \overline{\mathbf{T}}_{i(n+1)} \cdot \overline{\boldsymbol{\beta}}_{i0} \cdot \mathbf{a} \\ + \psi^t(k_0, \mathbf{r}_{n+1}) \cdot \overline{\mathbf{T}}_{n+1(n+1)} \cdot \overline{\boldsymbol{\beta}}_{n+1,0} \cdot \mathbf{a}.\end{aligned} \tag{2.3.64}$$

The first and last terms on the right-hand side of (2.3.64) can be viewed as the total incident field impinging upon the previous n scatterers. Remember that $\overline{\mathbf{T}}_{i(n)}$ relates the scattered field from scatterer i to the total incident field expressed in terms of the local coordinate system of the i-th scatterer. Therefore, the scattered field from scatterer i in the $(n+1)$-scatterer problem can be related to $\overline{\mathbf{T}}_{i(n)}$, the solution of the n-scatterer problem, by

$$\overline{\mathbf{T}}_{i(n+1)} \cdot \overline{\boldsymbol{\beta}}_{i0} = \overline{\mathbf{T}}_{i(n)} \cdot [\overline{\boldsymbol{\beta}}_{i0} + \overline{\boldsymbol{\alpha}}_{i,n+1} \cdot \overline{\mathbf{T}}_{n+1(n+1)} \cdot \overline{\boldsymbol{\beta}}_{n+1,0}], \quad i = 1, 2, \ldots, n. \tag{2.3.65}$$

From (2.3.57), we have

$$\overline{\mathbf{T}}_{n+1(n+1)} \cdot \overline{\boldsymbol{\beta}}_{n+1,0} \cdot \mathbf{a} = \overline{\mathbf{T}}_{n+1(1)} \cdot \left[\overline{\boldsymbol{\beta}}_{n+1,0} + \sum_{i=1}^{n} \overline{\boldsymbol{\alpha}}_{n+1,i} \cdot \overline{\mathbf{T}}_{i(n+1)} \cdot \overline{\boldsymbol{\beta}}_{i0} \right] \cdot \mathbf{a}. \tag{2.3.66}$$

Solving (2.3.65) and (2.3.66) for the $\overline{\mathbf{T}}_{n+1(n+1)} \cdot \overline{\boldsymbol{\beta}}_{n+1,0}$, we have

$$\begin{aligned}\overline{\mathbf{T}}_{n+1(n+1)} \cdot \overline{\boldsymbol{\beta}}_{n+1,0} = \left[\overline{\mathbf{I}} - \overline{\mathbf{T}}_{n+1(1)} \cdot \sum_{i=1}^{n} \overline{\boldsymbol{\alpha}}_{n+1,i} \cdot \overline{\mathbf{T}}_{i(n)} \cdot \overline{\boldsymbol{\alpha}}_{i,n+1} \right]^{-1} \\ \cdot \overline{\mathbf{T}}_{n+1(1)} \cdot \left[\overline{\boldsymbol{\beta}}_{n+1,0} + \sum_{i=1}^{n} \overline{\boldsymbol{\alpha}}_{n+1,i} \cdot \overline{\mathbf{T}}_{i(n)} \cdot \overline{\boldsymbol{\beta}}_{i0} \right].\end{aligned} \tag{2.3.67}$$

From (2.3.65), we have

$$\overline{\mathbf{T}}_{i(n+1)} \cdot \overline{\boldsymbol{\beta}}_{i0} = \overline{\mathbf{T}}_{i(n)} \cdot [\overline{\boldsymbol{\beta}}_{i0} + \overline{\boldsymbol{\alpha}}_{i,n+1} \cdot \overline{\mathbf{T}}_{n+1(n+1)} \cdot \overline{\boldsymbol{\beta}}_{n+1,0}],$$

$$i = 1, 2, \ldots, n. \quad (2.3.68)$$

From (2.3.67) and (2.3.68), we obtain

$$\overline{\mathbf{T}}_{n+1(n+1)} = \left[\overline{\mathbf{I}} - \overline{\mathbf{T}}_{n+1(1)} \cdot \sum_{i=1}^{n} \overline{\boldsymbol{\alpha}}_{n+1,i} \cdot \overline{\mathbf{T}}_{i(n)} \cdot \overline{\boldsymbol{\alpha}}_{i,n+1}\right]^{-1}$$

$$\cdot \overline{\mathbf{T}}_{n+1(1)} \cdot \left[\overline{\mathbf{I}} + \sum_{i=1}^{n} \overline{\boldsymbol{\alpha}}_{n+1,i} \cdot \overline{\mathbf{T}}_{i(n)} \cdot \overline{\boldsymbol{\beta}}_{i,n+1}\right]. \quad (2.3.69)$$

$$\overline{\mathbf{T}}_{i(n+1)} = \overline{\mathbf{T}}_{i(n)} \cdot [\overline{\mathbf{I}} + \overline{\boldsymbol{\alpha}}_{i,n+1} \cdot \overline{\mathbf{T}}_{n+1(n+1)} \cdot \overline{\boldsymbol{\beta}}_{n+1,i}],$$

$$i = 1, 2, \ldots, n. \quad (2.3.70)$$

In the above, the relations $\overline{\boldsymbol{\beta}}_{i0}^{-1} = \overline{\boldsymbol{\beta}}_{0i}$ and $\overline{\boldsymbol{\beta}}_{i0} \cdot \overline{\boldsymbol{\beta}}_{0j} = \overline{\boldsymbol{\beta}}_{ij}$ have been applied. Equations (2.3.69) and (2.3.70), or (2.3.67) and (2.3.68), together comprise the recursive relations from which the $\overline{\mathbf{T}}_{i(n+1)}$ matrices, $i = 1, 2, \ldots, n+1$, can be found given the $\overline{\mathbf{T}}_{i(n)}$ matrices, $i = 1, 2, \ldots, n$.

Next, we shall investigate the domain of validity of (2.3.69) and (2.3.70). We shall start our discussion with Equations (2.3.65) and (2.3.66) to determine the conditions under which (2.3.65) and (2.3.66) hold. First, we shall look at the conditions under which Equation (2.3.65) is held. Equation (2.3.65) is

$$\overline{\mathbf{T}}_{i(n+1)} \cdot \overline{\boldsymbol{\beta}}_{i0} = \overline{\mathbf{T}}_{i(n)} \cdot [\overline{\boldsymbol{\beta}}_{i0} + \overline{\boldsymbol{\alpha}}_{i,n+1} \cdot \overline{\mathbf{T}}_{n+1(n+1)} \cdot \overline{\boldsymbol{\beta}}_{n+1,0}]. \quad (2.3.71)$$

In order to determine the constraint conditions of the above equation, we need to write $\overline{\mathbf{T}}_{i(n)}$ explicitly by applying Equation (2.3.70) with the subscript n being replaced by $n-1$. Notice that this step is only suitable for

$i = 1, 2, \ldots, n-1$. Then, we obtain

$$\overline{\mathbf{T}}_{i(n+1)} \cdot \overline{\boldsymbol{\beta}}_{i0} = \overline{\mathbf{T}}_{i(n-1)} \cdot [\overline{\mathbf{I}} + \underbrace{\overline{\boldsymbol{\alpha}}_{i,n} \cdot \overline{\mathbf{T}}_{n(n)} \cdot \overline{\boldsymbol{\beta}}_{n,i}}_{\text{(I)}}]$$

$$[\overline{\boldsymbol{\beta}}_{i0} + \underbrace{\overline{\boldsymbol{\alpha}}_{i,n+1} \cdot \overline{\mathbf{T}}_{n+1(n+1)} \cdot \overline{\boldsymbol{\beta}}_{n+1,i}}_{\text{(II)}}]. \quad (2.3.72)$$

In the above equation, there are no constraints for all other terms except for the term from the product of (I) and (II), which is

$$\text{(I)} \cdot \text{(II)} = \overline{\boldsymbol{\alpha}}_{i,n} \cdot \overline{\mathbf{T}}_{n(n)} \cdot \overline{\boldsymbol{\beta}}_{n,i} \cdot \overline{\boldsymbol{\alpha}}_{i,n+1} \cdot \overline{\mathbf{T}}_{n+1(n+1)} \cdot \overline{\boldsymbol{\beta}}_{n+1,0}. \quad (2.3.73)$$

In order to find the constraint condition for (2.3.73), we need to examine (2.3.73) term by term from right to left. The first two entries $\overline{\mathbf{T}}_{n+1(n+1)} \cdot \overline{\boldsymbol{\beta}}_{n+1,0}$ represent the scattered field, the outgoing harmonics expressed in the local coordinate system of the scatterer $n+1$. The third entry $\overline{\boldsymbol{\alpha}}_{i,n+1}$ translates the expression of the above scattered field from the outgoing harmonics expressed in the local coordinate system of the $(n+1)$-th scatterer into the standing harmonics expressed in the local coordinate system of scatterer i. This translation is valid only for the field inside $C_{i,n+1}$. The fourth entry $\overline{\boldsymbol{\beta}}_{n,i}$ translates the above standing harmonics from the local coordinate system of the i-th scatterer into the local coordinate system of the n-th scatterer. From the constraint condition of $\overline{\boldsymbol{\alpha}}_{i,n+1}$, scatterer n has to be inside $C_{i,n+1}$. This is equivalent to saying that (2.3.73) is valid only when the scatterer $n+1$ is outside of $C_{i,n}$. This condition can be expressed mathematically as

$$\mathbf{r}_{n+1,0} \notin C_{i,n}. \quad (2.3.74)$$

Since (2.3.73) and (2.3.71) have the same constraint condition, (2.3.74) is also the constraint condition for (2.3.71). Moreover, the subscript i in Equation

(2.3.65) goes from 1 to n. But the step from (2.3.71) to (2.3.72) is only valid for $i = 1, 2, \ldots, n-1$. Therefore, (2.3.74) should hold for $i = 1, 2, \ldots, n-1$. Thus, the constraint condition for (66) with $i = 1, 2, \ldots, n-1$, becomes

$$\mathbf{r}_{n+1,0} \notin \bigcup_{i=1}^{n-1} C_{i,n-1}. \tag{2.3.75}$$

For $i = n$, (2.3.71) becomes

$$\overline{\mathbf{T}}_{n(n+1)} \cdot \overline{\boldsymbol{\beta}}_{n,0} = \overline{\mathbf{T}}_{n(n)} \cdot [\overline{\boldsymbol{\beta}}_{n,0} + \overline{\boldsymbol{\alpha}}_{n,n+1} \cdot \overline{\mathbf{T}}_{n+1(n+1)} \cdot \overline{\boldsymbol{\beta}}_{n+1,0}]. \tag{2.3.76}$$

Similarly, we shall write the $\overline{\mathbf{T}}_{n(n)}$ explicitly by applying Equation (2.3.69) with all the subscripts n being replaced by $n-1$. Then, we obtain

$$\overline{\mathbf{T}}_{n(n+1)} \cdot \overline{\boldsymbol{\beta}}_{n,0} = \left[\bar{\mathbf{I}} - \overline{\mathbf{T}}_{n(1)} \cdot \sum_{i=1}^{n-1} \overline{\boldsymbol{\alpha}}_{n,i} \cdot \overline{\mathbf{T}}_{i(n-1)} \cdot \overline{\boldsymbol{\alpha}}_{i,n}\right]^{-1}$$

$$\cdot \overline{\mathbf{T}}_{n(1)} \cdot [\bar{\mathbf{I}} + \underbrace{\sum_{i=1}^{n-1} \overline{\boldsymbol{\alpha}}_{n,i} \cdot \overline{\mathbf{T}}_{i(n-1)} \cdot \overline{\boldsymbol{\beta}}_{i,n}]}_{\text{(IV)}} \cdot [\overline{\boldsymbol{\beta}}_{n,0} + \underbrace{\overline{\boldsymbol{\alpha}}_{n,n+1} \cdot \overline{\mathbf{T}}_{n+1(n+1)} \cdot \overline{\boldsymbol{\beta}}_{n+1,0}}_{\text{(V)}}].$$

(2.3.77)

From the analysis following Equation (2.3.72), we see that the constraint condition comes from the terms which involve the product of $\overline{\boldsymbol{\beta}}$ and $\overline{\boldsymbol{\alpha}}$. In Equation (2.3.77), the only terms containing these products come from the product of (IV) and (V), which is

$$(\mathbf{IV}) \cdot (\mathbf{V}) = \sum_{i=1}^{n-1} \overline{\boldsymbol{\alpha}}_{n,i} \cdot \overline{\mathbf{T}}_{i(n-1)} \cdot \overline{\boldsymbol{\beta}}_{i,n} \cdot \overline{\boldsymbol{\alpha}}_{n,n+1} \cdot \overline{\mathbf{T}}_{n+1(n+1)} \cdot \overline{\boldsymbol{\beta}}_{n+1,0}. \tag{2.3.78}$$

Equation (2.3.78) is an eligible expression only if $\overline{\beta}_{i,n} \cdot \overline{\alpha}_{n,n+1}$, for all $i = 1, 2, \ldots, n-1$, holds. Following the argument from (2.3.72) to (2.3.75), scatterer $n+1$ has to be outside of all $C_{n,i}$, $i = 1, 2, \ldots, n-1$. This condition can be expressed as

$$\mathbf{r}_{n+1,0} \notin \bigcup_{i=1}^{n-1} C_{n,i}. \tag{2.3.79}$$

Equations (2.3.75) and (2.3.79) comprise the constraint condition for the validity of Equation (2.3.65). Meanwhile, Equation (2.3.66) is always true if scatterer $n+1$ is outside of the previous n scatterers. Since the recursive relations (2.3.69) and (2.3.70) are derived from (2.3.65) and (2.3.66), they share the same constraint conditions. Combining (2.3.75) and (2.3.79), the constraint condition for the validity of the recursive relations (2.3.69) and (2.3.70) finally becomes

$$\mathbf{r}_{n+1,0} \notin (\bigcup_{i=1}^{n-1} C_{i,n}) \bigcup (\bigcup_{i=1}^{n-1} C_{n,i}). \tag{2.3.80}$$

The above is equivalent to

$$d_{n+1,n} > \max(d_{i,n}, i = 1, 2, \ldots, n-1), \tag{2.3.81}$$

and

$$d_{i,n+1} > d_{i,n}, \qquad i = 1, 2, \ldots, n-1. \tag{2.3.82}$$

Equations (2.3.81) and (2.3.82) need to hold for each recursive step from 2 to N. Therefore, at the n-th step, all $C_{i,j}$, $i, j = 1, 2, \ldots, n-1$, will be contained in $(\cup_{i=1}^{n-1} C_{n,i}) \bigcup (\cup_{i=1}^{n-1} C_{i,n})$. Thus, the condition (2.3.81) is equivalent to

$$\mathbf{r}_{n+1,0} \notin \bigcup_{i,j=1}^{n} C_{i,j}. \tag{2.3.83}$$

Equation (2.3.83) is a very strong constraint condition for the application of the recursive relations (2.3.69) and (2.3.70). Moreover, the locations of the scatterers for any specific problem are predetermined. For most of the problems, condition (2.3.83) is too strong to be satisfied. Therefore, it is difficult to apply the recursive relations (2.3.69) and (2.3.70) to most of the general multiple scattering problems. Fortunately, the constraint condition (2.3.62) for the recursive relations (2.3.59) and (2.3.60) is easily satisfied for most application problems. The only case for which condition (2.3.62) may be violated is when there are more than two scatterers located at the same circle centered at the origin of the global coordinate system. In this case, we may move some of the scatterers, which are located on the same circle, a small distance δ to satisfy (2.3.62). If δ is much smaller than the typical dimension of the scatterers, for example, 10^{-6} of the radius of the smallest scatterer in the problem, the error contributed by these shifts will be proportional to δ. Therefore, if we choose δ much smaller than the required accuracy of the problem, these shifts actually do not affect the accuracy of the solution. Thus, from a practical point of view, condition (2.3.62) can always be satisfied by reordering and shifting the scatterers without sacrificing the accuracy of the solution. Consequently, the recursive relations (2.3.59) and (2.3.60) are legitimate recursive relations for the solution of the multiple scattering problem.

From now on, we shall concentrate on the recursive relations (2.3.59) and (2.3.60) because their constraint condition (2.3.62) can be easily satisfied in the solution of the multiple scattering problem. Theoretically, the recursive relations (2.3.59) and (2.3.60) give an exact solution of the scattering problem if the dimensions of the matrices in (2.3.59) and (2.3.60) are infinite. In order to implement the algorithm numerically, the matrices have to be truncated

to finite dimensions. For an N-scatterer problem, if the field around each scatterer is approximated by M harmonics, the total number of unknowns of the problem will be NM. In this case, $\overline{\mathbf{T}}_{i(n)} \cdot \overline{\boldsymbol{\beta}}_{i0} \cdot \mathbf{a}$ in (2.3.61) is an M element column vector. When the subobjects are much smaller than the wavelength, M could be kept small. However, the number of terms in the translation formulas should be large enough to maintain their accuracy. In other words, $\overline{\mathbf{T}}_{i(n)} \cdot \overline{\boldsymbol{\beta}}_{i0}$ need not be square—it should be $M \times P$ where P is large enough to keep the translation accurate.

For the convenience of discussion of the computational complexity of the algorithm, let us rewrite (2.3.59) and (2.3.60) with the dimension indices included

$$\overbrace{\overline{\mathbf{T}}_{n+1(n+1)} \cdot \overline{\boldsymbol{\beta}}_{n+1,0}}^{M\times P} = [\bar{\mathbf{I}} - \overbrace{\overline{\mathbf{T}}_{n+1(1)}}^{M\times M} \cdot \sum_{i=1}^{n} \overbrace{\overline{\boldsymbol{\alpha}}_{n+1,i}}^{M\times M} \cdot \overbrace{\overline{\mathbf{T}}_{i(n)} \cdot \overline{\boldsymbol{\beta}}_{i0}}^{M\times P} \cdot \overbrace{\overline{\boldsymbol{\alpha}}_{0,n+1}}^{P\times M}]^{-1}$$

$$\cdot \underbrace{\overline{\mathbf{T}}_{n+1(1)}}_{M\times M} \cdot [\underbrace{\overline{\boldsymbol{\beta}}_{n+1,0}}_{M\times P} + \sum_{i=1}^{n} \underbrace{\overline{\boldsymbol{\alpha}}_{n+1,i}}_{M\times M} \cdot \underbrace{\overline{\mathbf{T}}_{i(n)} \cdot \overline{\boldsymbol{\beta}}_{i0}}_{M\times P}], \quad (2.3.84)$$

$$\underbrace{\overline{\mathbf{T}}_{i(n+1)} \cdot \overline{\boldsymbol{\beta}}_{i0}}_{M\times P} = \underbrace{\overline{\mathbf{T}}_{i(n)} \cdot \overline{\boldsymbol{\beta}}_{i0}}_{M\times P} + (\underbrace{\overline{\mathbf{T}}_{i(n)} \cdot \overline{\boldsymbol{\beta}}_{i0}}_{M\times P} \cdot \underbrace{\overline{\boldsymbol{\alpha}}_{0,n+1}}_{P\times M}) \cdot \underbrace{\overline{\mathbf{T}}_{n+1(n+1)} \cdot \overline{\boldsymbol{\beta}}_{n+1,0}}_{M\times P}. \quad (2.3.85)$$

In the above $\overline{\mathbf{T}}_{i(n+1)} \cdot \overline{\boldsymbol{\beta}}_{i0}$ is the unknown function to be solved recursively. It is an $M \times P$ matrix. The dimensions of the matrices are indicated above. The number of floating-point operations required to multiply an $M \times P$ matrix with a $P \times M$ matrix, or an $M \times M$ matrix with an $M \times P$ matrix, is equal to M^2P. Assuming $M \ll P$, the other matrix multiplications and inversions are subdominant. Therefore, at each recursion, the number of floating-point operations is $O(nM^2P)$. Consequently, after applying the recursion relations to N scatterers, the number of floating-point operations is $O(N^2M^2P)$.

A study of the translation formula shows that for accurate results, $P > kd$, where d is the distance of translation. In the long wavelength limit, this is easily met. Hence, the algorithm scales as N^2 for static and quasi-static problems.

As the object becomes larger compared to the wavelength, or the wavelength becomes shorter for wave scattering problems, P is proportional to the radius of the object. In two dimensions, the radius of the object is proportional to $\sqrt{N}$, while in three dimensions, it is proportional to $N^{1/3}$. Hence, this algorithm scales as $N^{5/2}$, in two dimensions, and as $N^{7/3}$ in three dimensions.

The N scatterer problem is also expressible as an NM unknown problem by solving NM linear algebraic equations. However, this would require $O(N^3M^3)$ floating-point operations if these NM linear algebraic equations were solved with Gauss' elimination. If the conjugate gradient method is used here, the $O(N^2M^2)$ algorithm is possible, but the conjugate gradient method solves the matrix equation $\overline{\mathbf{A}}\cdot\mathbf{x} = \mathbf{b}$ with a fixed right-hand side. It has to be redone if the right-hand side of the equation changes. Hence, if the incident angle of the wave changes, the equation has to be solved again. However, the above algorithm is independent of the incident angle of the incident wave.

2.4 N Recursive Algorithm

In the last section, an N^2 algorithm has been developed by using a recursive operator algorithm. In that algorithm, at the n-th recursion, since the interactions between the $(n+1)$-th scatterer and the previous n scatterers have to be taken into account, the computational labor is proportional to $O(n)$ for each recursion. Consequently, after N recursions, the number of

floating-point operations is $O(N^2)$. (At this point, in order to simplify the analysis, the floating-point operations involved in matrix operations at each recursion have not been taken into account.) From the above, it is clear that in order to make an algorithm linear in N, the floating-point operations in each recursion have to be independent of the number of the scatterers such that after N recursions, it will yield an $O(N)$ algorithm.

2.4.1 Recursive formulas

In order to make the floating-point operations at each recursion independent of the number of the scatterers involved, we need to find a way to remove the summations in the recursive relation (2.3.84). Actually, the two summations in (2.3.84) are the same, because $\overline{\alpha}_{0,n+1}$ in the first term involving the summation in (2.3.84) can be taken out of the summation. The physical interpretation of $\sum_{i=1}^{n} \overline{\alpha}_{n+1,i} \cdot \overline{\mathbf{T}}_{i(n)} \cdot \overline{\beta}_{i,n+1}$ is that the outgoing harmonics expressed in the local coordinate systems of the corresponding scatterers, from scatterers i, $i = 1, 2, \ldots, n$, have been translated to the standing harmonics in the local coordinate system of scatterer $n+1$. Since these translations are relative between i, for $i = 1, 2, \ldots, n$, and $n+1$, they have to be repeated in every recursion step.

Since the scatterers of the problem have been ordered according to Equation (2.3.62), the following identity is always valid

$$\overline{\alpha}_{n+1,i} = \overline{\alpha}_{n+1,0} \cdot \overline{\beta}_{0,i}, \qquad \text{for all } i < n+1. \tag{2.4.1}$$

On substituting (2.4.1) into (2.3.84) and removing $\overline{\alpha}_{n+1,0}$ from the summa-

tions, we obtain

$$\overline{\mathbf{T}}_{n+1(n+1)} \cdot \overline{\boldsymbol{\beta}}_{n+1,0} = [\overline{\mathbf{I}} - \overline{\mathbf{T}}_{n+1(1)} \cdot \overline{\boldsymbol{\alpha}}_{n+1,0} \cdot \sum_{i=1}^{n} \overline{\boldsymbol{\beta}}_{0i} \cdot \overline{\mathbf{T}}_{i(n)} \cdot \overline{\boldsymbol{\beta}}_{i0} \cdot \overline{\boldsymbol{\alpha}}_{0,n+1}]^{-1}$$

$$\cdot \overline{\mathbf{T}}_{n+1(1)} \cdot [\overline{\boldsymbol{\beta}}_{n+1,0} + \overline{\boldsymbol{\alpha}}_{n+1,0} \cdot \sum_{i=1}^{n} \overline{\boldsymbol{\beta}}_{0i} \cdot \overline{\mathbf{T}}_{i(n)} \cdot \overline{\boldsymbol{\beta}}_{i0}]. \quad (2.4.2)$$

Now, we define an aggregate transition matrix $\overline{\boldsymbol{\tau}}$ as

$$\overline{\boldsymbol{\tau}}_{(n)} = \sum_{i=1}^{n} \overline{\boldsymbol{\beta}}_{0i} \cdot \overline{\mathbf{T}}_{i(n)} \cdot \overline{\boldsymbol{\beta}}_{i0}. \quad (2.4.3)$$

On substituting Equation (2.4.3) into Equation (2.4.2), we have

$$\overbrace{\overline{\mathbf{T}}_{n+1(n+1)} \cdot \overline{\boldsymbol{\beta}}_{n+1,0}}^{M\times P} = [\overbrace{\overline{\mathbf{I}}}^{M\times M} - \overbrace{\overline{\mathbf{T}}_{n+1(1)}}^{M\times M} \cdot \overbrace{\overline{\boldsymbol{\alpha}}_{n+1,0}}^{M\times P} \cdot \overbrace{\overline{\boldsymbol{\tau}}_{(n)}}^{P\times P} \cdot \overbrace{\overline{\boldsymbol{\alpha}}_{0,n+1}}^{P\times M}]^{-1}$$

$$\cdot \underbrace{\overline{\mathbf{T}}_{n+1(1)}}_{M\times M} \cdot [\underbrace{\overline{\boldsymbol{\beta}}_{n+1,0}}_{M\times P} + \underbrace{\overline{\boldsymbol{\alpha}}_{n+1,0}}_{M\times P} \cdot \underbrace{\overline{\boldsymbol{\tau}}_{(n)}}_{P\times P}]. \quad (2.4.4)$$

Multiplying Equation (2.3.85) from the left by $\overline{\boldsymbol{\beta}}_{0i}$, summing over i from 1 to n, and adding $\overline{\boldsymbol{\beta}}_{0,n+1} \cdot \overline{\mathbf{T}}_{n+1(n+1)} \cdot \overline{\boldsymbol{\beta}}_{n+1,0}$ to the both sides of the equation, we finally obtain

$$\overbrace{\overline{\boldsymbol{\tau}}_{(n+1)}}^{P\times P} = \overbrace{\overline{\boldsymbol{\tau}}_{(n)}}^{P\times P} + \overbrace{\overline{\boldsymbol{\beta}}_{0,n+1}}^{P\times M} \cdot \overbrace{\overline{\mathbf{T}}_{n+1(n+1)} \cdot \overline{\boldsymbol{\beta}}_{n+1,0}}^{M\times P} + \overbrace{\overline{\boldsymbol{\tau}}_{(n)}}^{P\times P} \cdot \overbrace{\overline{\boldsymbol{\alpha}}_{0,n+1}}^{P\times M} \cdot \overbrace{\overline{\mathbf{T}}_{n+1(n+1)} \cdot \overline{\boldsymbol{\beta}}_{n+1,0}}^{M\times P}. \quad (2.4.5)$$

Equations (2.4.4) and (2.4.5) together constitute the recursive formulas for $\overline{\boldsymbol{\tau}}$. Obviously, the number of matrix multiplications in the recursive equations (2.4.4) and (2.4.5) is independent of n, the recursive ordinal. Therefore, the total floating-point operations after N recursions will be linear in N if P

and M are fixed. With the aggregate $\overline{\tau}$-matrix expression, Equation (2.3.61) becomes

$$\phi(\mathbf{r}) = \Re g\psi^t(k_0, \mathbf{r}_0) \cdot \mathbf{a} + \psi^t(k_0, \mathbf{r}_0) \cdot \overline{\tau}_{(N)} \cdot \mathbf{a}. \tag{2.4.6}$$

The aggregate $\overline{\tau}$ matrix defined in Equation (2.4.3) is a global representation of the $\overline{\mathbf{T}}$ (transition) matrices by translating every $\overline{\mathbf{T}}_{i(n)}$-matrix from its own local coordinate system related to the i-th scatterer to the origin of a global coordinate system. Hence, Equation (2.4.4) actually is an equation for a two-body scattering problem: one scatterer is an assembly of the previous n scatterers characterized by the n-th aggregate $\overline{\tau}_{(n)}$-matrix located at the origin of the global coordinate system, the other is the $(n+1)$-th scatterer characterized by an isolated single $\overline{\mathbf{T}}_{n+1(1)}$ matrix located at $\mathbf{r}_{n+1(0)}$. This will become more obvious when we compare Equation (2.4.4) with Equation (2.3.84). Let n equal 1 in Equation (2.3.84) and suppose that scatterer 1 is located at the origin of the global coordinate system, then, two equations will be exactly the same if we replace $\overline{\tau}_{(n)}$ in Equation (2.4.4) with $\overline{\mathbf{T}}_{1(1)}$.

Because Equation (2.4.4) always involves a two-body scattering problem at each recursion, the number of matrix multiplications will be a constant, which is independent of the ordinal number of the recursion. In Equation (2.4.4), indices P and M represent the number of harmonics in the translation formulas and the number of harmonics in the isolated scatterer $\overline{\mathbf{T}}$ matrix of the subobject, respectively. In Equations (2.4.4) and (2.4.5), matrix operations include matrix multiplication of an $M \times P$ matrix and a $P \times P$ matrix, or a $P \times P$ matrix and a $P \times M$ matrix, matrix multiplication of a $P \times M$ matrix and an $M \times P$ matrix, and matrix inversion of an $M \times M$ matrix, etc. The number of floating-point operations required for a matrix multiplication of a $P \times P$ matrix and a $P \times M$ matrix, or an $M \times P$ matrix and

a $P \times P$ matrix is equal to MP^2. Under the assumption of $M \ll P$, this matrix operation will be dominant compared to the other matrix operations in Equations (2.4.4) and (2.4.5). Therefore, at each recursion, the number of floating-point operations is proportional to MP^2. Finally, after applying the recursion relations to N scatterers, the number of floating-point operations is $O(NMP^2)$.

As we mentioned in the last section, to achieve the required accuracy in the translation formulas, P, the number of the harmonics used in the translation formulas, should satisfy the relation of $P > kd$, where d is the distance of translation. In the low frequency limit, this could be easily met by choosing a fixed P, because the dimension of the object is always less than the wavelength. Therefore, the computational complexity will be linear in N for static and quasi-static problems.

When the scatterer becomes larger compared to the wavelength, P will be proportional to the radius of the object, and N, the number of subobjects, is proportional to the square of the radius of the object in two dimensions, or the cube of the radius of the object in three dimensions. Therefore, when the wavelength becomes shorter, P will be proportional to $N^{1/2}$ in two dimensions, and $N^{1/3}$ in three dimensions. Finally, the computational complexity of the algorithm will scale as N^2 in two dimensions and as $N^{5/3}$ in three dimensions.

2.4.2 Field inside the scatterers

The field expression (2.4.6) is only valid outside of a big circle which closely embraces all of the subobjects. Therefore, the field inside the object cannot be directly obtained by using the aggregate $\overline{\tau}$ matrix expression of

the field. In order to calculate the field inside the object, the $\overline{\mathbf{T}}_{i(N)}$ matrices, $i = 1, ..., N$, have to be found. This could be achieved by a backward recursion scheme. From the recursive relations (2.4.4) and (2.4.5), we already have the $\overline{\mathbf{T}}_{i(i)} \cdot \overline{\boldsymbol{\beta}}_{i0}$ matrices for $i = 1, 2, ..., N$. From Equation (2.3.62), for any $i < j$, the i-th scatterer is inside of $C_{0,j}$. Now, to find the $T_{N-1(N)}$ matrix, we consider an $(N-1)$-scatterer problem with a composite incident field which consists of the original incident field and the field scattered from scatterer N represented by $\overline{\mathbf{T}}_{N(N)} \cdot \overline{\boldsymbol{\beta}}_{N,0}$ which is known. With $\overline{\mathbf{T}}_{N-1(N-1)} \cdot \overline{\boldsymbol{\beta}}_{N-1,0}$ on hand, the $\overline{\mathbf{T}}_{N-1(N)} \cdot \overline{\boldsymbol{\beta}}_{N-1,0}$ can be directly obtained from

$$\overline{\mathbf{T}}_{N-1(N)} \cdot \overline{\boldsymbol{\beta}}_{N-1,0} = \overline{\mathbf{T}}_{N-1(N-1)} \cdot \overline{\boldsymbol{\beta}}_{N-1,0} \cdot [\overline{\mathbf{I}} + \overline{\boldsymbol{\alpha}}_{0,N} \cdot \overline{\mathbf{T}}_{N(N)} \cdot \overline{\boldsymbol{\beta}}_{N,0}]. \quad (2.4.7)$$

Similarly, for $(N-2)$-th scatterer, we have

$$\overline{\mathbf{T}}_{N-2(N)} \cdot \overline{\boldsymbol{\beta}}_{N-2,0} = \overline{\mathbf{T}}_{N-2(N-2)} \cdot \overline{\boldsymbol{\beta}}_{N-2,0} \cdot [\overline{\mathbf{I}} + \overline{\boldsymbol{\alpha}}_{0,N} \cdot \overline{\mathbf{T}}_{N(N)} \cdot \overline{\boldsymbol{\beta}}_{N,0} + \overline{\boldsymbol{\alpha}}_{0,N-1} \cdot \overline{\mathbf{T}}_{N-1(N)} \cdot \overline{\boldsymbol{\beta}}_{N-1,0}]. \quad (2.4.8)$$

Generally, knowing $\overline{\mathbf{T}}_{N(N)} \cdot \overline{\boldsymbol{\beta}}_{N,0}$, $\overline{\mathbf{T}}_{N-1(N)} \cdot \overline{\boldsymbol{\beta}}_{N-1,0}$, ..., $\overline{\mathbf{T}}_{N-i+1(N)} \cdot \overline{\boldsymbol{\beta}}_{N-i+1,0}$, and $\overline{\mathbf{T}}_{i(i)} \cdot \overline{\boldsymbol{\beta}}_{i0}$, the recursive equation for $\overline{\mathbf{T}}_{N-i(N)} \cdot \overline{\boldsymbol{\beta}}_{N-i,0}$ matrix is

$$\overline{\mathbf{T}}_{N-i(N)} \cdot \overline{\boldsymbol{\beta}}_{N-i,0} = \overline{\mathbf{T}}_{N-i(N-i)} \cdot \overline{\boldsymbol{\beta}}_{N-i,0} \cdot [\overline{\mathbf{I}} + \sum_{j=0}^{i-1} \overline{\boldsymbol{\alpha}}_{0,N-j} \cdot \overline{\mathbf{T}}_{N-j(N)} \cdot \overline{\boldsymbol{\beta}}_{N-j,0}]. \quad (2.4.9)$$

We define a complementary partial N-th aggregate $\widetilde{\overline{\boldsymbol{\tau}}}_{i(N)}$ as

$$\widetilde{\overline{\boldsymbol{\tau}}}_{i(N)} = \sum_{j=0}^{i-1} \overline{\boldsymbol{\alpha}}_{0,N-j} \cdot \overline{\mathbf{T}}_{N-j(N)} \cdot \overline{\boldsymbol{\beta}}_{N-i,0}. \quad (2.4.10)$$

Using (2.4.10) in (2.4.9), we have

$$\overline{\mathbf{T}}_{N-i(N)} \cdot \overline{\boldsymbol{\beta}}_{N-i,0} = \overline{\mathbf{T}}_{N-i(N-i)} \cdot \overline{\boldsymbol{\beta}}_{N-i,0} \cdot [\overline{\mathbf{I}} + \widetilde{\overline{\boldsymbol{\tau}}}_{i(N)}]. \quad (2.4.11)$$

From (2.4.10), the next complementary partial aggregate matrix $\widetilde{\overline{\tau}}$ can be obtained from

$$\widetilde{\overline{\tau}}_{i+1(N)} = \widetilde{\overline{\tau}}_{i(N)} + \overline{\alpha}_{0,N-i} \cdot \overline{\mathbf{T}}_{N-i(N)} \cdot \overline{\beta}_{N-i,0}. \tag{2.4.12}$$

Equations (2.4.11) and (2.4.12) constitute the backward recursive relation for $\overline{\mathbf{T}}_{N-i(N)} \cdot \overline{\beta}_{N-i,0}, i = 1, 2, ..., N-1$. The computational complexity of the backward recursive scheme of (2.4.11) and (2.4.12) is the same as that of the forward recursive scheme of (2.4.4) and (2.4.5).

Once $\overline{\mathbf{T}}_{j(N)}$ for scatterer j is known, the field internal to scatterer j is readily calculated by matching the boundary condition at the scatterer's surface. For example, if $\overline{\mathbf{T}}_{i(N)}$ for $i = 1, \cdots, N$, are known, then the field exterior to the scatterer can be written as

$$\phi(\mathbf{r}) = \Re g\psi^t(k_0, \mathbf{r}_0) \cdot \mathbf{a} + \sum_{i=1}^{N} \psi^t(k_0, \mathbf{r}_i) \cdot \overline{\mathbf{T}}_{i(N)} \cdot \overline{\beta}_{i0} \cdot \mathbf{a}. \tag{2.4.13}$$

If the internal field interior to the j-th scatterer is of interest, the fields of the other scatterers can be expressed in terms of the j-th coordinate system as

$$\phi(\mathbf{r}) = \Re g\psi^t(k_0, \mathbf{r}_j)\overline{\beta}_{j0} \cdot \mathbf{a} + \sum_{i \neq j} \Re g\psi^t(k_0, \mathbf{r}_j) \cdot \overline{\alpha}_{ji} \cdot \overline{\mathbf{T}}_{i(N)} \cdot \overline{\beta}_{i0} \cdot \mathbf{a} + \psi^t(k_0, \mathbf{r}_j) \cdot \overline{\mathbf{T}}_{j(N)} \cdot \overline{\beta}_{j0} \cdot \mathbf{a}. \tag{2.4.14}$$

The first two terms on the right-hand side of (2.4.14) can be treated as the total incident field impinging upon scatterer j. Therefore, the scattered amplitude $\overline{\mathbf{T}}_{j(N)} \cdot \overline{\beta}_{j0}$ could be related to the isolated transition matrix of the scatterer j, $\overline{\mathbf{T}}_{j(1)}$, and the total incident field as

$$\overline{\mathbf{T}}_{j(1)} \cdot \left[\overline{\beta}_{j0} + \sum_{i \neq j} \overline{\alpha}_{ji} \cdot \overline{\mathbf{T}}_{i(N)} \cdot \overline{\beta}_{i0} \right] \cdot \mathbf{a} = \overline{\mathbf{T}}_{j(N)} \cdot \overline{\beta}_{j0} \cdot \mathbf{a}, \tag{2.4.15a}$$

or

$$\left[\overline{\beta}_{j0}+\sum_{i\neq j}\overline{\alpha}_{ji}\cdot\overline{\mathbf{T}}_{i(N)}\cdot\overline{\beta}_{i0}\right]\cdot\mathbf{a}=\overline{\mathbf{T}}_{j(1)}^{-1}\cdot\overline{\mathbf{T}}_{j(N)}\cdot\overline{\beta}_{j0}\cdot\mathbf{a}. \qquad (2.4.15b)$$

The left-hand side of (2.4.15b) is the total incident-field amplitude on scatterer j, but the right-hand side of (2.4.15b) provides an exceedingly simple way to calculate this total incident-field amplitude. Once the total incident-field amplitude on the j-th scatterer is found, the internal field of scatterer j can be found using the isolated transmission matrix $\overline{\overline{\mathbf{W}}}_{j(1)}$ as

$$\phi(\mathbf{r})=\Re g\psi^{t}(k_j,\mathbf{r}_j)\cdot\overline{\overline{\mathbf{W}}}_{j(1)}\cdot\overline{\mathbf{T}}_{j(1)}^{-1}\cdot\overline{\mathbf{T}}_{j(N)}\cdot\overline{\beta}_{j0}\cdot\mathbf{a}, \qquad \mathbf{r}\in\Omega_j, \qquad (2.4.16)$$

where

$$\Omega_j\equiv\{\mathbf{r}|\mathbf{r}\text{ inside the scatterer j}\} \qquad (2.4.17)$$

and

$$k_j=k_0\sqrt{\epsilon_j}. \qquad (2.4.18)$$

Moreover, the field inside of the circle that closely embraces all the scatterers, that is, $\mathbf{r}\in C_{0,N}$, but external to all the scatterers, that is, $\mathbf{r}\notin\bigcup_{i=1}^{N}\Omega_i$, is given by (2.4.13).

2.5 Numerical Implementation and Results

The two recursive algorithms discussed above have been implemented for a two-dimensional dielectric scattering problem depicted in Figure 2.4. The object is an inhomogeneous cylinder. To apply the recursive algorithms, the problem has to be discretized. Here, we decompose the object into N subobjects. The dimension of the subobjects is much smaller than the wavelength in high frequency cases, or the characteristic length of the object within

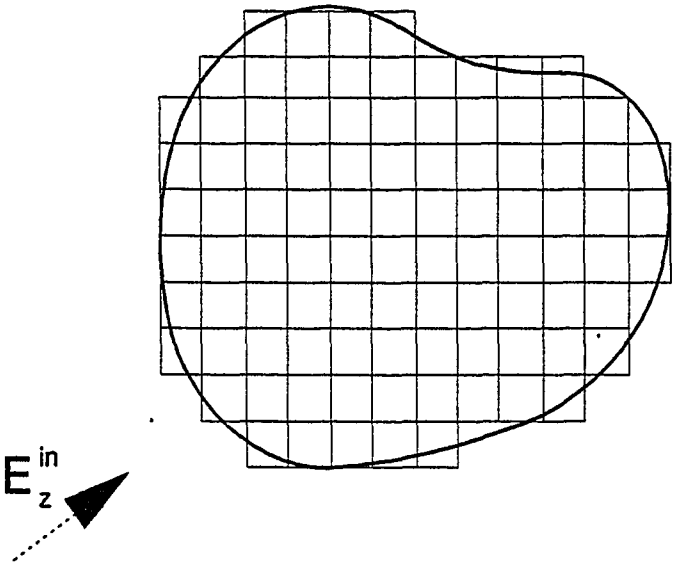

Figure 2.4. Configuration of a two-dimensional scattering problem.

which the permittivity has a significant change in low frequency cases. By considering each subobject as a single scatterer in an N-scatterer problem, the solution of the problem can been obtained by applying the two recursive algorithms developed above. The incident field is a TE wave with the electric field vector perpendicular to the paper.

2.5.1 N^2 recursive algorithm

The N^2 recursive operator algorithm discussed in Section 2.3 has been implemented for a two-dimensional scattering problem shown in Figure 2.4. The two-dimensional translational formulas are given in Appendix A. The incident field is a TE wave with the electric field vector perpendicular to the paper in Figure 2.4.

For efficiency, we expect to make both M and P as small as possible. Since the object has been discretized by about $10-12$ points per wavelength, we can assume that the field in each subobject is nearly a constant. For TE waves, the induced current in the subobject is also nearly a constant. Therefore, only the monopole term in the transition matrices is important. Hence, we can keep only a basic mode in the expansion of the scattered field from each subobject, implying that we can choose $M = 1$, without any significant loss of accuracy. When the dimension of the mesh is much smaller than the wavelength, in two-dimensional cases, the square mesh could be replaced by a circular mesh with the same area [16,17,18]. With such a replacement, the isolated scatterer $\overline{\mathbf{T}}_{i(1)}$ matrices could be obtained analytically. Meanwhile, P should be chosen just large enough to satisfy the relation of $P > kd$ to maintain a desired accuracy.

In order to check the accuracy of the algorithm, we calculated the scattered field from a circular cylinder using both the N^2 algorithm and the

method of moments [16]. The code of the method of moments has been validated by comparing the scattered field with that from a closed-form solution for a uniform circular cylinder.

The test case consists of a circular cylinder. The radius of the object is 0.6 m. The frequency is 3×10^8 Hz. The dielectric constant of the scatterer is $2\epsilon_0$. Therefore, the diameter of the object is about 1.7 wavelengths. The scatterer is divided into 373 subobjects so that N is 373, and M is 1 while P is taken to be 9.

Figure 2.5(a) shows the scattered field intensity as a function of angle for an observation point 5 m from the scatterer. The phase of the scattered field is shown in Figure 2.5(b). The results from the recursive algorithm and the method of moments are indistinguishable.

2.5.2 N recursive algorithm

The N algorithm discussed in Section 2.3 has also been implemented for a two-dimensional dielectric scattering problem shown in Figure 2.4. The incident field is a TE wave with the electric field vector perpendicular to the paper.

The problem has been discretized in the same way as in Section 2.5.1. Following the same arguments as those in Section 2.5.1, we can choose $M = 1$ for a TE polarized incident field without any significant loss of accuracy. Meanwhile, the square meshes have been replaced by the circular cylinders with the same area, since we know that the size of the meshes is much smaller than the wavelength in the problem. In this case, the isolated scatterer $\overline{\mathbf{T}}_{i(1)}$ matrices could be obtained analytically. P is chosen just large enough to satisfy the relation of $P > kd$ to maintain a desired accuracy.

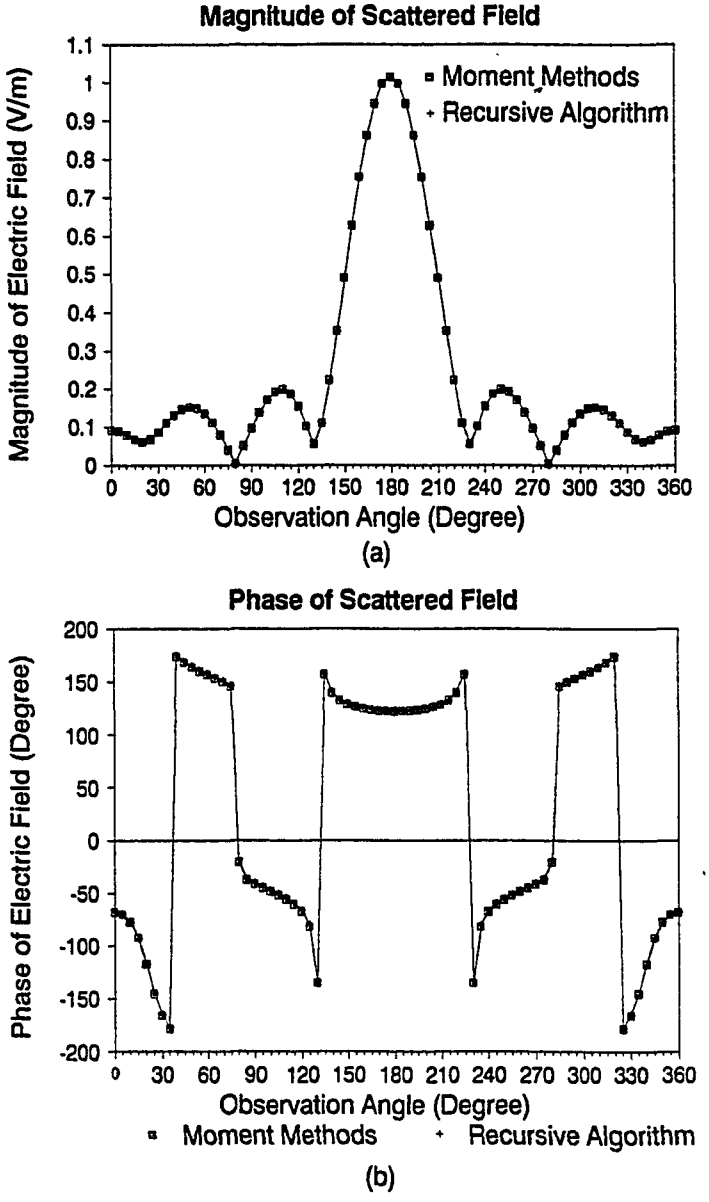

Figure 2.5. Comparison of the scattered fields by using the recursive operator algorithm and the method of moments. (a) Amplitude of the scattered field as a function of the observation angles. (b) Phase of the scattered field as a function of the observation angles.

First, we calculated the scattered field from a uniform circular cylinder using the N algorithm and the method of moments to check the accuracy of the algorithm. The radius of the object is one meter. The frequency of the incident wave is 3 MHz. The relative permittivity of the object is 2. Therefore, the diameter of the object is about 2.8 wavelengths. The scatterer is divided into 777 subobjects. M is one and P is taken as 25. The field is measured at the points on a circle whose radius is 10 m. Figure 2.6 shows the comparison of the results from the method of moments and the aggregate $\overline{\tau}$ matrix method. The dashed curves are the results from the method of moments, and the solid-curves are the results from the aggregate $\overline{\tau}$ matrix method. Figure 2.6(a) gives the magnitude of the scattered field as a function of the observation angles. The results from the two methods are almost indistinguishable. Figure 2.6(b) gives the phase of the scattered field as a function of the observation angles. The results are also in excellent agreement, and the only observable discrepancies are in the neighborhoods of 60 degrees and 300 degrees. As we see, the errors are quite small and acceptable. The numerical result of the aggregate $\overline{\tau}$-matrix method in Figure 2.6 was obtained on a CRAY-2 supercomputer.

In Figure 2.7, a comparison is made between the solutions from the method of moments and the recursive algorithm for an inhomogeneous dielectric scatterer with radius $\rho_0 = 0.6$ m and relative permittivity profile

$$\epsilon_r(\rho, \phi) = 1 + \frac{(1 + \sin\phi)}{2} \sin\left(\frac{\pi\rho}{\rho_0}\right), \quad 0 < \rho < \rho_0. \tag{2.5.1}$$

The agreement is excellent for both amplitude and phase. The inhomogeneous dielectric cylinder is illuminated with a plane wave of 300 MHz incident from the positive x axis ($\phi = 0$). The fields are computed at 5 m from the

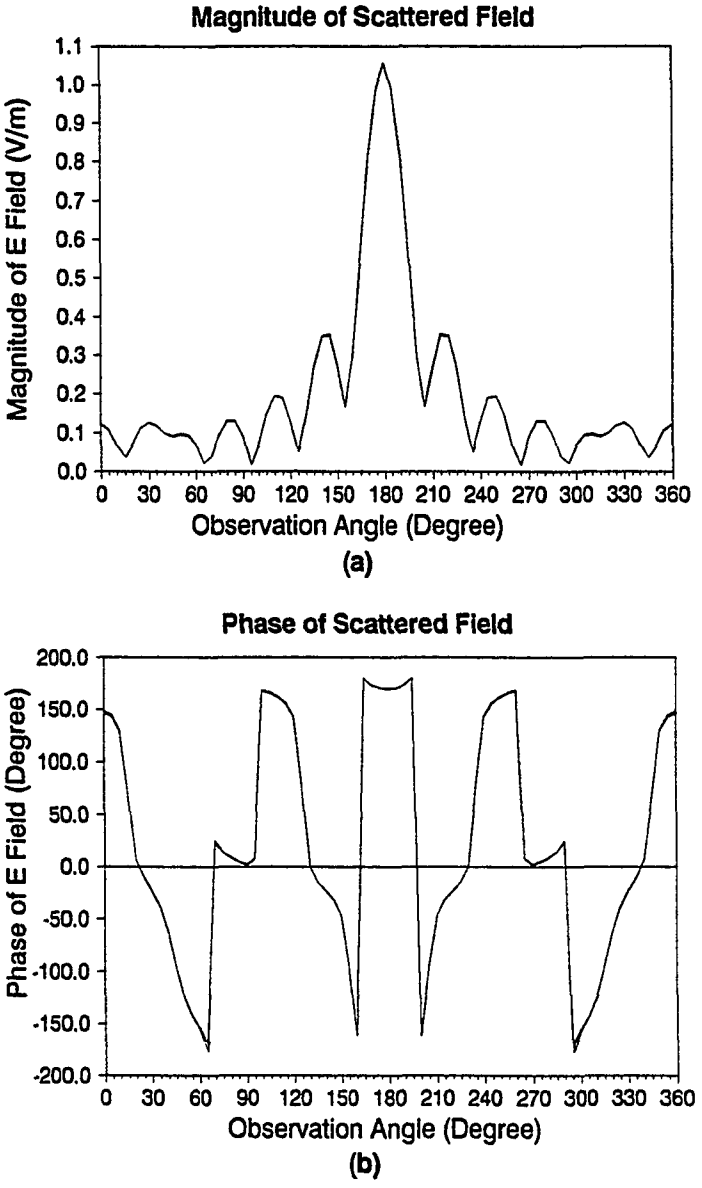

Figure 2.6. Comparison of the scattered fields by using the aggregate τ matrix method and the method of moments. (a) Amplitude of the scattered field as a function of the observation angles. (b) Phase of the scattered field as a function of the observation angles.

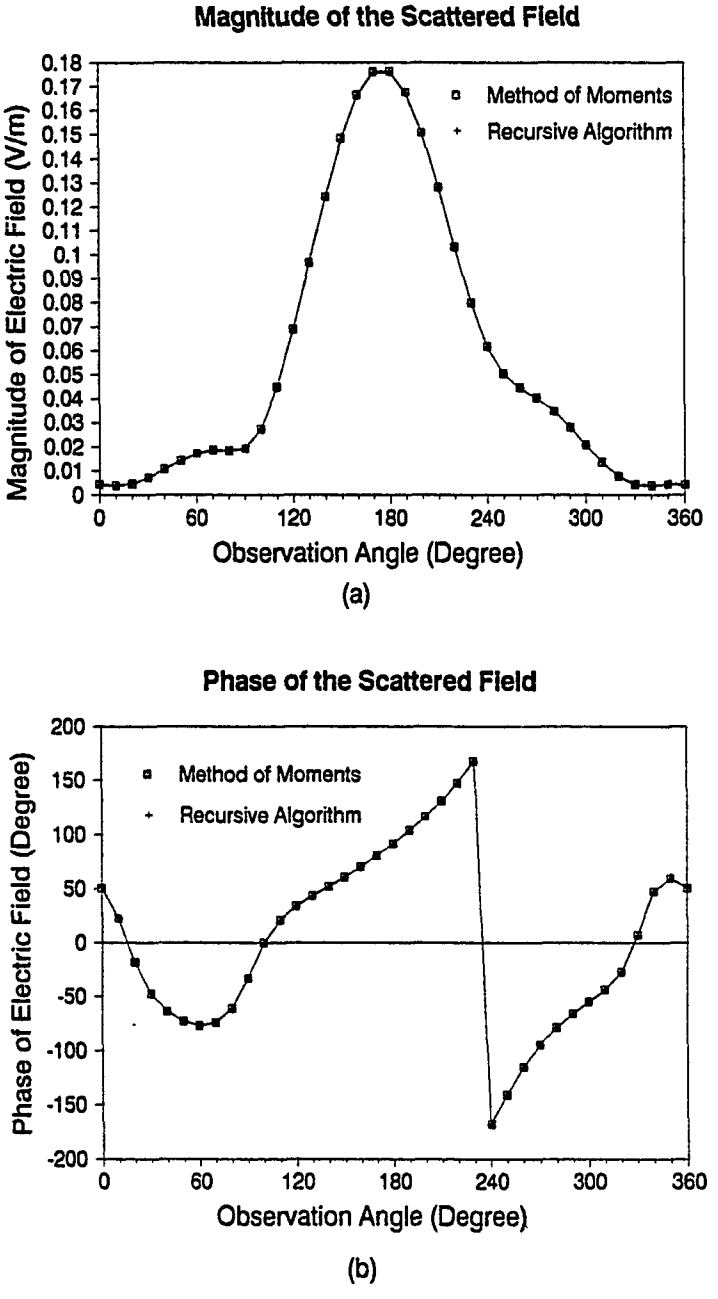

Figure 2.7. Comparison of the solutions from the method of moments and the fast recursive algorithm for an inhomogeneous dielectric scatterer. (a) Amplitude of the scattered field versus observation angle ϕ. (b) Phase of the scattered field versus observation angle ϕ.

center of the scatterer. For this case, $N = 377$, $P = 9$, and $M = 1$. The calculation was performed on a SUN-SPARC workstation. The CPU time taken for the method of moments is 1,401 sec while that for the recursive algorithm is 54.2 sec, which is approximately 26 times faster.

Figure 2.8 shows the comparison of the computation times for the method of moments, the N^2 recursive algorithm, and the Nrecursive algorithm as the number of unknowns N is increased. The top curve in Figure 2.8 is the result for the method of moments. The method of moments has a large overhead in the matrix fill time because numerical integration is needed to accurately evaluate the matrix elements. Since the matrix fill time is proportional to N^2, the moment method curve has an N^2 slope in the beginning, and finally takes off with an N^3 slope. To simplify the comparison for the N^2 algorithm and the $\overline{\tau}$-matrix alroithm, we have a fixed P for all the simulations. P is chosen according to the requirement for the largest object such that it will yield the required accuracy for the largest object, or the largest number of unknowns in the simulations. In choosing P this way, we can guarantee that the algorithms will give a satisfactory accuracy for all the simulations in Figure 2.8. Here, P has been chosen as 15. The middle curve shows the results for the N^2 algorithm discussed in Section 2.3. It has a slope of N^2. The bottom curve is obtained by the N recursive operator method discussed in Section 2.4. It has a slope of N as expected. The simulation in Figure 2.8 is performed on a SUN SPARC workstation. The results show that the N^2 algorithm is consistently more efficient than the method of moments, and the aggregate $\overline{\tau}$ matrix algorithm is the most efficient algorithm in the above three methods.

Up to now, we have only checked the scattered field outside the scatterer. Since the field inside the scatterer is calculated by Equation (2.4.16), the

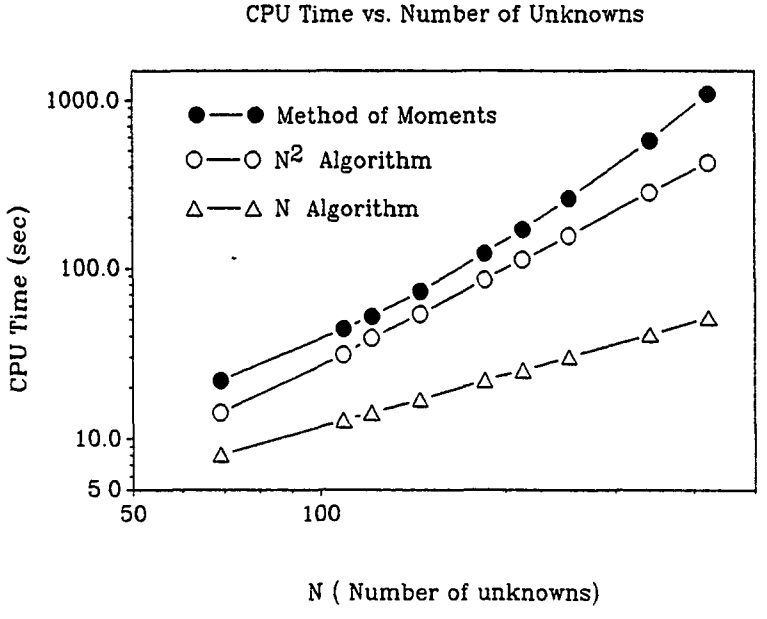

Figure 2.8. The computer times for the method of moments, the N^2 recursive algorithm, and the N recursive algorithm.

backward recursive relations (11) and (12) have to be implemented to find $\overline{\mathbf{T}}_{i(N)}$, $i = 1,2,\ldots,N$, from the aggregate transition matrices $\overline{\tau}$ and $\overline{\mathbf{T}}_{i(i)}$, $i = 1,2,\ldots,N$. The object is a uniform dielectric cylinder. The radius of the object is 0.5 m. The relative permittivity of the object is 2. The frequency of the incident wave is 300 MHz. Figure 2.9(a) shows the amplitude of the internal field derived using the $\overline{\tau}$ matrix algorithm and the method of moments. Figure 2.9(b) shows the phase of the internal field. The agreement is excellent. The knowledge of the internal field is important in a number of applications such as inverse scattering [31,32] or biomedical applications.

2.5.3 Solution of large inhomogeneous scatterers

In the last two subsections, the two recursive algorithms have been validated by comparing their simulation results with those obtained by the method of moments for small scatterers of one or two wavelengths. The CPU time shown in Figure 2.8 demonstrates that the two recursive algorithms are much more efficient than the method of moments. But for large scatterers, the method of moments is extremely inefficient due to its N^3 complexity.

We have used the N recursive algorithm to calculate the scattering solution from a large cylinder, which is about $10\lambda \times 10\lambda$ and can be approximated by $11,905$ unknowns. Since the method of moments is extremely inefficient in this regime, we validate our solution by comparing it with the closed-form solution of a circular, homogeneous cylinder, which is solvable by harmonic expansions.

Figure 2.10(a) shows the amplitude of the scattered field obtained by the recursive algorithm and the closed-form solution. The agreement is excellent.

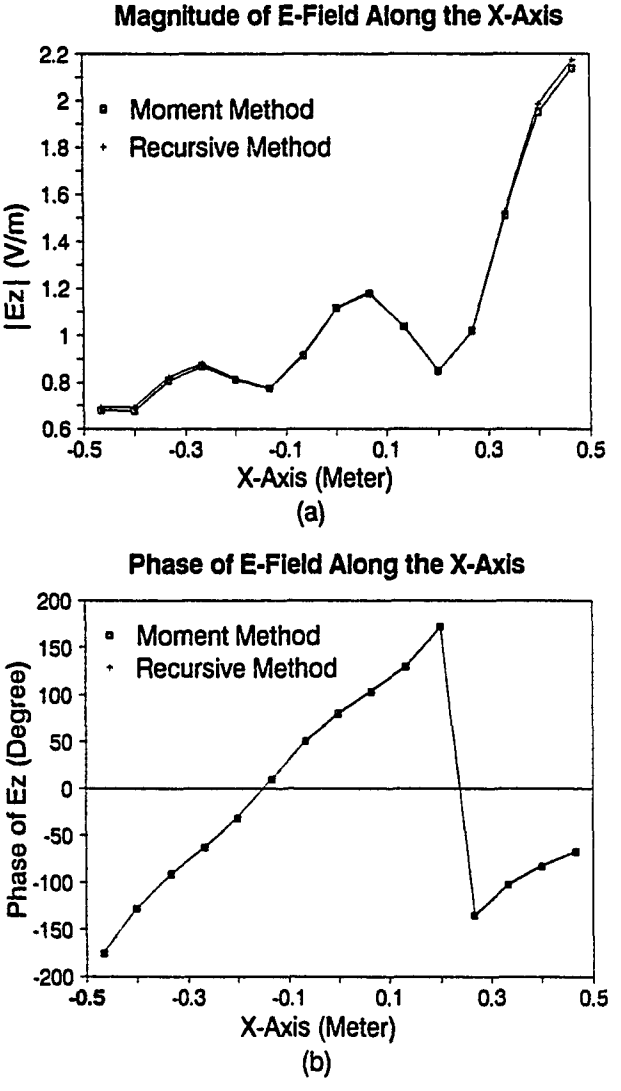

Figure 2.9. Comparison of the fields inside the scatterer by using the method of moments and the recursive operator algorithm. (a) Amplitude of the field along the x-axis. (b) Phase of the field along the x-axis.

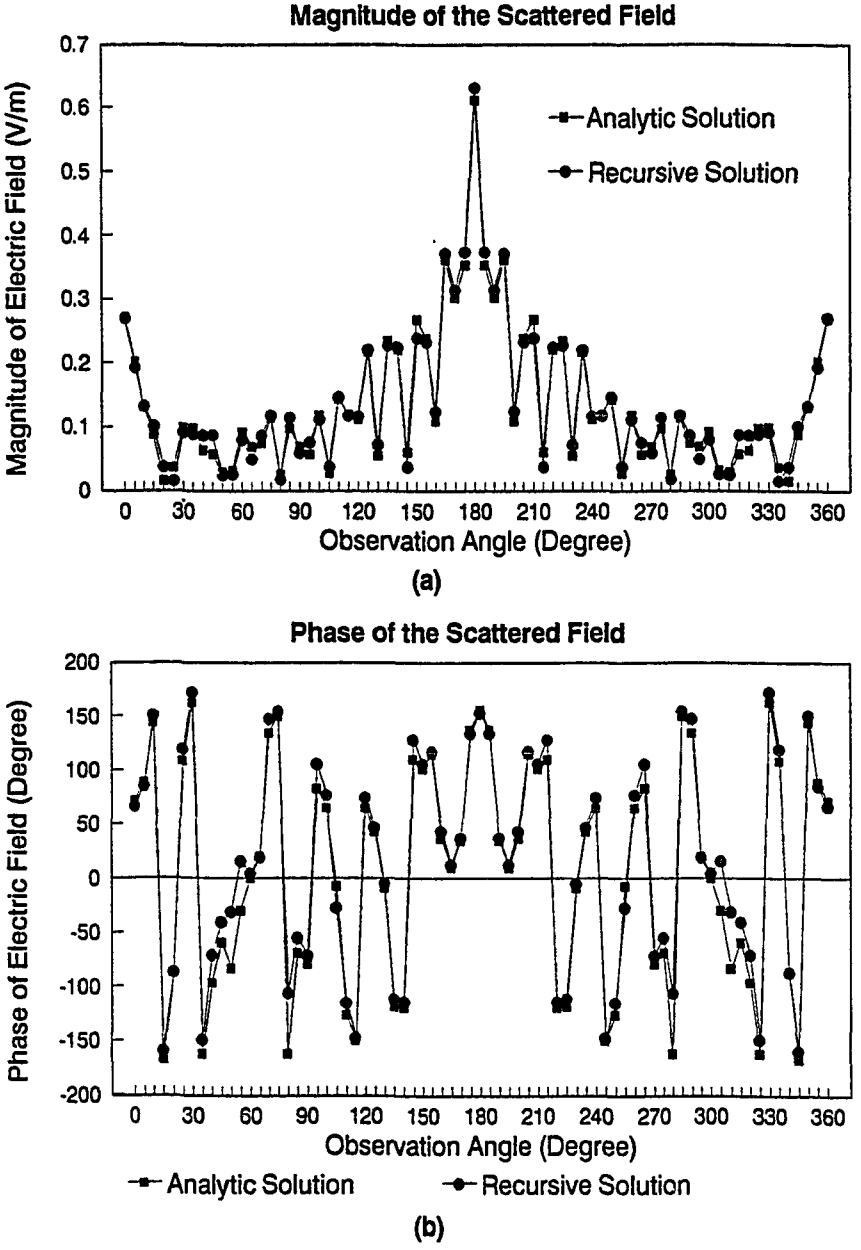

Figure 2.10. Comparison of the scattered fields using the recursive algorithm and the closed-form solution. (a) Amplitude of the scattered field as a function of the observation angles. (b) Phase of the scattered field as a function of the observation angles.

Figure 2.10(b) shows the phase of the scattered field by the recursive algorithm and the closed-form solution. We observe excellent agreements except for some angles of observation. However, for such a wavelength, note that if the diameter of the object is changed by 0.5%, a phase error of about 9° is possible, which indicates that the phase of the scattered field is very sensitive to the size of the object.

In order to use the recursive algorithm, the subscatterers have to be ordered so that they are of increasing distance from the origin [22–24]. We have used the Heapsort algorithm [33,34] to order the subscatterers with computer time proportional to $N \log_2 N$. If a naive sorting algorithm of $O(N^2)$ complexity is used, the sorting time could constitute as much as 40% of the total computer time.

On a CRAY-2 supercomputer, the 11,905-unknown problem is solved in about 30 sec. In this simulation, we pick $M = 1$ and $P = 30$. Though the CRAY-2 has a peak performance of about 1.7 GFLOPS, this peak is in general not attainable for practical applications. For instance, for a simple fully vectorizable "DO" loop, the throughput of the CRAY-2 is about 100 MFLOPS unless a special programming technique is used [35]. In general, the throughput is about 20 to 40 MFLOPS. We assume 30 MFLOPS throughput and that $N^3/3$ floating-point operations are required to invert an $N \times N$ matrix. Then multiplying by a factor of 4 for complex floating-point operations, we estimate that it will take about 20 hours to solve this problem by the method of moments. Figure 2.11 shows the computer times on a CRAY-2 supercomputer of the fast recursive algorithm and the method of moments versus the number of unknowns. The 11,905-unknown points for the method of moments is extrapolated since it is too expensive to solve a problem with such a large number of unknowns.

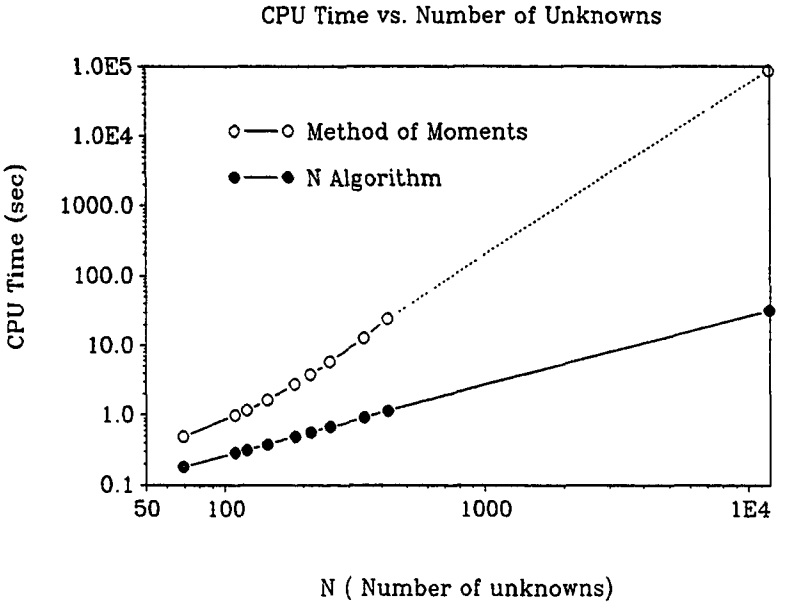

Figure 2.11. Comparison of the computer times for the fast recursive algorithm and the method of moments.

In this program, the isolated scatterer $\overline{\mathbf{T}}$ matrix and the translation formulas are calculated as they are needed. Hence, the dominant part of the memory is used to store the grid which is proportional to the number of unknowns N, whereas a matrix method such as MOM would have required storage proportional to N^2.

Even though the simulation given above is for a homogeneous cylinder, it provides solid evidence of the capability of the algorithm for the solution of a large inhomogeneous 2-D scatterer. The arguments are as follows. First, we have treated the problem as an inhomogeneous scatterer problem and have taken no advantage of the homogeneity and symmetry of the problem. Second, due to the recursive nature of the algorithm, it could easily become unstable if the numerical errors in the algorithm are amplified by the recursive procedure. However, in the above simulation, a reasonably accurate result has been obtained even after about 12,000 recursive steps. Last, the subscatterers have been sorted according to their distances from the origin of the global coordinate system, which is the center of the cylinder in the above simulation. The $n+1$-th scatterer is added to the previous n scatterers in an asymmetric fashion. There is no built-in symmetry in our algorithm that exploits the symmetry of the simulated example. Nevertheless, the solution we have obtained for the circular, cylindrical scatterer is very symmetrical as can be observed from Figure 2.10. On the other hand, if our algorithm had been unstable, an asymmetric result would have been obtained for our simulation.

Table I shows the breakdown of the computer time spent on various parts of the computer program. About 16% of the time is spent in reading in the input for the program. This could be sped up by using binary data files.

Table I. The breakdown of the computer time spent on various parts of the computer program.

	Percentage of the Total CPU	CPU Time (second)	Times Been Called
Recursive Part	44.928	14.327	1
Translation Matrices	19.928	6.355	11,905
Input Data	16.176	5.158	1
Bessel Functions	16.013	5.106	35,862
$T_{i(1)}$ Matrices	2.062	0.657	11,905
Sorting	0.606	0.193	1
Main Program	0.287	0.092	1

Total CPU = 31.888 second
Total Memory = 0.385 MWord

Note that the memory used is about 0.385 MWord. A full matrix method as in the method of moments would have required 290 MWord of memory.

2.6 Conclusions

The recursive algorithms for the solution of the multiple scattering problem have been formulated using the two different approaches. One is formulated by using $\overline{\mathbf{T}}_i(n)$ as the building blocks in the recursive procedure. The other is formulated by using $\overline{\mathbf{T}}_{i(n)} \cdot \overline{\boldsymbol{\beta}}_{i0}$ as the building blocks in the recursive procedure. The investigations on the domain of validity of the two algorithms reveal that the constraint condition for the method with $\overline{\mathbf{T}}_{i(n)}$ as the building blocks is too strong to be satisfied for most of the applications, while the constraint condition for the method with $\overline{\mathbf{T}}_{i(n)} \cdot \overline{\boldsymbol{\beta}}_{i0}$ as the building blocks can always be satisfied by reordering and shifting scatterers without sacrificing the accuracy of the problem. Therefore, the recursive algorithm using $\overline{\mathbf{T}}_{i(n)} \cdot \overline{\boldsymbol{\beta}}_{i0}$ as the building blocks is a legitimate algorithm for the solution of a general multiple scattering problem. The analysis of the computational complexity of the algorithm shows that it is an N^2 algorithm for static and quasi-static problems, an $N^{5/2}$ algorithm for two-dimensional wave scattering problems, and an $N^{7/3}$ algorithm for three-dimensional wave scattering problems.

By introducing an aggregate transmission matrix $\overline{\boldsymbol{\tau}}$, an algorithm with an N computational complexity for static and quasi-static problems has been developed from the algorithm with the use of $\overline{\mathbf{T}}_{i(n)} \cdot \overline{\boldsymbol{\beta}}_{i0}$ as the building blocks. The scattered field exterior to the object can be easily calculated from the $\overline{\boldsymbol{\tau}}$ matrix. The field interior to the object is obtained by a backward recursive scheme, which has the same computational complexity as that of the forward

recursive scheme for the calculation of the $\overline{\tau}$ matrix. For wave scattering problems, the computational complexity of the $\overline{\tau}$ matrix algorithm is N^2 for two-dimensional cases and $N^{5/3}$ for three-dimensional cases.

Both the $\overline{\mathbf{T}}_{i(n)} \cdot \overline{\beta}_{i0}$ algorithm and the $\overline{\tau}$ matrix algorithm have been implemented in two dimensions. The algorithms have been verified by comparing their results with that from the method of moments. The computational times for the method of moments, the $\overline{\mathbf{T}}_{i(n)} \cdot \overline{\beta}_{i0}$ algorithm, and the $\overline{\tau}$ matrix algorithm demonstrate that the algorithms introduced in this chapter are more efficient than the method of moments, and the $\overline{\tau}$ matrix algorithm is the most efficient of the three methods. The $\overline{\tau}$ matrix algorithm has been applied to solve a $10\lambda \times 10\lambda$ problem with $11,905$ unknowns, in less than 32 sec on a CRAY-2 supercomputer with a typical throughput of about 30 MFLOPS. Unlike the finite-element method, this method can be easily implemented on a rectilinear mesh, and its implementation is rather straightforward. Moreover, the method provides a solution that naturally satisfies the radiation condition at infinity and a full scattering solution valid for all angles of incidence.

References

[1] P. C. Waterman, "Matrix formulation of electromagnetic scattering," *Proc. IEEE*, vol. 53, pp. 805-811, 1965.

[2] P. C. Waterman, "New formulation of acoustic scattering," *J. Acoust. Soc.*, vol. 45, pp. 1417-1429, 1969.

[3] P. C. Waterman, "Symmetry, unitarity, and geometry in electromagnetic scattering," *Phys. Rev. D.*, vol. 3, no. 4, pp. 825-829, 1971.

[4] M. Lax, "Multiple scattering of waves II," *Phys. Rev.*, vol. 85, pp. 261–269, 1952.

[5] V. Twersky, "On scattering of waves by random distribution, I and II," *J. Math. Phys.*, vol. 3, pp. 700–734, 1962.

[6] J. G. Fikioris and P. C. Waterman, "Multiple scattering of waves II," *J. Math. Phys.*, vol. 5, pp. 1413–1420, 1964.

[7] J. H. Bruning and Y. T. Lo, "Multiple scattering of EM waves by spheres, Parts I and II, *IEEE Trans. Antennas Propagat.*, vol. AP-19, no. 3, pp. 378–400, 1971.

[8] N. R. Zitron and S. N. Karp, "Higher-order approximations in multiple scattering: I—two-dimensional scalar cases, and II—three dimensional scalar cases," *J. Math. Phys.*, vol. 2, pp. 394–406, 1961.

[9] B. Peterson and S. Ström, "T-matrix for electromagnetic scattering from an arbitrary number of scatterers and representation of E(3)," *Phys. Rev.*, vol. D8, no. 10, pp. 3661–3677, 1973.

[10] B. Peterson and S. Ström, "Matrix formulation of acoustic scattering from an arbitrary number of scatterers," *J. Acoust. Soc. Am.*, vol. 56, no. 3, pp. 771–780, 1974.

[11] M. Danos and L. C. Maximon, "Multipole matrix elements of the translation operator," *J. Math. Phys.*, vol. 6, no. 5, pp. 766-778, 1965.

[12] L. Tsang and J. A. Kong, "Multiple scattering of electromagnetic waves by random distributions of discrete scatterers with coherent potential and quantum mechanical formulism," *J. Appl. Phys.*, vol. 51, no. 7, p. 1824, 1980.

[13] L. Tsang, "Scattering of electromagnetic waves from a half-space of non-spherical particles," *Radio Sci.*, vol. 19, no. 6, pp. 1450–1460, 1984.

[14] W. C. Chew, "An N^2 algorithm for the multiple scattering solution of N scatterers," *Micro. Opt. Tech. Lett.*, vol. 2, no. 11, pp. 380-383, Nov. 1989.

[15] W. C. Chew, J. Friedrich, and R. Geiger, "A multiple scattering solution for the effective permittivity of a sphere mixture," *IEEE Geosci. Remote Sensing*, vol. 28, no. 2, p. 207-214, March 1990.

[16] R. Harrington, *Field Computation by Moment Method.* Malabar, Florida: Krieger Publishing, 1983.

[17] J. H. Richmond, "Scattering from a dielectric cylinder of arbitrary cross section shape," *IEEE Trans. Antennas Propagat.*, vol. AP-13, pp. 334–341, 1965.

[18] A. J. Poggio and E. K. Miller, "Integral equation solution of three dimensional scattering problems," *Computer Techniques for Electromagnetics*, R. Mittra, ed. New York: Pergamon Press, 1973 (also, New York: Hemisphere Publishing, 1987).

[19] D. T. Borup, D. M. Sullivan, and O. P. Gandhi, "Comparison of two FFT conjugate gradient methods and the finite-difference time-domain method for the 2-d absorption problem," *IEEE Trans. Microwave Theory Tech.*, vol. MTT-35, no. 4, pp. 383-395, April 1987.

[20] C. C. Su, "Calculation of electromagnetic scattering from a dielectric cylinder using the conjugate gradient method and FFT," *IEEE Trans. Antennas Propagat.*, vol. AP-35, no. 12, pp. 1418-1425, December 1987.

[21] C. Y. Shen, K. J. Glover, M. I. Sancer, and A. D. Varvatsis, "The discrete Fourier transform method of solving differential-integral equations

in scattering theory," *IEEE Trans. Antennas Propagat.*, vol. AP-37, no. 8, pp. 1032-1041, August 1989.

[22] Y. M. Wang and W. C. Chew, "An efficient algorithm for solution of a scattering problem," *Micro. Opt. Tech. Lett.*, vol. 3, no. 3, pp. 102-106, March 1990.

[23] W. C. Chew and Y. M. Wang, "A fast algorithm for solution of a scattering problem using a recursive aggregate tau matrix method," *Micro. Opt. Tech. Lett.*, vol. 3, no. 5, pp. 164-169, May 1990.

[24] Y. M. Wang and W. C. Chew, "Solution of large inhomogeneous scatterers by a fast recursive algorithm," Submitted for publication.

[25] J. A. Kong, *Electromagnetic Wave Theory.* New York: John Wiley & Sons, 1986.

[26] R. H. Harrington, *Time-harmonic Electromagnetic Fields.* New York: McGraw-Hill, 1961.

[27] J. A. Stratton, *Electromagnetic Theory.* New York: McGraw-Hill, 1941.

[28] W. C. Chew, *Waves and Fields in Inhomogeneous Media.* New York: Van Nostrand Reinhold, 1990.

[29] M. Abramowitz and I. A. Stegun, *Handbook of Mathematical Functions.* New York: Dover Publications, 1965.

[30] O. R. Cruzan, "Translational addition theorems for spherical vector wave functions," *Quarterly Appl. Math.*, vol. 20, no. 1, pp. 33–40, 1962.

[31] Y. M. Wang and W. C. Chew, "An iterative solution of two-dimensional electromagnetic inverse scattering problem," *Int. J. Imaging Syst. Technol.*, vol. 1, no. 1, pp. 100-108, 1989.

[32] W. C. Chew and Y. M. Wang, "Reconstruction of two-dimensional permittivity distribution using the distorted Born iterative method," *IEEE Trans. Medical Imag.*, vol. 9, no. 2, pp. 218-225, June 1990.

[33] D. E. Knuth, *Sorting and Searching: The Art of Computer Programming*, vol. 3. Mass.: Addison-Wesley, 1973.

[34] W. H. Press, B. P. Flannery, S. A. Teukolsky and W. T. Vetterling; *Numerical Recipes: The Art of Scientific Computing.* New York: Cambridge University Press, 1986.

[35] I. Dilber, "Matrix multiplication benchmarks on the CRAY-2 system," *Datalink* (NCSA, Univ. of Illinois, Urbana-Champaign), vol. 4, no. 5, pp. 15-18, May-June 1990.

[36] A. Erdélyi, W. Magnus, F. Oberhettinger, and F. Tricomi, *Higher Transcendental Functions*, vol. 2. New York: McGraw-Hill, 1953.

CHAPTER 3

ITERATIVE SOLUTION OF TWO-DIMENSIONAL ELECTROMAGNETIC INVERSE SCATTERING PROBLEMS

3.1 Introduction

The electromagnetics inverse problems in a general sense are aimed at determining the field source or the property of the scatterer from indirect information about an electromagnetic field. These types of problems arise in a variety of science branches and in different applications. There are two kinds of inverse problems which can be distinguished from each other. One, the inverse problem in the narrow sense, determines the field source or the property of the scatterer from the measured radiation patterns or scattered field. The other constructs a source distribution which could generate an electromagnetic radiation with specified characteristics. The latter category of the electromagnetics inverse problems is called the design problem or electromagnetic synthesis problem. The problem investigated in this thesis is the two-dimensional electromagnetic inverse scattering problem. In this chapter, two iterative methods are introduced to solve the nonlinear electromagnetic inverse scattering problem. Electromagnetic inverse scattering is also called electromagnetic imaging.

It is well recognized that electromagnetic imaging has several potential advantages over other techniques. Of particular interest is the ability to image parameters such as permittivity and conductivity over a wide range of frequencies. It can provide additional information which could be complementary to that obtained by other imaging techniques. Furthermore,

electromagnetic imaging is of interest to various disciplines such as medical imaging, geophysical exploration, remote sensing and nondestructive evaluation.

In electromagnetic imaging, diffraction effects are important and cannot be neglected without decreasing the quality of the imaging. In weak scattering cases, the diffraction tomography (DT) approach has been introduced and investigated within the framework of the Born and the Rytov approximations [1–4], where the diffraction effects are supposed to be weak but not negligible. Unfortunately, these conditions are not frequently satisfied in practical problems. The limitations of the Born and the Rytov approximations have been investigated by Keller [5], and Slaney et al. [6]. To consider the effects of strong diffraction, the nonlinear inverse scattering problems have to be solved without the Born approximation.

One-dimensional electromagnetic inverse scattering problems have been investigated by many researchers for many years. Using the time domain analysis, Tijhuis [7] proposed an iterative technique for one-dimensional permittivity distribution reconstruction. An iterative procedure called the distorted Born approximation, which is equivalent to the Newton iteration method, had been proposed by Chew and Chuang [8] and Habashy et al. [9] for one-dimensional reconstruction of permittivity and conductivity distributions. For higher dimensional problems, Wolf [10] proposed a method for reconstructing the permittivity distribution of the object from its hologram taken at different angles of irradiation. Recently, a point matching method was used to reconstruct dielectric properties of a three-dimensional model of the human body within the framework of the first-order Born approximations [11]. A method called pseudoinverse transformation [12] was proposed

to reconstruct two-dimensional dielectric distributions. However, the success of the method depends on the solution of the inverse source problem, for which the stability of the solution is difficult to ensure because of the existence of nonradiating sources [13–15]. A double iterative algorithm based on expansion of both ϵ_r and the total electric field E was proposed to solve the two-dimensional inverse scattering problem by using sinc basis functions and multiple source techniques [16,17,18,19].

In this chapter, two iteration algorithms will be discussed to solve the two-dimensional nonlinear electromagnetic inverse scattering problem. They are the Born iterative method [20] and the distorted Born iterative method [21]. We first present the formulation of the methods in Section 3.2. In Section 3.3, the numrical simulations will be given using both methods.

3.2 Theory and Formulations

The geometry of the two-dimensional inverse problem is shown in Figure 3.1. A cylindrical medium with an arbitrary cross section is inhomogeneous in the xy plane but is homogeneous in the z-axis. The receivers are located around the cylindrical object at finite discrete points. The object is illuminated by either a plane wave or the field excited by an electrical current line source indicated as T in Figure 3.1. In this thesis, TM incident waves are assumed in both the plane wave and line source cases since the operator involved in the basic equation becomes much simpler for TM irradiation than that for TE irradiations [22] and, consequently, yields a better accuracy for the scattered field solution [23]. In the following, the time dependence $e^{-i\omega t}$ is suppressed. For the pure TM incident wave, Maxwell's

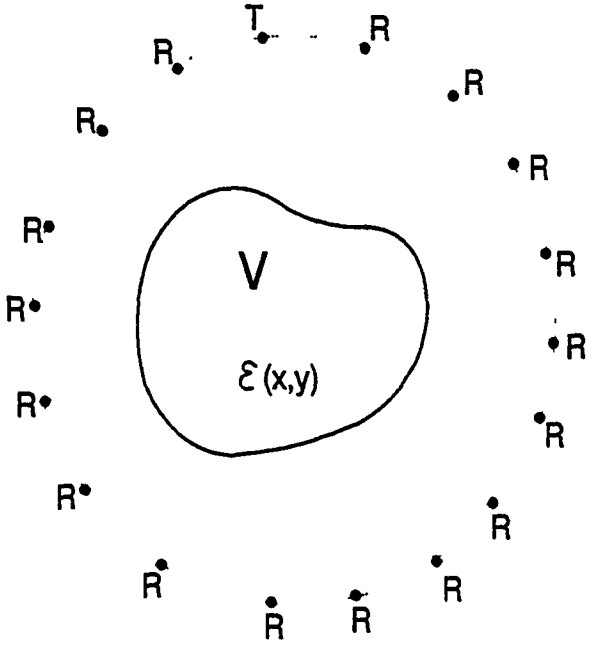

Figure 3.1. Geometrical configuration of the problem.

equations reduce to a scalar equation

$$\nabla_s^2 E_z(x,y) + k^2(x,y) E_z(x,y) = -i\omega\mu_0 J_z^i. \tag{3.2.1}$$

Here, normal incidence has been assumed, and

$$\nabla_s^2 \equiv \frac{\partial^2}{\partial x^2} + \frac{\partial^2}{\partial y^2},$$

$$k^2 = \omega^2 \mu_0 \epsilon(x,y).$$

The inverse scattering problem is to reconstruct $k^2(x,y)$ from the measured scattered fields $E_z^s(\boldsymbol{\rho}_j)$, $j = 1,2,...,M$, exterior to the scatterer. Equation (3.2.1) can be cast into an integral equation as

$$E_z(\boldsymbol{\rho}_j) = E_z^i(\boldsymbol{\rho}_j) + \iint_S G(\boldsymbol{\rho}_j - \boldsymbol{\rho}', \epsilon_b) O(\boldsymbol{\rho}') E_z(x',y') dx'dy',$$

$$j = 1,2,\ldots,M, \tag{3.2.2}$$

where S is the scatterer cross section, and $G(\boldsymbol{\rho}-\boldsymbol{\rho}', \epsilon_b)$ is the Green's function which is the solution of

$$\nabla^2 G(\mathbf{r}-\mathbf{r}', \epsilon_b) + k_b^2(\mathbf{r}) G_0(\mathbf{r}-\mathbf{r}', \epsilon_b) = -\delta(\mathbf{r}-\mathbf{r}'), \tag{3.2.3}$$

and

$$O(\boldsymbol{\rho}) = k_0(\epsilon_r(\boldsymbol{\rho}) - \epsilon_b(\boldsymbol{\rho}))$$

is the object function to be recovered.

Moving the incident field $E_z^{in}(\boldsymbol{\rho}_j)$ of Equation (3.2.2) to the left-hand side of the equation, we have

$$E_z^s(\boldsymbol{\rho}_j) = \iint_S G(\boldsymbol{\rho}_j - \boldsymbol{\rho}', \epsilon_b) O(\boldsymbol{\rho}') E_z(x',y') dx'dy',$$

$$j = 1,2,\ldots,M, \tag{3.2.4}$$

where

$$E_z^s(\boldsymbol{\rho}_j) = E_z(\boldsymbol{\rho}_j) - E_z^{in}(\boldsymbol{\rho}_j), \quad j = 1, 2, \ldots, M, \tag{3.2.5}$$

is the scattered field measured at the observation points $\boldsymbol{\rho}_j$, $j = 1, 2, \ldots, M$, outside of the scatterer. Here, we have deliberately restricted the number of measurement locations to a finite number M to distinguish the practical application of the inverse scattering problem from the mathematical inverse problem, in which the field on an arbitrarily closed surface completely embracing the object is assumed to be known. Furthermore, we have relaxed the locations of the observation points to arbitrary regions outside the object.

For the inverse scattering problem, both the object function $O(\boldsymbol{\rho})$ and the total field $E(\boldsymbol{\rho})$ in the integrand of the integral equation (3.2.4) are unknown. Since the total field inside the scatterer is a functional of $\epsilon_r(\boldsymbol{\rho})$, Equation (3.2.4) is a nonlinear integral equation for $\epsilon_r(\boldsymbol{\rho})$. This will become very clear if we substitute the Neumann series solution of the total field $E(\boldsymbol{\rho})$ into the integrand of Equation (3.2.4),

$$\begin{aligned} E_z^s(\boldsymbol{\rho}) = & \iint_S d\boldsymbol{\rho}' G(\boldsymbol{\rho} - \boldsymbol{\rho}', \epsilon_b) O(\boldsymbol{\rho}') E_z^{in}(\boldsymbol{\rho}') \\ & + \iint_S d\boldsymbol{\rho}' G(\boldsymbol{\rho} - \boldsymbol{\rho}', \epsilon_b) O(\boldsymbol{\rho}') \iint_S d\boldsymbol{\rho}'' G(\boldsymbol{\rho}' - \boldsymbol{\rho}'', \epsilon_b) O(\boldsymbol{\rho}'') E_z^{in}(\boldsymbol{\rho}'') \\ & + \ldots . \end{aligned} \tag{3.2.6}$$

The terms after the second term of the right-hand side of the equation come from the multiple scattering of the wave in the object. In weak scattering cases, in which the scattered field is much smaller than the incident field, the integral equation (3.2.4) can be solved for $\delta\epsilon_r$ under the Born or Rytov approximations. Unfortunately, the distortions of the reconstructed profile become intolerable under the first Born approximation when the criteria are

not satisfied. In these cases, the strong diffraction effects have to be considered, which means that the inherent nonlinearity of the integral equation (3.2.4) has to be taken into account. In this section, two iterative methods for the solution of the nonlinear integral equation (3.2.4) are introduced. They are the Born iterative method and the distorted Born iterative method.

3.2.1 Born iterative method

Since $E_z(\boldsymbol{\rho})$, the field interior to the object, is unknown in the integral equation (3.2.4), we cannot directly solve Equation (3.2.4) for the object function $O(\boldsymbol{\rho})$. In order to solve the nonlinear integral equation (3.2.4), iterative procedures have to be developed so that we need to deal only with a linear problem at each iteration step. In this subsection, the Born iterative method should be introduced to solve Equation (3.2.4). In this method, $G(\boldsymbol{\rho}-\boldsymbol{\rho}', \epsilon_b)$, the kernel of the integral operator, is chosen as the Green's function of the uniform background medium, and remains unchanged in the iteration procedure. Without losing the generality, we can assume that the background is free space, that is $\epsilon_b = \epsilon_0$. The free-space two-dimensional Green's function is

$$G(\boldsymbol{\rho}-\boldsymbol{\rho}', \epsilon_0) \equiv G_0(\boldsymbol{\rho}-\boldsymbol{\rho}) = \frac{i}{4} H_0^{(1)}(k_0|\boldsymbol{\rho}-\boldsymbol{\rho}'|). \tag{3.2.7}$$

Since ϵ_b remains unchanged during the iteration procedure, the integral equation (3.2.4) becomes

$$\hat{E}_z^s(\boldsymbol{\rho}_j) = \iint_V d\boldsymbol{\rho}' G(\boldsymbol{\rho}_j - \boldsymbol{\rho}', \epsilon_0) O(\boldsymbol{\rho}') E_z(\boldsymbol{\rho}'), \quad j = 1, 2, \ldots, M, \tag{3.2.8}$$

where

$$O(\boldsymbol{\rho}) = k_0^2(\epsilon_r(\boldsymbol{\rho}) - 1.), \tag{3.2.9}$$

and $\hat{E}_z^s$ is the measured scattered field at the receivers. To linearize the integral equation (3.2.8), we approximate the total field interior to the scatterer by the incident field, that is $E_z(\boldsymbol{\rho}) = E_z^{in}$ in the integrand of Equation (3.2.8). Then, (8) becomes

$$E_z^s(\boldsymbol{\rho}_j) = \iint_V d\boldsymbol{\rho}' G(\boldsymbol{\rho}_j - \boldsymbol{\rho}', \epsilon_0) O(\boldsymbol{\rho}') E_z^{in}(\boldsymbol{\rho}'),$$

$$j = 1, 2, \ldots, M. \quad (3.2.10)$$

The above equation is a linear integral equation of the unknown object function $O(\boldsymbol{\rho})$. Equation (3.2.10) is the Born approximation of Equation (3.2.4). Solution of (3.2.10) gives an approximate solution of the object function $O^{(1)}(\boldsymbol{\rho})$. Here, we assume that the integral equation (3.2.10) is solvable. The topics related to the ill-posed problem and stability of the solution will be discussed later. With this approximately reconstructed object function $O^{(1)}(\boldsymbol{\rho})$, an iterative solution of the nonlinear integral equation (3.2.8) can be obtained by the following procedures:

(a) Solve the scattering problem for the field in the object and at the observation points with the last reconstructed distribution function.

(b) Substitute the field in the object obtained in step (a) into the integrand in the integral equation and solve the inverse problem to recover the next order distribution function. Once again, we assume that the pertinent linear integral equation is solvable.

(c) Go to step (a) and compare the field scattered by the reconstructed distribution function with the measured data which, in our case, are the simulated fields for the exact distribution function at the receiver points. If the relative residual error (RRE) (see definition below) is less than the

convergent criterion or is larger than the RRE of the last reconstructed profile, the iteration terminates. Otherwise, repeat the cycle until the solution converges.

The definition of the relative residual error (RRE) in the jth iteration is

$$\mathrm{RRE} = \frac{\sum_{i=1}^{M}(E_z^s(\boldsymbol{\rho}_i) - E_z^{s^{(j)}}(\boldsymbol{\rho}_i))}{\sum_{i=1}^{M} E^s(\boldsymbol{\rho}_i)}, \tag{3.2.11}$$

where the summation is over the receiver points.

The relative residual error (RRE) defined by (3.2.9) gives an objective estimate of the "goodness" of the reconstructed data and is the only estimate in practical situations to judge the convergence of the solution of inverse scattering problems. In step (c) of the above iteration procedure, there are two cases in which the iteration will be terminated. One is that the RRE is less than the convergent criterion. In this case, we assume that a convergent solution of the integral equation (3.2.8) has been achieved. The other case is that the RRE of the recently obtained reconstructed object function $O^{(j)}(\boldsymbol{\rho})$ is larger than that of the previous one $O^{(j-1)}(\boldsymbol{\rho})$. In the latter case, we either find an approximated solution or do not find a convergent solution depending on the absolute value of the RRE and the convergent criterion being given. In the noiseless case, if we make the convergent criterion too small, for example 10^{-8}, then the RRE increases when the RRE is a relatively small number but still larger than the convergent criterion, for example, 10^{-4}. At this point, we still consider that a good approximate solution has been achieved. However, if the RRE is too large, for example, RRE = 0.1 which means about 10% error in the scattered field from the reconstructed object function, then we may assume that the satisfactory reconstruction of the object function is not

achieved. In the noisy case, in which the signal received at the receivers has been contaminated with noise, if the RRE increases in the iteration procedure but has the same order as that of the signal-to-noise ratio of the problem, then we can assume that an acceptable reconstruction of the object function is obtained since for noise data it is unnecessary to fit the measured data more accurately than the signal-to-noise ratio of the measured data. However, if the RRE increases and is much larger than the signal-to-noise ratio of the measured data, then we should assume that the convergent solution is not obtained. An empirical criterion for the region of the convergent solution of the method will be given in Section 3.4.

As we see in this method, only the fields in the integrand are updated in each iteration step, while the Green's function remains unchanged throughout the solution process. We call this the Born iterative method because in each iteration, the kernel of the integral operator remains unchanged; only the field in the scatterer is updated.

3.2.2 Distorted Born iterative method

One immediate extension of the Born iterative method is to update the Green's function as well as the field in the scatterer. We call this the distorted Born iterative method. Since the Green's function, the kernel of the integral equation, changes during the iteration procedure, the right-hand side of Equation (3.2.4), which is the scattered field due to the inhomogeneity of the scatterer relative to the background distribution $\epsilon_r^b(\boldsymbol{\rho})$, has to make the corresponding change too. Therefore, Equation (3.2.4) becomes

$$E_z^s(\boldsymbol{\rho}_j, \delta O) = \iint_S d\boldsymbol{\rho}'\, G(\boldsymbol{\rho}_j - \boldsymbol{\rho}', \epsilon_r^b)\delta O(\boldsymbol{\rho}')E_z(\boldsymbol{\rho}'),$$

$$j = 1, 2, \ldots, M, \quad (3.2.12)$$

where

$$\delta O(\boldsymbol{\rho}) = k_0[\epsilon_r(\boldsymbol{\rho}) - \epsilon_r^b(\boldsymbol{\rho})] \tag{3.2.13}$$

and

$$E_z^s(\boldsymbol{\rho}_j, \delta O) = \hat{E}_z^s(\boldsymbol{\rho}_j) - E_z^s(\boldsymbol{\rho}_j, \epsilon_r^b), \quad j = 1, 2, \ldots, M, \tag{3.2.14}$$

where $E_z^s(\boldsymbol{\rho}, \epsilon_r^b)$ is the scattered field from the inhomogeneous background medium, $\epsilon_b(\boldsymbol{\rho})$, $\hat{E}_z^s(\boldsymbol{\rho})$ is the measured scattered field at the receiver locations, and the Green's function $G(\boldsymbol{\rho} - \boldsymbol{\rho}', \epsilon_r^b)$ is the solution of Equation (3.2.3).

The permittivity distribution is obtained from (3.2.11). That is,

$$\epsilon_r(\boldsymbol{\rho}) = \frac{\delta O(\boldsymbol{\rho})}{k_0^2} + \epsilon_r^b(\boldsymbol{\rho}). \tag{3.2.15}$$

Equation (3.2.12) has to be linearized in each iteration to solve this nonlinear integral equation. Similar to the Born iterative method, we first solve Equation (3.2.12) under the Born approximation, that is, we approximate the total field interior of the scatterer by the original incident field $E_z^{in}(\boldsymbol{\rho}, \epsilon_0)$. Then (3.2.12) becomes

$$E_z^s(\boldsymbol{\rho}_j, \epsilon_0) = \iint_V d\boldsymbol{\rho}' G(\boldsymbol{\rho}_j - \boldsymbol{\rho}', \epsilon_0) O^{(1)}(\boldsymbol{\rho}') E_z^{in}(\boldsymbol{\rho}'),$$

$$j = 1, 2, \ldots, M. \tag{3.2.16}$$

The solution of (3.2.16) gives an approximate solution of the object function $O^{(1)}(\boldsymbol{\rho})$. Then the first-order solution of the permittivity distribution is given by

$$\epsilon_r^{(1)}(\boldsymbol{\rho}) = \frac{O^{(1)}(\boldsymbol{\rho})}{k_0^2} + 1. \tag{3.2.17}$$

With this approximately reconstructed permittivity distribution $\epsilon_b^{(1)}(\boldsymbol{\rho})$, the distorted Born iterative solution can be obtained by the following procedures:

(a) Solve the direct scattering problem for the field in the object and at the observation points with the last reconstructed distribution function. Next, calculate the point-source response in the object for every observation point with the last reconstructed object function. The second part of this step is to calculate the Green's function $G(\boldsymbol{\rho}-\boldsymbol{\rho}', \epsilon_r^b)$ with the last reconstructed permittivity distribution as the background permittivity $\epsilon_r^b(x, y)$.

(b) Substitute the new Green's function and the field inside the scatterer obtained in step (a) into the integrand, and subtract the scattered field due to the last reconstructed distribution function from the measured scattered field at the receivers to obtain $E_z^s(\boldsymbol{\rho}_j, \epsilon_r^b)$, the right-hand side of Equation (3.2.12), where $\epsilon_r^b(\boldsymbol{\rho})$ is the last reconstructed distribution function. Then solve the above inverse problem for the corrections to the last reconstructed profile. Generate the new profile by adding the corrections to the previous profile.

(c) Repeat step (a) and compare the field scattered by the reconstructed distribution function and the measured data, which, in our case, are the simulated fields for the exact distribution function at the receiver points. If the relative residual error (RRE) is less than the criterion given before or is larger than the RRE of the last reconstructed profile, the iteration terminates. Otherwise, repeat the cycle until the solution converges.

3.2.3 Scattering solution and the Green's function

To implement the above two iterative methods on a computer, both the direct (step (a) and step (c)) and the inverse (the Born approximate solutions and step (b)) problems need to be discretized. For consistency,

we choose the same basis function $f_i(x,y)$ for both of them. For simplicity, the pulse basis function $f_i(x,y)$ has been used in discretizing both the direct and the inverse scattering problems. The point-matching method [22,23] is employed in solving the direct scattering problem and in calculating the Green's function with the permittivity distribution at every iteration step for the distorted Born iterative method.

The field and the permittivity of the object are represented as

$$E_z(x,y) = \sum_{i=1}^{N} E_i f_i(x,y), \tag{3.2.18}$$

$$\delta\epsilon_r(x,y) = \sum_{i=1}^{N} a_i f_i(x,y). \tag{3.2.19}$$

For the direct scattering problem, by substituting (3.2.18) into Equation (3.2.4), we have

$$\sum_{i=1}^{N} E_i f_i(\boldsymbol{\rho}) = E_z^{in}(\boldsymbol{\rho}) + \iint_S \delta\boldsymbol{\rho}' G_0(\boldsymbol{\rho}_i - \boldsymbol{\rho}') k_0^2 \delta\epsilon_r(\boldsymbol{\rho}') \sum_{j=1}^{N} E_j f_j(\boldsymbol{\rho}'). \tag{3.2.20}$$

Using the point-matching method, we have

$$\overline{\Gamma} \cdot \mathbf{a} = \mathbf{b}, \tag{3.2.21}$$

where $\mathbf{a}$ is an unknown column vector whose entries are the expansion coefficients of $E_z(x,y)$ expressed in Equation (3.2.18), and $\mathbf{b}$ is a column vector whose components are the expansion coefficients of the incident field in the

first term on the right-hand side of Equation (3.2.20). The elements of matrix $\overline{\boldsymbol{\Gamma}}$ are

$$\Gamma_{ij} = \delta_{ij} - \iint_{S_i} \delta\boldsymbol{\rho}' \, G_0(\boldsymbol{\rho}_i - \boldsymbol{\rho}') k_0^2 \delta\epsilon_r f_j(\boldsymbol{\rho}'). \qquad (3.2.22)$$

In the distorted Born iterative method, the linear system of equations for calculating the Green's function is the same as Equation (3.2.21) except that the entries in the column vector **b** are the incident field generated by a two-dimensional point source located at the corresponding receiver point.

Notice that to calculate the Green's function numerically in every iterative step, the matrix inverse needed is exactly that used for solving the direct scattering problem. Therefore, if the matrix has been inverted in solving the direct scattering problem, the same matrix inverse is directly applied to calculate the Green's function so that the extra computational effort is proportional to MN^2, where M is the number of receivers and N is the number of basis functions used in the discretization of the problem. In most practical situations, the number of unknowns is much larger than that of the receivers, i.e., $N \gg M$. Therefore, compared to the computational time spent on solving the direct problem, which is proportional to N^3, the extra time spent on the calculation of the Green's function in each iterative step is not that significant.

3.2.4 Inverse scattering solution

For a linearized version of the integral Equation (3.2.4), the linear system of equations for the inverse scattering problem is

$$E_z^{s(l)}(x_j, y_j) = \sum_{i=1}^{N} a_i^{(l+1)} \iint_{S_i} G_l(\boldsymbol{\rho}_j - \boldsymbol{\rho}', \epsilon_r^l) k_0^2 f_i(x', y') E_z^{(l)}(x', y') dx' dy'$$

$$j = 1, ..., M, \quad (3.2.23)$$

where S_i is the domain of the pulse function $f_i(x,y)$, and $E_z^{(l)}$ is the l-th direct scattering solution with the l-th permittivity distribution function. For $l = 0$, it is the incident field in the object. Equation (3.2.10) has been used to express $\delta\epsilon_r$ in terms of the basis function $f_i(x,y)$. $G_l(\boldsymbol{\rho}_j - \boldsymbol{\rho}', \epsilon_r^l)$ is the Green's function with the permittivity distribution ϵ_r^l which has been obtained numerically.

Equation (3.2.23) for the inverse scattering problem can be written as the matrix equation

$$\mathbf{u} = \overline{\mathbf{K}} \cdot \mathbf{z}, \tag{3.2.24}$$

where

$$\mathbf{u} = [E_z^s(\boldsymbol{\rho}_1), E_z^s(\boldsymbol{\rho}_2), ..., E_z^s(\boldsymbol{\rho}_M)]^T,$$

$$\mathbf{z} = [a_1, a_2, ..., a_N]^T,$$

where a_i, $i = 1, 2, \ldots, N$, are the expansion coefficients of ϵ_r in (3.2.18), and $\overline{\mathbf{K}}$ is an $M \times N$ matrix whose elements are

$$K_{ji} = \iint_{S_i} k_0^2 G_l(\boldsymbol{\rho}_j - \boldsymbol{\rho}', \epsilon_r^l) E_z^{(l)}(x', y') f_i(x', y') dx' dy'$$

$$i = 1, ..., N, j = 1, ..., M.$$

Equation (3.2.24) can also be considered as a general "operator" equation, where

$$\mathbf{u} \in U, \text{ and, } \mathbf{z} \in Z. \tag{3.2.25}$$

Here, U is the data space and Z is the image space. According to Hadamard [24,25,26], a problem defined by Equations (3.2.24) and (3.2.25) is correctly (or well) posed if the following conditions are fulfilled: (i) for each $\mathbf{u} \in U$ there exists a solution $\mathbf{z} \in Z$; (ii) the solution is unique, and (iii) the solution

depends continuously on $\mathbf{u}$ (it is stable against small variations of $\mathbf{u}$). If even one of the above conditions is not satisfied, then the problem is called ill-posed.

Unfortunately, the matrix equation (3.2.24) obtained by discretizing the linearized integral equation (3.2.4) is ill-posed [24–30], which comes from the unbounded nature of K^{-1}. Thus, the solution of (3.2.24) is unstable against small variation of the measured data $\mathbf{u}$ [27,29,30].

One way to deal with the ill-posed problem is to use Tikhonov's regularization procedure. In this method, instead of solving Equation (3.2.24), we seek a solution which will minimize the following Tikhonov's functional:

$$T(\mathbf{z}, \overline{\mathbf{K}}, u) = \|\overline{\mathbf{K}} \cdot \mathbf{z} - \mathbf{u}\|^2 + \gamma \|\overline{\mathbf{H}} \cdot \mathbf{z}\|^2, \tag{3.2.26}$$

where γ is the regularization parameter, and $\overline{\mathbf{H}}$ is the regularization operator (or the stabilizing operator).

For the matrix equation, the minimization of (3.2.26) leads to

$$[\overline{\mathbf{K}}^{\dagger} \cdot \overline{\mathbf{K}} + \gamma \overline{\mathbf{H}}^{\dagger} \cdot \overline{\mathbf{H}}] \cdot \mathbf{z} = \overline{\mathbf{K}}^{\dagger} \cdot \mathbf{u}, \tag{3.2.27}$$

where $\overline{\mathbf{K}}^{\dagger}$ and $\overline{\mathbf{H}}^{\dagger}$ are the conjugate transpose of $\overline{\mathbf{K}}$ and $\overline{\mathbf{H}}$, respectively. In this thesis, the zeroth-order regularization in which $\overline{\mathbf{H}}$ is the identity matrix of order N has been used to generate the results given in the next section. The solution of Equation (3.2.27) is given by

$$\mathbf{z} = [\overline{\mathbf{K}}^{\dagger} \cdot \overline{\mathbf{K}} + \gamma \overline{\mathbf{H}}^{\dagger} \cdot \overline{\mathbf{H}}]^{-1} \cdot \overline{\mathbf{K}}^{\dagger} \cdot \mathbf{u}. \tag{3.2.28}$$

The choice of the arbitrary regularization parameter γ is important in the regularization procedure. It must be properly balanced so that it is large

enough to filter out unstable high frequency components to obtain a stable solution, but not too large so as to filter out too many useful frequency components in the solution. Generally speaking, however, there is no universal strategy for selecting the optimum γ, and it is probably best to regard γ as effectively undefined in any specific case. A safer approach would be to base the selection of γ on the numerical simulations.

In practice, the range of γ over which the stable solution could be obtained also plays an important role in the inverse procedure. If the solution is too sensitive to the parameter γ, i.e., the range of γ which gives the stable solution is too small (for instance less than one order), then the problem may not be properly defined for the inverse solution because the information contained in the data is not enough to recover the profile with the expected accuracy. According to our experience, for a robust inversion algorithm, the range of γ, which gives the stable solution should, at least, be three to five orders of magnitude, for example from 10^{-10} to 10^{-15}. One practical point that should be mentioned is that to have a convergent solution using the iterative procedure proposed in this thesis, one must have a suitable and robust standard inverse algorithm which has to pass the test by using numerical simulations in which the first-order Born approximation is valid.

3.2.5 Operator forms of the inverse scattering problem

In the following, the solution of the inverse scattering problem should be expressed in terms of the operator notations to gain a deeper understanding of the problem and view the problem from another perspective. First, we should consider the Born iterative method. In the operator representation, Equation (3.2.2) becomes

$$E\rangle = E_{inc}\rangle + \overline{G}_0 \cdot \overline{O} \cdot E\rangle, \tag{3.2.29}$$

where $E\rangle$ is a state vector of the **E** field, $\overline{G}_0$ is a Green's function operator in a homogeneous medium, and $\overline{O}$ is an operator related to the object function $k_0^2[\epsilon_r(\mathbf{r}) - 1]$. The operator equation (3.2.29) expresses the scattering equation in an abstract linear vector space, which is independent of the particular space being considered. In the following, all derivations will be performed formally in this abstract space although a specific space has to be specified when we implement the final formulas numerically. For instance, the coordinate space representation of Equation (3.2.29) can be retrieved by evaluating the inner product of Equation (3.2.29) with a coordinate vector $\mathbf{r}$. Then, Equation (3.2.29) becomes

$$\langle \mathbf{r}, E\rangle = \langle \mathbf{r}, E_{inc}\rangle + \langle \mathbf{r}, \overline{G}_0 \cdot \overline{O} \cdot E\rangle. \tag{3.2.30}$$

Furthermore, noticing that an identity operator [29] is

$$\overline{I} = \int d\mathbf{r}\, \mathbf{r}\rangle\langle \mathbf{r}, \tag{3.2.31}$$

and substituting (3.2.31) into (3.2.30), we have

$$\langle \mathbf{r}, E\rangle = \langle \mathbf{r}, E_{inc}\rangle + \int d\mathbf{r}' d\mathbf{r}'' \langle \mathbf{r}, \overline{G}_0, \mathbf{r}'\rangle\langle \mathbf{r}', \overline{O}, \mathbf{r}''\rangle\langle \mathbf{r}'', E\rangle. \tag{3.2.32}$$

On identifying

$$\langle \mathbf{r}, E\rangle = E(\mathbf{r}), \qquad \langle \mathbf{r}, E_{inc}\rangle = E_{inc}(\mathbf{r}), \tag{3.2.33a}$$

$$\langle \mathbf{r}, \overline{G}_0, \mathbf{r}'\rangle = G_0(\mathbf{r}, \mathbf{r}'), \qquad \langle \mathbf{r}', \overline{O}, \mathbf{r}''\rangle = \delta(\mathbf{r}' - \mathbf{r}'')[k^2(\mathbf{r}') - k_0^2], \tag{3.2.33b}$$

Equation (3.2.32) is identical to Equation (3.2.8). In the coordinate space representation, the operator $\overline{O}$ is diagonal and is related to the object function to be reconstructed in the inverse scattering problem. Following a similar procedure, Equation (3.2.29) can also be represented in other spaces of representations, e.g., the spectral space.

Equation (3.2.29) could be formally solved for $E\rangle$ to yield

$$E\rangle = (\overline{I} - \overline{G}_0 \cdot \overline{O})^{-1} \cdot E_{inc}\rangle. \tag{3.2.34}$$

Substituting (3.2.35) into the right-hand side of (3.2.29), we have

$$E_{sca}\rangle = \overline{G}_0 \cdot \overline{O} \cdot (\overline{I} - \overline{G}_0 \cdot \overline{O})^{-1} \cdot E_{inc}\rangle. \tag{3.2.35}$$

Notice that the scattered field is a nonlinear functional of $\overline{O}$, the operator for the object function. From another viewpoint, the nonlinearity can also be interpreted as the consequence of the multiple scattering effect contributed by the operator $(\overline{I} - \overline{G}_0 \cdot \overline{O})^{-1}$. By expanding the operator $(\overline{I} - \overline{G}_0 \cdot \overline{O})^{-1}$ in Equation (3.2.35) into a geometrical series, we have

$$E_{sca}\rangle = [\overline{G}_0 \cdot \overline{O} + \overline{G}_0 \cdot \overline{O} \cdot \overline{G}_0 \cdot \overline{O} + \overline{G}_0 \cdot \overline{O} \cdot \overline{G}_0 \cdot \overline{O} \cdot \overline{G}_0 \cdot \overline{O} + \cdots] \cdot E_{inc}\rangle, \tag{3.2.36}$$

where $E_{sca}\rangle$ is the scattered field, which is obtained by subtracting the incident field $E_{inc}\rangle$ from the total field $E\rangle$. Equation (3.2.36) is the operator representation of (3.2.6). The n-th term in the above series corresponds to the n-th multiple scattering of the incident field in the object. Equation (3.2.36) is also known as the Neumann series expansion of the pertinent integral equation in the operator form representation.

In the inverse scattering problem, we want to minimize the norm of the difference between the measured scattered field $\hat{E}_{sca}\rangle$ and the calculated scattered field from the reconstructed object. This is equivalent to the following optimization problem:

$$\text{Min}\{\|\hat{E}_{sca}\rangle - \overline{G}_0 \cdot \overline{O} \cdot (\overline{I} - \overline{G}_0 \cdot \overline{O})^{-1} \cdot E_{inc}\rangle\|\}. \tag{3.2.37}$$

Equation (3.2.37) is a nonlinear optimization problem since the norm in the above is a nonlinear functional of the object operator $\overline{O}$. In order to

solve the above nonlinear optimization problem, iterative schemes have to be introduced so that one needs to deal only with a linear optimization problem at each iteration step. In the Born iterative method, the total field inside the object, which is $(\overline{I} - \overline{G}_0 \cdot \overline{O})^{-1} \cdot E_{inc}\rangle$, is approximated iteratively. First, the total field $E\rangle$ is assumed to be approximately $E_{inc}\rangle$ or the field in the presence of an initial guessed permittivity distribution. Then, the object function $\overline{O}$ is solved for as a linear optimization problem in (3.2.37). The new object function thus found is then used to estimate $E\rangle = (\overline{I} - \overline{G}_0 \cdot \overline{O})^{-1} \cdot E_{inc}\rangle$, the total field inside the object. The process is repeated until (3.2.37) is minimized. Meanwhile, the regularization procedure is employed at every iteration step [24,27,30] to circumvent the inherent instability and nonuniqueness [13,14,15,24-30] of the inverse scattering problem.

As we have mentioned before, the operator expression of a nonlinear optimization problem is independent of the particular linear space being considered. Therefore, the minimization of (3.2.37) can be performed in any linear space of representations, e.g., coordinate space or spectral space. The effort needed to find the operator $(\overline{I}-\overline{G}_0\cdot\overline{O})^{-1}$ at each iteration step is exactly equivalent to that of the solution of the pertinent direct scattering problem with the object operator $\overline{O}$ at the corresponding iteration step. For example, if we assume that $\{n\rangle, i = 1, 2, \cdots\}$ is a complete set of basis vectors of a vector space of representation, then the matrix representation of the operator $\overline{G}_0 \cdot \overline{O}$ under such a basis set is $\langle m, \overline{G}_0 \cdot \overline{O}, n\rangle$; the matrix representation of $(\overline{I} - \overline{G}_0 \cdot \overline{O})$ under the basis set $\{n\rangle, n = 1, 2, \cdots\}$ is $\langle m, (\overline{I} - \overline{G}_0 \cdot \overline{O}), n\rangle$. Therefore, the matrix representation of $(\overline{I}-\overline{G}_0\cdot\overline{O})^{-1}$ can be obtained by the inversion of the matrix $\langle m, (\overline{I}-\overline{G}_0\cdot\overline{O}), n\rangle$. The above procedure is equivalent

to using the method of moments [16,17] to solve the direct scattering problem corresponding to the integral equation (3.2.2).

In the distorted Born iterative method, the incident field is the field in the presence of an inhomogeneous background medium; hence, the corresponding Green's function is the point source response in the inhomogeneous background medium. In the presence of an inhomogeneous background medium, the corresponding scattering equation from (3.2.12) is

$$E\rangle = E_{b,inc}\rangle + \overline{G}_b \cdot \delta\overline{O} \cdot E\rangle, \tag{3.2.38}$$

where

$$E_{b,inc}\rangle = E_{inc}\rangle + \overline{G}_0 \cdot \overline{O}_b \cdot E_{b,inc}\rangle, \tag{3.2.39a}$$

$$\overline{G}_b = \overline{G}_0 + \overline{G}_0 \cdot \overline{O}_b \cdot \overline{G}_b, \tag{3.2.39b}$$

$$\overline{O} = \overline{O}_b + \delta\overline{O}. \tag{3.2.39c}$$

In the above, the object operator is a diagonal matrix with diagonal element $k^2(\mathbf{r}) - k_b^2$ under the coordinate space representation. Because the incident field $E_{b,inc}\rangle$ is the solution of the direct scattering problem presented by Equation (3.2.39a), it is the field when an inhomogeneous background is present. Similarly, Equation (3.2.39b) states that the Green's function operator $\overline{G}_b$ is the point source response in the presence of an inhomogeneous background medium characterized by the background object operator $\overline{O}_b$ in Equation (3.2.39b).

In the inverse scattering problem, the object operator $\delta\overline{O}$ is the unknown to be sought. Since the measurement data are the scattered fields at the remote receivers outside of the object, we can formally recast Equation (3.2.38) into

$$E\rangle = E_{b,inc}\rangle + \overline{G}_b \cdot \delta\overline{O} \cdot (\overline{I} - \overline{G}_b \cdot \delta\overline{O})^{-1} \cdot E_{b,inc}\rangle. \tag{3.2.40}$$

Moving the first term on the right-hand side of the above equation to the left-hand side of the equation, we have

$$E_{b,sca}\rangle = \overline{G}_b \cdot \delta\overline{O} \cdot (\overline{I} - \overline{G}_b \cdot \delta\overline{O})^{-1} \cdot E_{b,inc}\rangle, \tag{3.2.41}$$

where $E_{b,sca}\rangle$ is the scattered field which is defined as the difference between the total field $E\rangle$ and the incident field $E_{b,inc}\rangle$. Given the measurement data $\hat{E}_{sca}\rangle$ and a background object operator $\overline{O}_b$, $\hat{E}_{b,sca}\rangle$ can be calculated. Consequently, an optimization problem can be set up to minimize

$$\left\| \hat{E}_{b,sca}\rangle - \overline{G}_b \cdot \delta\overline{O} \cdot \overline{E}\rangle \right\|. \tag{3.2.42}$$

The above can be solved for $\delta\overline{O}$ by assuming first that

$$E\rangle = (\overline{I} - \overline{G}_b \cdot \delta\overline{O})^{-1} \cdot E_{inc}\rangle \approx E_{b,inc}\rangle \tag{3.2.43}$$

in Equation (3.2.42). Under such an approximation, the nonlinear optimization problem (3.2.42) is converted into a linear optimization problem. Then, $\delta\overline{O}$ is ascertained by the solution of the corresponding linear optimization problem. Given $\delta\overline{O}$, a new $\overline{O}$ given by (3.2.39c) can be used as the new $\overline{O}_b$, hence yielding new $\overline{G}_b$ and $E_{b,inc}\rangle$. Consequently, the process can be repeated until (3.2.42) is minimized. As in the Born iterative method, the regularization procedure has to be employed at each iteration step to circumvent the inherent instability of the inverse problem.

3.2.6. Convergence of the algorithms

Now, we should discuss the convergent speed of the two iterative algorithms discussed above. We should consider the distorted Born iterative

method first. In the distorted Born iterative method, the problem is represented by (3.2.41) which is

$$E_{b,sca}\rangle = \overline{G}_b \cdot \delta\overline{O} \cdot (\overline{I} - \overline{G}_b \cdot \delta\overline{O})^{-1} \cdot E_{b,inc}\rangle, \tag{3.2.44}$$

where $E_{b,sca}\rangle$ is the scattered field which is defined as the difference between the total field $E\rangle$ and the incident field $E_{b,inc}\rangle$. Using the series expansion of $(\overline{I} - \overline{G}_b \cdot \delta\overline{O})^{-1}$, we have

$$E_{b,sca}\rangle = \overline{G}_b \cdot \delta\overline{O} \cdot (\overline{I} + \overline{G}_b \cdot \delta\overline{O} + \dots) \cdot E_{b,inc}\rangle. \tag{3.2.45}$$

In each iteration step of the distorted Born iterative method, only the first term in the parentheses remains in order to linearize the problem. From (3.2.45), we can see that the error is proportional to $(\delta\overline{O})^2$. Here, $\delta\overline{O}$ is the correction of the object function at this iteration step. Therefore, the distorted Born iterative method converges quadratically. The quadratic convergence of the solution means that the error at each iteration is proportional to the square of the correction of the solution. Hence, the distorted Born iterative method is similar to the Newton method for the solution of a one variable function.

In the Born iterative method, the problem is expressed by (3.2.29), which is

$$E\rangle = E_{inc}\rangle + \overline{G}_0 \cdot \overline{O} \cdot E\rangle. \tag{3.2.46}$$

Using (3.2.40) in the above equation and moving the first term of the right-hand side of the equation to the left-hand side, we have

$$E_{sca}\rangle = \overline{G}_0 \cdot \overline{O} \cdot (I - \overline{G}_b \cdot \delta\overline{O})^{-1} E_{b,inc}\rangle, \tag{3.2.47}$$

where $\overline{G}_b$ is the Green's function of the inhomogeneous medium $\epsilon_r^b(\boldsymbol{\rho})$, which is the last reconstructed object function in the iteration procedure, and $E_{b,inc}\rangle$

is the direct scattering problem with the last reconstructed object function. Using the series expansion of $(\overline{I} - \overline{G}_b \cdot \delta\overline{O})^{-1}$, we have

$$E_{sca}\rangle = \overline{G}_0 \cdot \overline{O} \cdot (I + \overline{G}_b \cdot \delta\overline{O} + \ldots) \cdot E_{b,inc}\rangle. \qquad (3.2.48)$$

In each iteration step of the Born iterative method, only the first term in the parentheses remains in order to linearize the problem. The error at each iteration is proportional to $\delta\overline{O}$, the correction of the object function at this iteration step. Thus, the Born iterative method is said to converge linearly just as the bisection method for the solution of a one variable function.

3.3 Simulations and Results

3.3.1 Born iterative method

In this subsection, some simulated results are obtained for several cases from low-frequency to high-frequency electromagnetic images by using the Born iterative method. Figure 3.2 shows the relative dielectric distribution reconstruction of a sinelike function with a peak value of 11. The frequency of the incident wave is 10 MHz. The diameter of the object is about one-tenth of the wavelength. Four incident plane waves from the different directions are illuminated in this and the following examples in this subsection. The receivers are located around the object as indicated in Figure 3.1. The number of the receivers in this and the following examples varies from 26 to 36 depending on the number of unknowns in the problem. The measured data for all of the examples in this subsection were simulated on a computer by solving the direct scattering problem with the original dielectric distribution functions for the scattered fields at the receivers.

Figure 3.2 shows clearly the evolution of the convergence of the solution

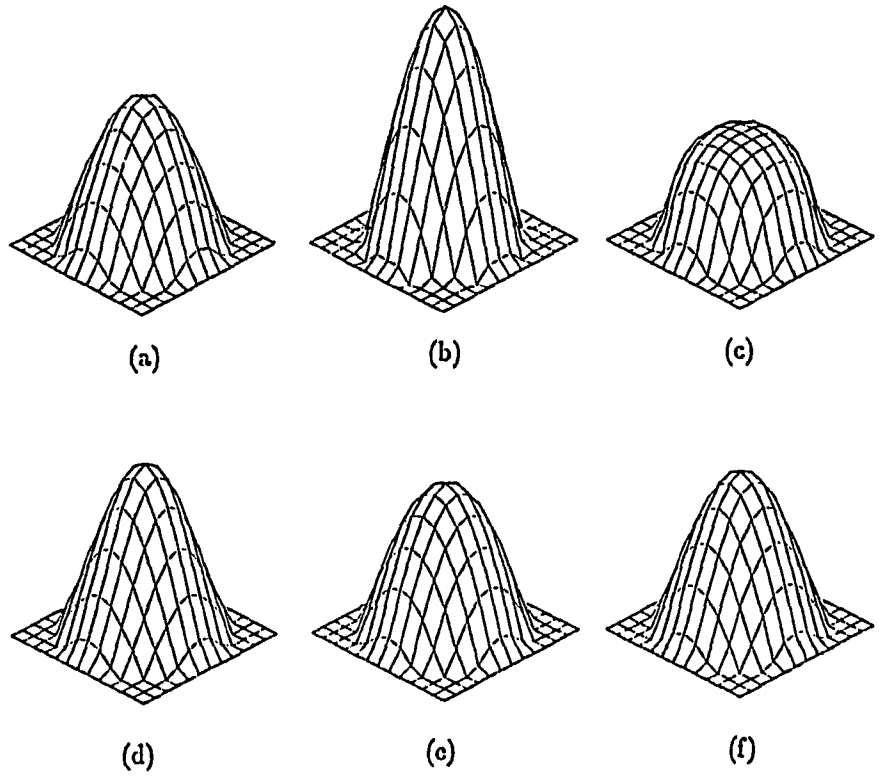

Figure 3.2. Reconstruction of a sinelike permittivity distribution with operating frequency at 10 MHz. The peak value of the relative permittivity is 11. The diameter of the object is one-tenth of the wavelength. (a) is the original distribution. (b) is the result of the first-order approximation. (c) to (e) are the results from the second iteration to the fourth iteration. (f) is the final convergent solution after five iterations.

given by the Born iterative algorithm. Figure 3.2(a) is the original dielectric distribution function. Figure 3.2(b) is the reconstructed result of the first-order approximation, i.e., the Born approximation. Here, we can see that the Born approximation fails for the quantitative reconstruction of the dielectric distribution function in this case. Figures 3.2(c)–3.2(f) are iteration results from the second iteration to the fifth iteration. The solution converges to the original dielectric distribution function after five iterations. The above example shows that the algorithm works very well even when the Born approximation fails to reconstruct the distribution function in the low frequency inverse scattering problem.

Figure 3.3 shows the dielectric distribution reconstruction of a sinelike function with the operating frequency at 100 MHz. The peak value of the relative dielectric constant in the object is 1.80. The diameter of the object in this case is about 1λ. Figure 3.3(a) is the original dielectric distribution. Figure 3.3(b) is the reconstructed dielectric distribution of the first iteration, i.e., the Born approximation. Figures 3.3(c)–3.3(h) are the iteration results from the second iteration to the seventh iteration. Figure 3.3(i) is the final convergent solution after eight iterations.

All simulation results given in this subsection are obtained on the SUN 4/110 workstation. As is well-known, to guarantee the accuracy of the calculated scattered field by using the moment method, the mesh density has to be about $100/\lambda^2$ [19]. Due to the limitation of the memory provided by the SUN workstation, the maximum size of the object we can deal with on the SUN is about 2λ. In Figure 3.4, the operating frequency is 200 MHz. The diameter of the object is about 2λ. In this example, eight plane waves are illuminated from different directions. Figure 3.4(a) is the original dielectric

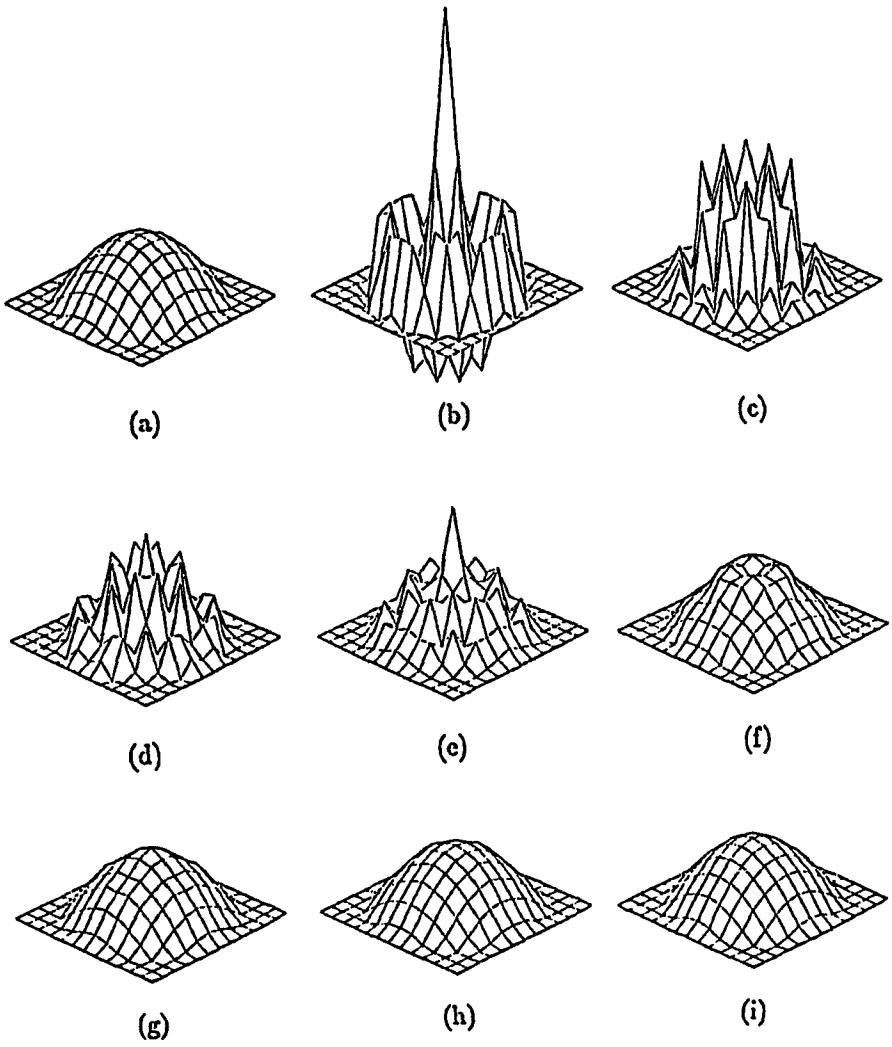

Figure 3.3. Reconstruction of a sinelike permittivity distribution with operating frequency at 100 MHz. The peak value of the relativity permittivity is 1.80. The diameter of the object is 1λ. (a) is the original distribution. (b) is the result of the first-order approximation. (c) to (h) are the results from the second iteration to the seventh iteration. (i) is the final convergent solution after eight iterations.

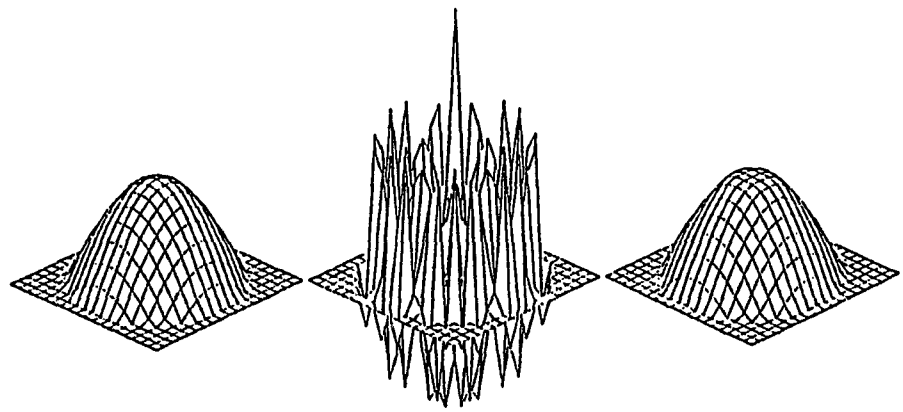

Figure 3.4. Reconstruction of a sinelike permittivity distribution with operating frequency at 200 MHz. The peak value of the relativity permittivity is 1.80. The diameter of the object is 2λ. (a) is the original distribution. (b) is the result of the first-order approximation. (c) is the final convergent solution after twelve iterations.

distribution. Figure 3.4(b) is the reconstructed distribution of the first iteration. Figure 3.4(c) is the convergent solution of the dielectric distribution function after twelve iterations.

Some common features appear in all the examples given above. First, the Born approximation fails to give a quantitative reconstruction of the dielectric distribution in all the examples. Second, the final convergent solutions obtained by the algorithm proposed in the paper converge to the exact distribution functions after a few iterations with the negligible errors less than 1% at grid points. The reason for such good accuracy of the reconstructed dielectric distributions in the above examples is that the property of the constraint we employed in the inverse procedure coincides with that of the original distribution functions, i.e., continuity of the distribution functions. In the next two examples, the dielectric distribution functions with a discontinuity, i.e., step function, are considered. The result will give us an idea on how the algorithm works and what we can expect for a discontinuous distribution function.

Figure 3.5 shows the dielectric distribution reconstruction of a step function to illustrate the band-limited nature of the algorithm. The regularization employed in the inverse procedure causes the algorithm to exhibit some low-pass-filtering effect. In Figure 3.5, the final convergent solution is, as expected, a smoothed version of the original distribution function. In Figure 3.5, the operating frequency is 100 MHz. The diameter of the object is about 1λ; $\delta\epsilon_r$ is 0.60. Figure 3.5(a) gives the original dielectric distribution. Figure 3.5(b) is the result of the first iteration, i.e., the Born approximation. Figures 3.5(c)–3.5(i) are the results from the second iteration to the eighth iteration, respectively. The solution converges after eight iterations.

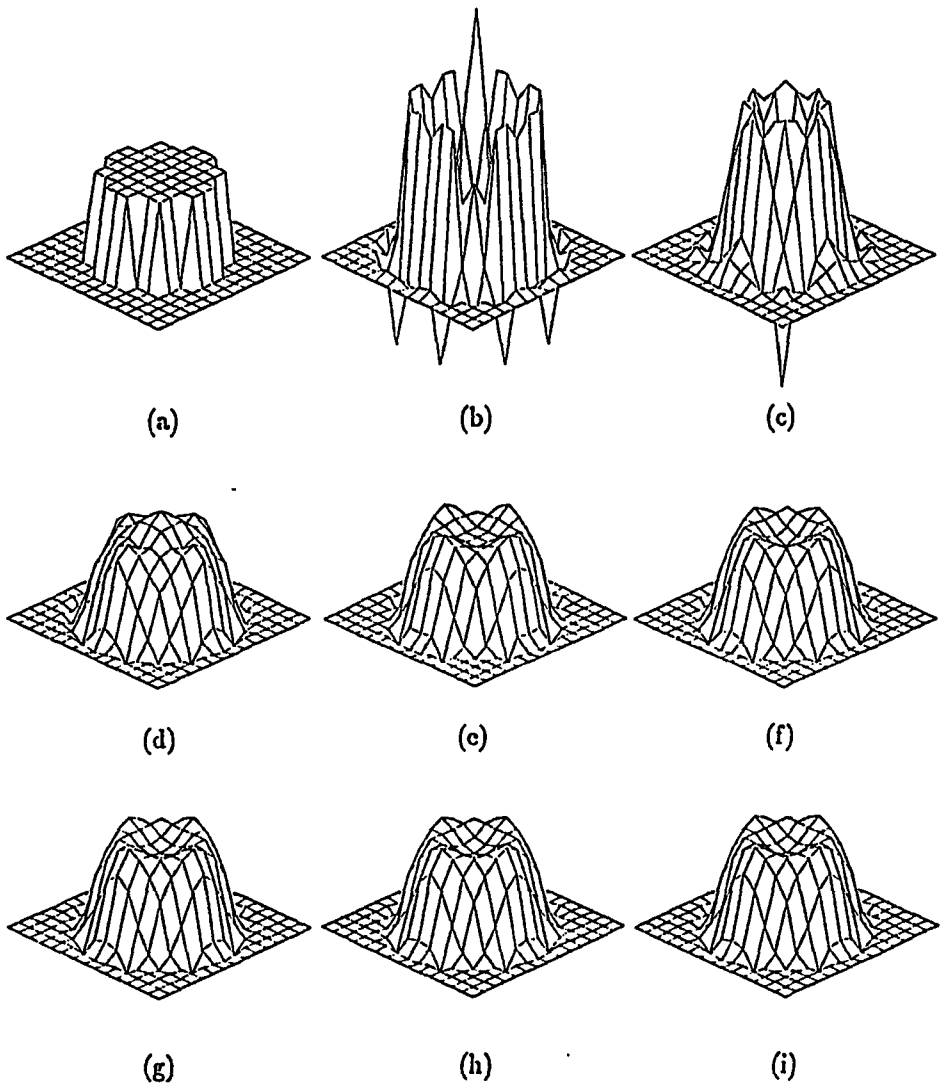

Figure 3.5. Reconstruction of a step permittivity distribution with operating frequency at 100 MHz. The contrast of the relativity permittivity is 1:1.60. The diameter of the object is 1λ. (a) is the original distribution. (b) is the result of the first-order approximation. (c) to (h) are the results from the second iteration to the seventh iteration. (i) is the final convergent solution after eight iterations.

Figure 3.6 shows a behavior similar to that seen in Figure 3.5. But in this example, the operating frequency is 10 MHz. The diameter of the object is about one-tenth of the wavelength. Here, $\delta\epsilon_r$ is 10. Figure 3.6(a) gives the original dielectric distribution. Figure 3.6(b) gives the result of the first iteration. Figure 3.6(c) is the final convergent solution after five iterations.

As the last example, Figure 3.7 shows that the convergent solution of the reconstruction of an asymmetric dielectric distribution agrees quite well with the original one. Figure 3.7(a) is the original dielectric distribution. Figure 3.7(b) is the convergent solution of the constructed distribution after six iterations. However, because of the band-limited nature of the algorithm, the result shows that high spectral frequency components of the distribution function were smoothed out.

Figure 3.8 gives the relative mean squared error (MSE) of the reconstructed object function in Figure 3.3 as a function of the iteration steps. The relative MSE is defined as

$$\text{MSE} = \sqrt{\frac{\iint_S [\epsilon_r^{(i)}(\boldsymbol{\rho}) - \epsilon_r(\boldsymbol{\rho})]^2 dx\, dy}{\iint_S [\epsilon_r(\boldsymbol{\rho})]^2\, dx\, dy}}, \tag{3.3.1}$$

where S is the scatterer's cross section, $\epsilon_r^{(i)}(\boldsymbol{\rho})$ is the reconstructed relative permittivity distribution in the i-th iteration, and $\epsilon_r(\boldsymbol{\rho})$ is the original relative permittivity distribution. In actual application, the MSE is unknown since $\epsilon_r(\boldsymbol{\rho})$ is not known.

The numerical simulations in this subsection covered a wide range of the electromagnetic inverse scattering applications, from low frequency with high-contrast cases to high frequency with moderate-contrast cases. According to the results of the numerical simulations, the algorithm can be successfully applied to the reconstruction of the dielectric distribution when the

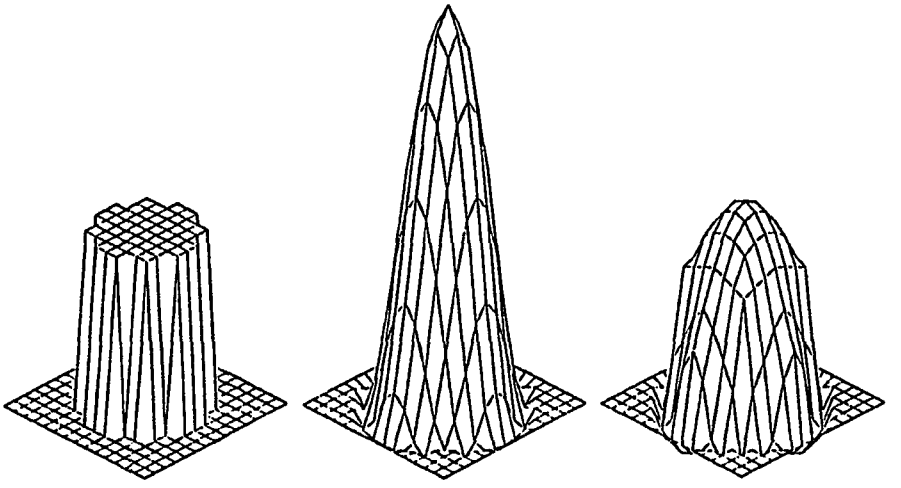

Figure 3.6. Reconstruction of a step permittivity distribution with operating frequency at 10 MHz. The contrast of the relativity permittivity is 1:11. The diameter of the object is 0.1λ. (a) is the original distribution. (b) is the result of the first-order approximation. (c) is the final convergent solution after five iterations.

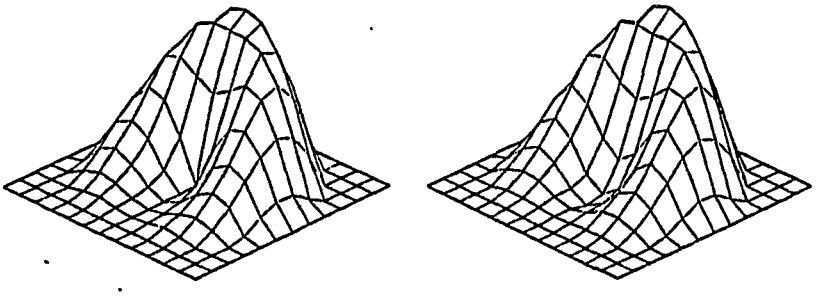

(a) (b)

Figure 3.7. Reconstruction of an axially asymmetric permittivity distribution with operating frequency at 100 MHz. The peak value of the relativity permittivity is 1.80. The diameter of the object is 1λ. (a) is the original distribution. (b) is the final convergent solution after six iterations.

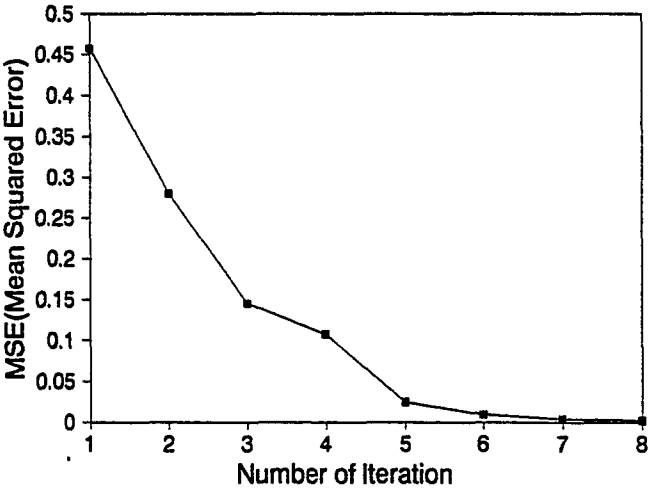

Figure 3.8. The relative MSE (Mean Square Error) of the reconstructed permittivity distribution in Figure 3.2 as a function of the iteration steps.

first-order Born approximation fails for the quantitative reconstruction. The simulations established that the maximum contrast of the relative dielectric constant, in which the algorithm gives a correct convergent solution, is ten times more than that for the Born approximation at the fixed frequency.

3.3.2. Distorted Born iterative method and comparison with the Born iterative method

As the first example, Figure 3.9 shows clearly the evolution of the convergence of the solution given by the distorted Born iterative algorithm for an asymmetric permittivity distribution. Figure 3.9(a) is the original dielectric distribution. Figure 3.9(b) is the first-order Born approximation. Figures 3.9(c)–3.9(h) are the iterative results from the second iteration to the seventh iteration. Figure 3.9(i) gives the final convergent solution after 25 iterations. Actually, it is hard to tell the difference between Figure 3.9(e) and Figure 3.9(i). The algorithm terminates after the twenty-fifth iteration because a relatively small RRE was chosen as the convergent criterion in this case (10^{-5}) in order to examine the convergence and the stability of the algorithm.

Figure 3.10 shows the relative mean square error (MSE) and relative residual error (RRE) of the reconstructed permittivity distribution in the last example as a function of the iteration steps. It is clear that the RRE drops to a negligible level after the fourth iteration. The MSE stays at 0.026 after the sixth iteration because of the band-limited effect of the algorithm. For example, a discontinuity at the origin of the original permittivity distribution is smoothed out in the reconstruction.

This example gives us an idea on how the distorted Born iterative algo-

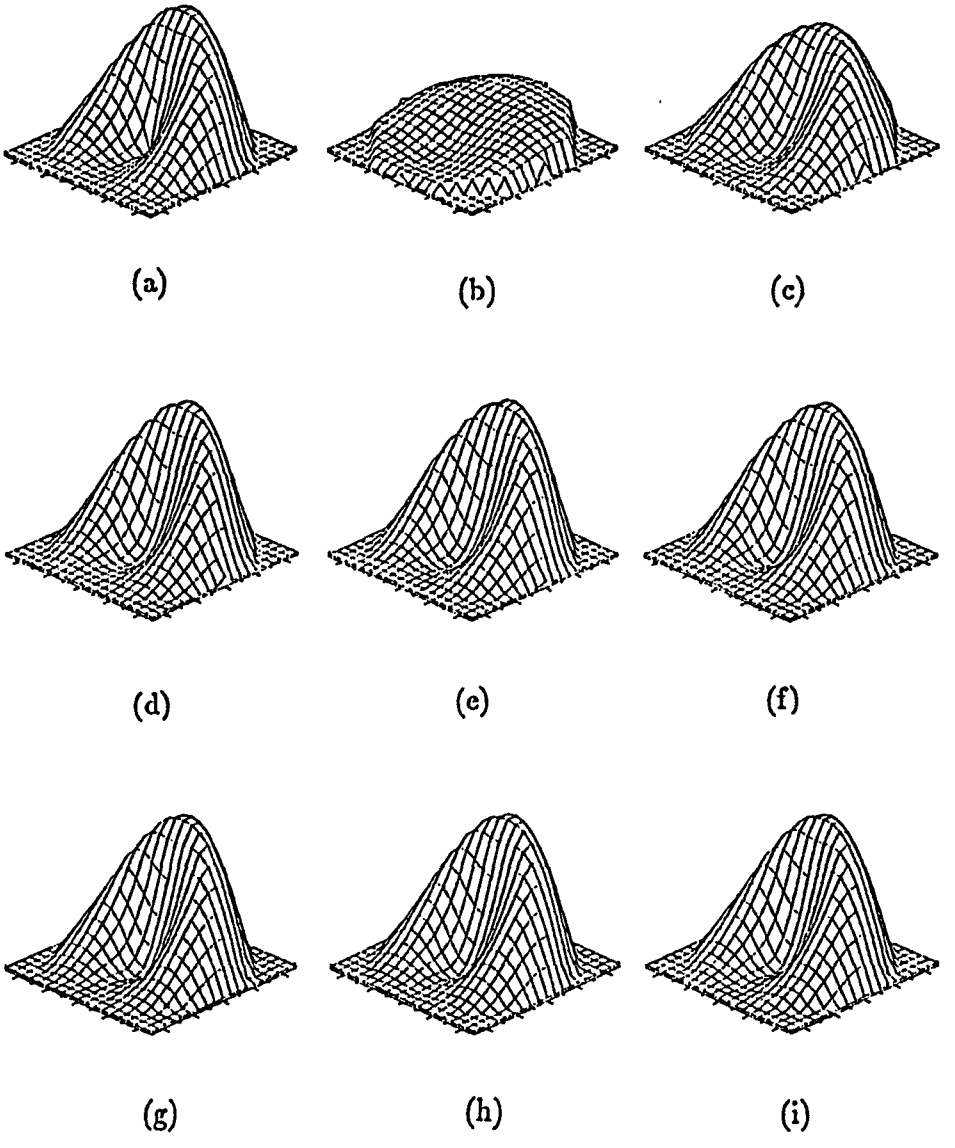

Figure 3.9. Reconstruction of an asymmetric distribution with operating frequency at 100 MHz. The peak value of the relativity permittivity is 1.8. The diameter of the object is 3.0 meters. (a) is the original distribution. (b) is the result of the first-order approximation. (c) to (h) are the results from the second iteration to the seventh iteration. (i) is the final convergent solution after twenty-five iterations.

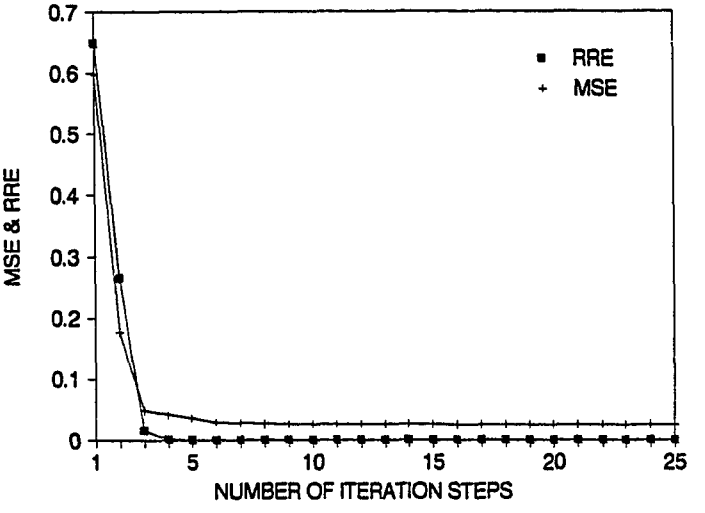

Figure 3.10. The relative MSE (Mean Square Error) and the RRE (Relative Residual Error) of the reconstructed permittivity distribution in Figure 3.9 as a function of the iteration steps.

rithm works for a general permittivity reconstruction problem for asymmetric and nonsmooth distributions.

In the following examples, both the results of the distorted Born iterative method and the Born iterative method are given for comparison for every case.

3.3.2.1 Sinelike distribution (noiseless)

Figure 3.11 shows the reconstruction of a sinelike permittivity distribution by using the distorted Born iterative method. The diameter of the object is about 1λ. Figure 3.11(a) is the original distribution. Figure 3.11(b) is the result of the first-order Born approximation. Figures 3.11(c)–3.11(e) are the iterative solutions from the second step to the fourth step. Figure 3.11(f) gives the convergent solution after the 15 iterations.

Figure 3.12 shows the reconstruction of the same distribution using the Born iterative method. The meaning of the curve surfaces is the same as that in Figure 3.11.

Figure 3.13 shows the relative mean square error and the relative residual error as a function of the iteration steps for both the distorted Born and the Born iterative methods. It shows that for the distorted Born iterative method, the convergent solution is achieved after the fourth iteration, while for the Born iterative method, the convergent solution is reached after the sixth iteration.

3.3.2.2 Two separated pulses (noiseless)

Figure 3.14 shows the reconstruction of the two-pulse distribution using the distorted Born iterative method. The dimension of the pulses is about

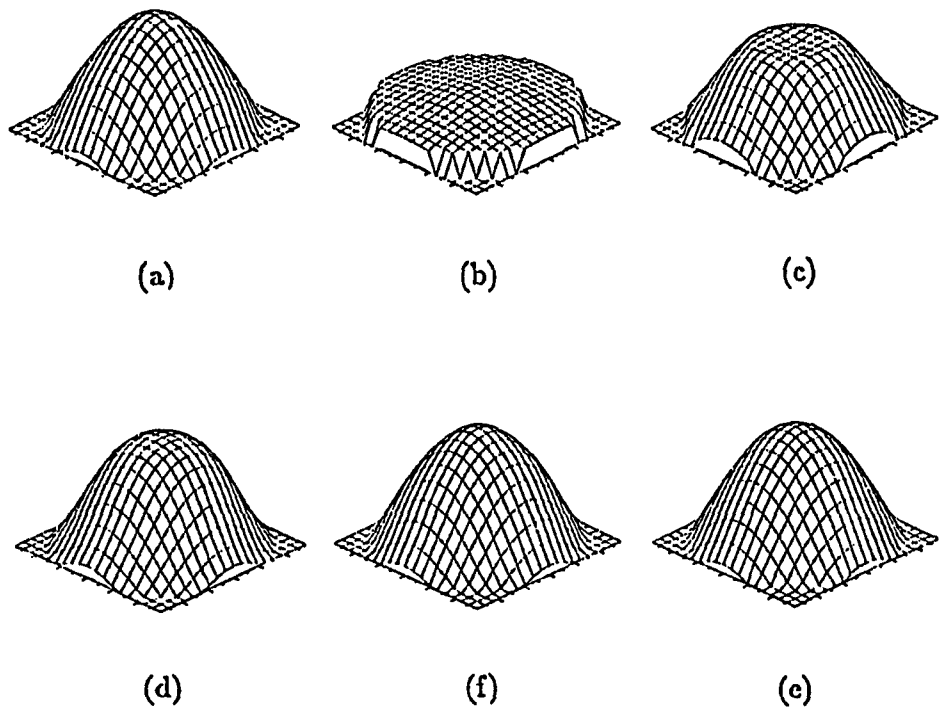

Figure 3.11. Reconstruction of a sinelike permittivity distribution by using the distorted Born iterative method with operating frequency at 100 MHz. The peak value of the relativity permittivity is 1.80. The diameter of the object is 3.0 meters. (a) is the original distribution. (b) is the result of the first-order approximation. (c) to (f) are the results from the second iteration to the fourth iteration. (e) is the final convergent solution after fifteen iterations.

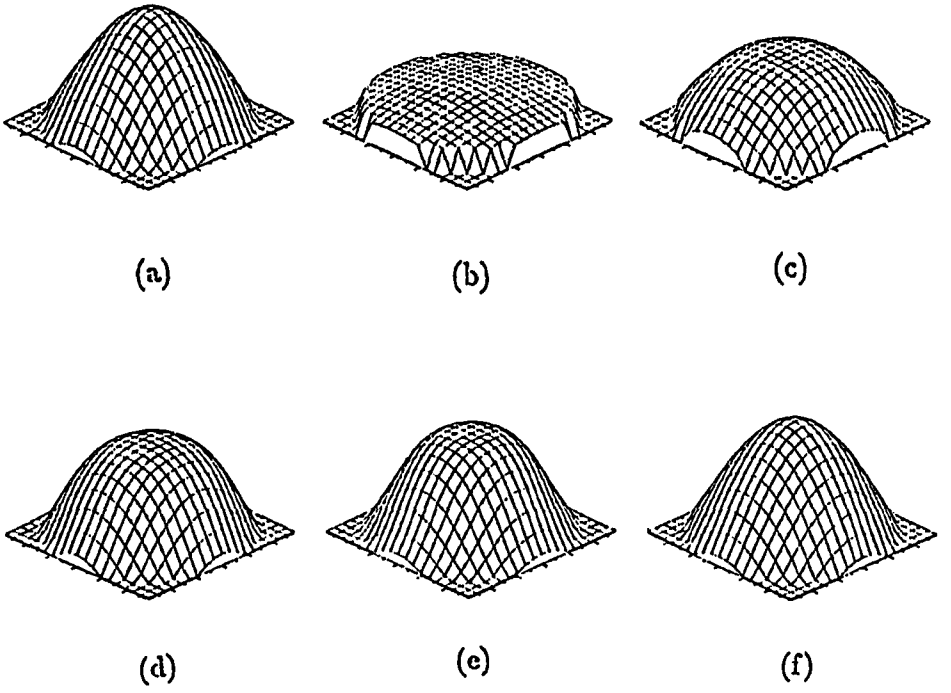

Figure 3.12. Reconstruction of a sinelike permittivity distribution by using the Born iterative method with operating frequency at 100 MHz. The peak value of the relativity permittivity is 1.80. The diameter of the object is 3.0 meters. (a) is the original distribution. (b) is the result of the first-order approximation. (c) to (e) are the results from the second iteration to the fourth iteration. (f) is the final convergent solution after fifteen iterations.

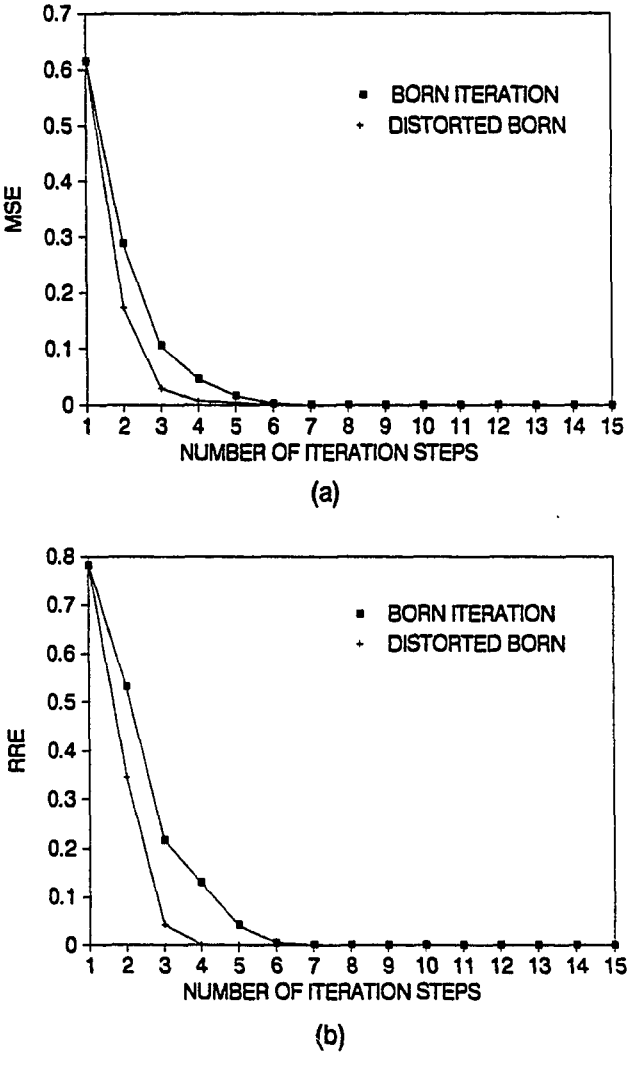

Figure 3.13. (a) is the relative MSE (Mean Square Error) and the RRE (Relative Residual Error) of the reconstructed object function in Figures 3.11 and 3.12 as a function of the iteration steps. (b) is the RRE (Relative Residual Error) of the reconstructed object function in Figures 3.11 and 3.12 as a function of the iteration steps.

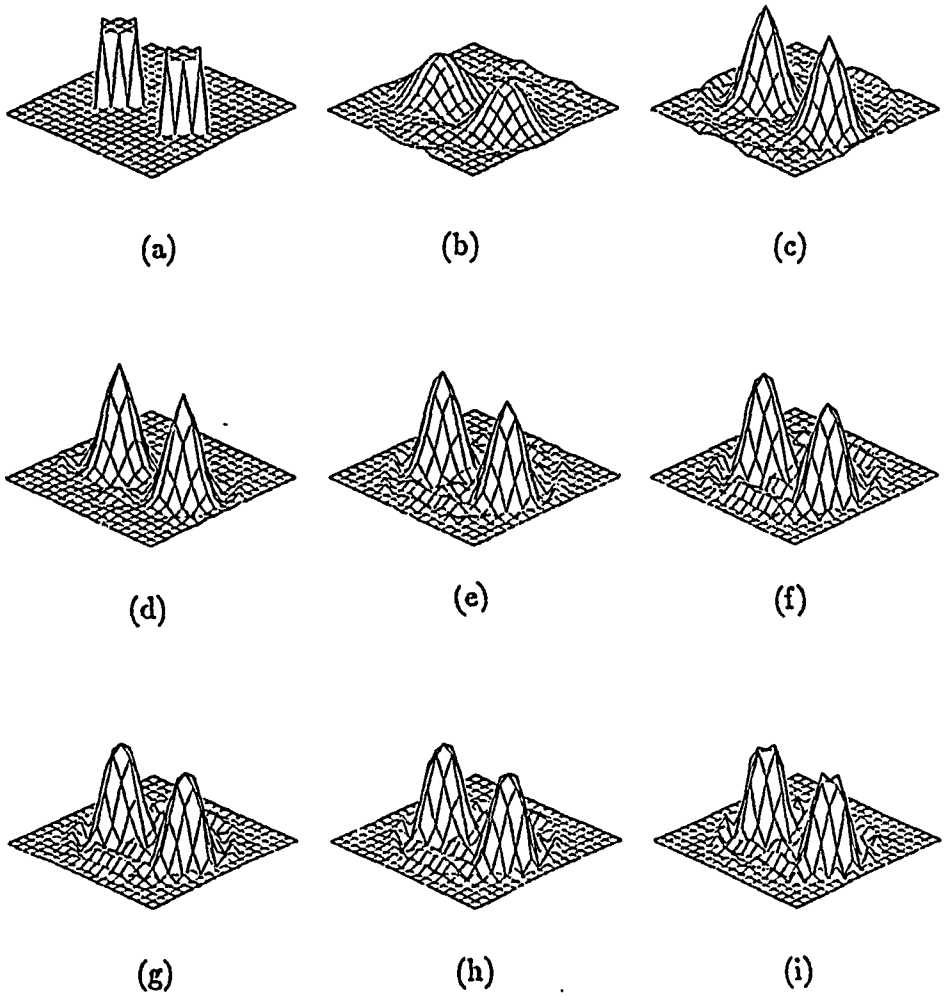

Figure 3.14. Reconstruction of a two-pulse distribution by using the distorted Born iterative method with operating frequency at 100 MHz. The peak value of the relative permittivity is 1.80. The diameter of the object is 3.0 meters. (a) is the original distribution. (b) is the result of the first-order approximation. (c) to (h) are the results from the second iteration to the seventh iteration. (i) is the final convergent solution after fifteen iterations.

$\lambda/2$. The distance between the two pulses is about $\lambda/4$. Figure 3.14(a) is the original distribution. Figure 3.14(b) is the reconstructed distribution of the first-order Born approximation. Figures 3.14(c)–3.14(h) are the reconstructed distributions from the second to the seventh iterations. Figure 3.14(i) is the result after 15 iterations.

Figure 3.15 shows the reconstruction of the same distribution by using the Born iterative method.

Figure 3.16 gives the relative residual error (RRE) of the reconstructed distributions as a function of the iteration steps for both the distorted Born and Born iterative methods.

From this example, we see that both methods successfully distinguish the two pulses from each other. However, the convergent speed of the Born iterative method seems much slower than that of the distorted Born iterative method.

3.3.2.3 Sinelike distribution with noise

Figure 3.17 shows the reconstruction of a sinelike permittivity distribution with 25 dB of the signal-to-noise ratio by using the distorted Born iterative method. The diameter of the object is 1λ. The peak value of the sinelike distribution is 1.8. Figure 3.17(a) is the reconstructed distribution of the first-order Born approximation. Figures 3.17(b)–3.17(e) are the iterative results from the second to fifth iterations. Figure 3.17(f) is the result after a filtering operation which will be described later. The algorithm terminates after five iterations because the relative residual error in the fifth iteration is larger than the RRE in the fourth iteration. The plot of the original permittivity distribution is given in Figure 3.18(a).

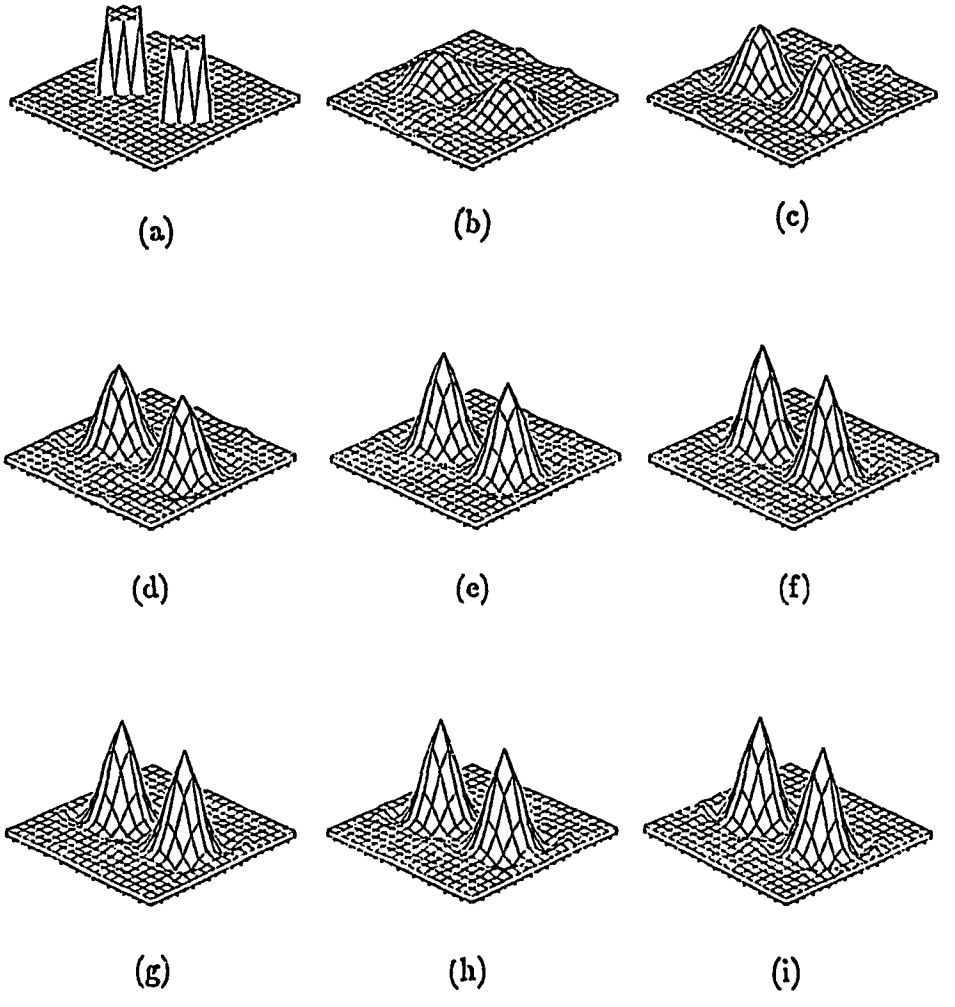

Figure 3.15. Reconstruction of a two-pulse distribution by using the Born iterative method with operating frequency at 100 MHz. The peak value of the relative permittivity is 1.80. The diameter of the object is 3.0 meters. (a) is the original distribution. (b) is the result of the first-order approximation. (c) to (h) are the results from the second iteration to the seventh iteration. (i) is the final convergent solution after fifteen iterations.

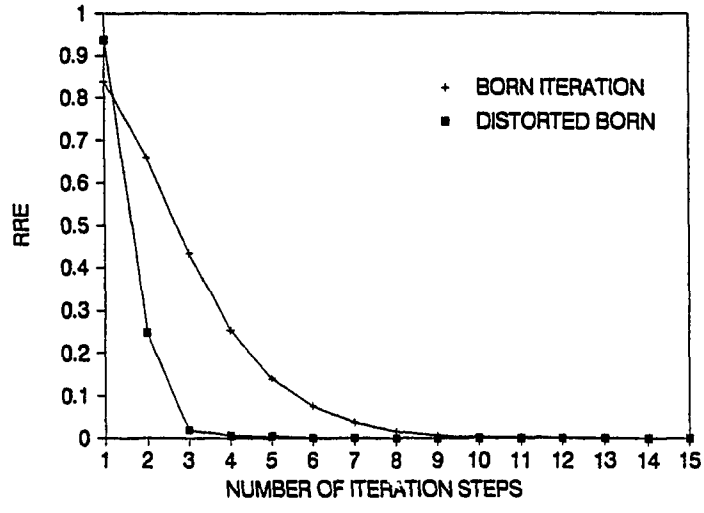

Figure 3.16. The RRE (Relative Residual Error) of the reconstructed permittivity distribution in Figures 3.14 and 3.15 as a function of the iteration steps.

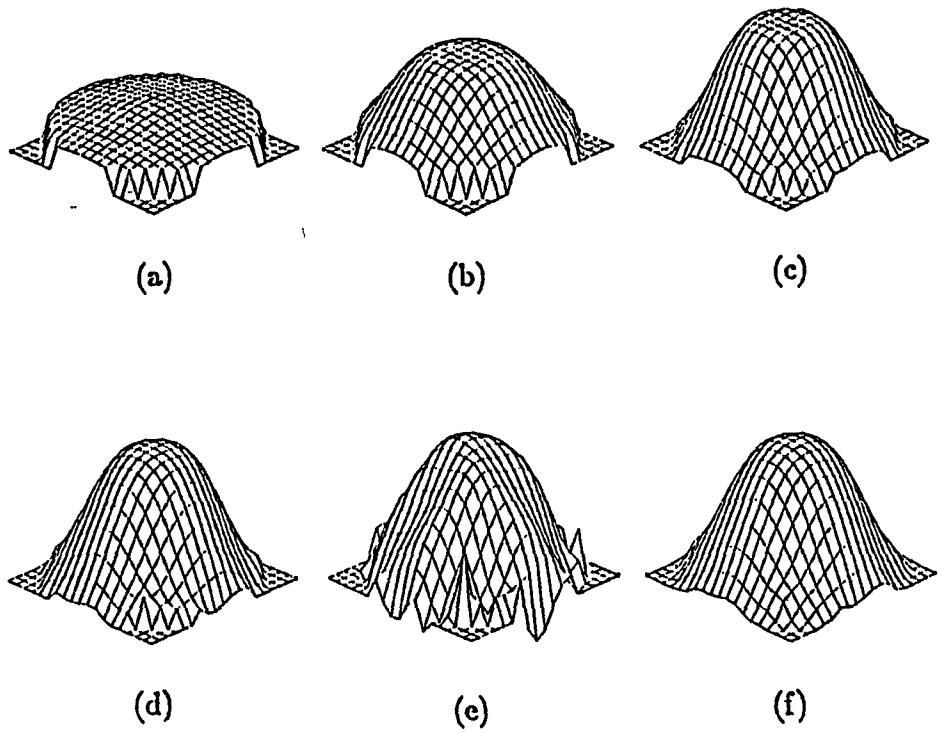

Figure 17. Reconstruction of a sinelike permittivity distribution with a 25 dB signal-to-noise ratio in the measurement field by using the distorted Born iterative method with operating frequency at 100 MHz. The peak value of the relative permittivity is 1.80. The diameter of the object is 1λ. (a) is the original distribution. (b) is the result of the first-order approximation. (c) to (e) are the results from the second iteration to the fourth iteration. (f) is the final distribution after operating the filter function on (d).

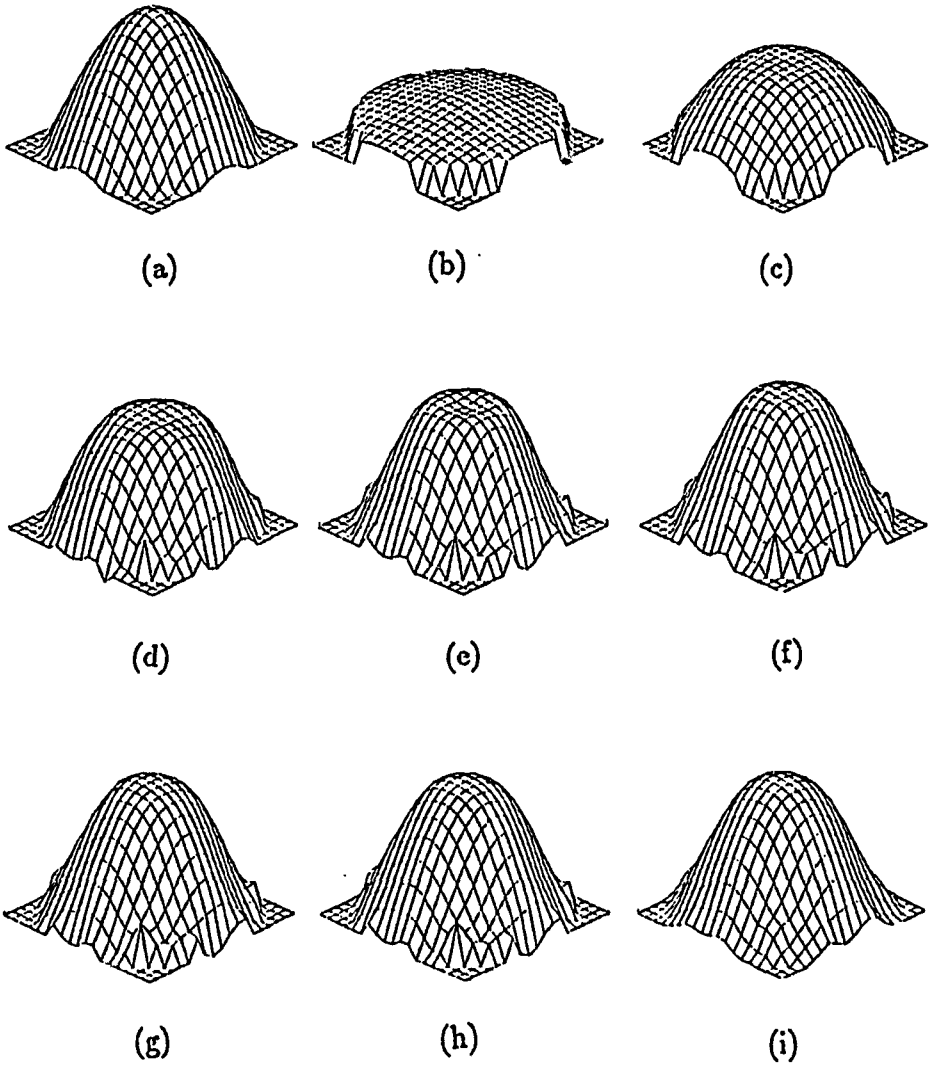

Figure 18. Reconstruction by using the Born iterative method for the same problem given in Figure 17. (a) is the original distribution. (b) is the result of the first-order approximation. (c) to (g) are the results from the second iteration to the sixth iteration. (h) is the convergent distribution after the fifteen iterations. (i) the reconstructed distribution after operating the filter function on (h).

Figure 3.18 shows the reconstruction of the same problem given in the above by using the Born iterative method. Figure 3.18(a) is the original distribution. Figure 3.18(b) is the reconstruction of the first-order Born approximation. Figures 3.18(c)–3.18(g) are the results from the second iteration to the sixth iteration. Figure 3.18(h) is the final result after 15 iterations. Here, we have set the maximum number of steps as 15. Figure 3.18(i) is the filtered result.

Figure 3.19 gives the MSE and the RRE as a function of iteration steps for both the distorted Born and the Born iterative methods. The MSE of the distorted Born iterative method increases at the fifth iteration step. This is consistent with Figure 3.18(e), which is noisier than that of Figure 3.18(d). Fortunately, at the same step, the RRE increases as well (see Figure 3.20(b)) so that the program is terminated after this step. However, the convergent behaviour of the Born iterative method is quite different. Both the RRE and MSE reach the final convergent solution after a few steps and both of them stay at that value until the program terminates after the iteration reaches the maximum number of iteration steps.

When noise exists, unwanted artifacts are present in the reconstructed distribution, which could be easily recognized in Figures 3.17(e) and 3.18(h). This image noise obscures the actual features of the object. For this reason, image filters are used to remove the noise so that the features can be identified [31]. The filter operates by passing a 5-cell window over the image, and replacing the center cell of the window with some function of all the cells in the window. One obvious function would be one that averages all the cells in the window. Unfortunately, this type of filter is too harsh because in addition to removing the noise in the image it also blurs the desired features of the distribution function of the object. In this thesis, the weighted average filter

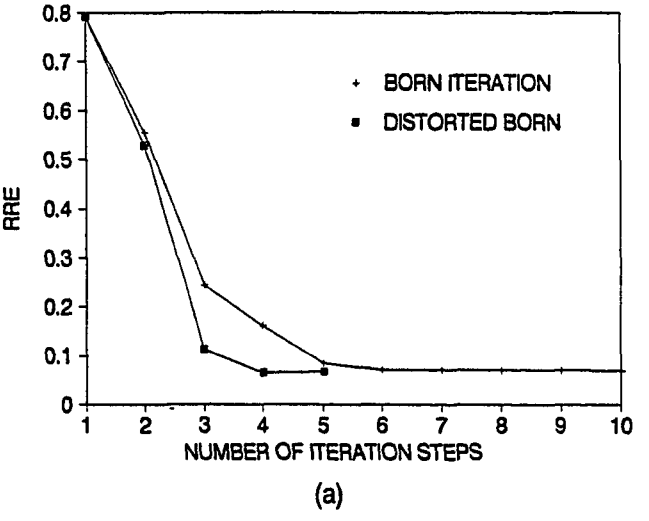

(a)

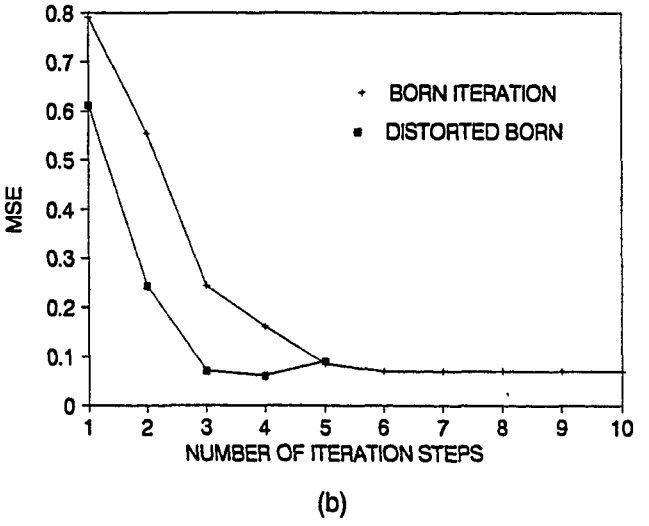

(b)

Figure 3.19. (a) is the RRE (Relative Residual Error) of the reconstructed object function in Figures 3.17 and 3.18 as a function of the iteration steps. (b) is the relative MSE (Mean Square Error) of the reconstructed object function in Figures 3.17 and 3.18 as a function of the iteration steps.

of all the cells in the window has been chosen in which weighting factors are chosen as 1.8 for the center cell and 0.8 for the other cells. Figures 3.18(f) and 3.18(i) are the final reconstructed distributions after applying the filter to Figures 3.17(d) and 3.18(e), respectively. The reason for using Figure 3.17(d) instead of Figure 3.18(e) is that both of the MSE and the RRE at step four are smaller than those at step five such that it is more reliable to use Figure 3.17(d) instead of Figure 3.17(e).

3.3.2.4 Single-pixel pulses

In the investigation of the inverse algorithms, it is of interest to assess the ability and quality of the reconstruction of a single-pixel pulse object function. For a unit height single-pixel pulse, this is also called the point spread function of the algorithm.

First, a unit height single-pixel pulse, that is $\delta\epsilon_r = 1$, will be reconstructed using both the Born and the distorted Born iterative methods.

Figure 3.20 shows the reconstruction of a unit height pulse using the distorted Born iterative method. The dimension of the reconstructed area is about 1λ. The area has been divided into the subobject with 169 pixels/λ^2. The operating frequency is 100 MHz. The unit height single-pixel pulse is located 3 pixels from the center of the object. Figure 3.20(a) is the original distribution. Figure 3.20(b) is the reconstructed distribution of the first-order Born approximation. Figures 3.20(c)–3.20(h) are the reconstructed distributions from the second to the seventh iterations. Figure 3.20(i) is the final convergent solution after 20 iterations.

Figure 3.21 shows the reconstruction of the same distribution by using the Born iterative method. Figure 3.21(a) is the original distribution. Figure

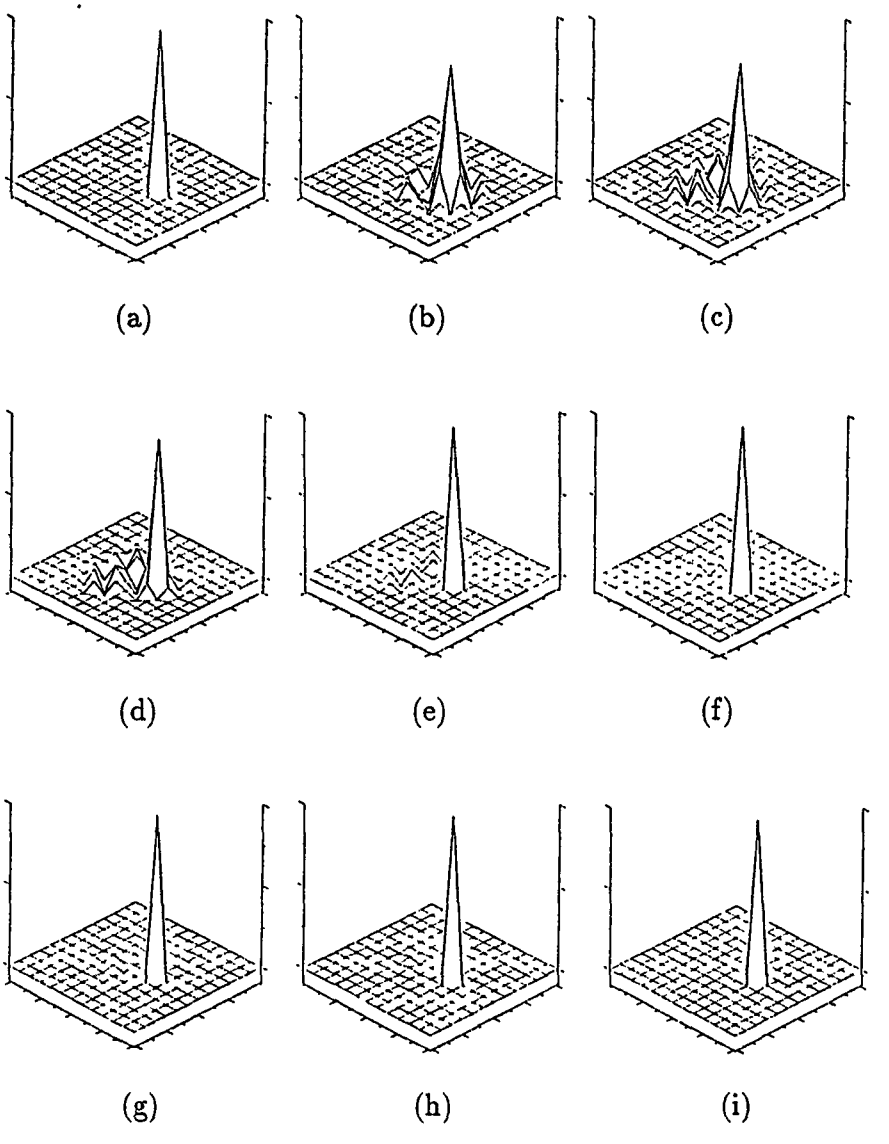

Figure 3.20. Reconstruction of a single-pixel pulse distribution by using the distorted Born iterative method with operating frequency at 100 MHz. The contrast of the relative permittivity is 1:2. The diameter of the reconstructed area is 1.5 meters. (a) is the original distribution. (b) is the result of the first-order approximation. (c) to (h) are the results from the second iteration to the seventh iteration. (i) is the final convergent solution after twenty iterations.

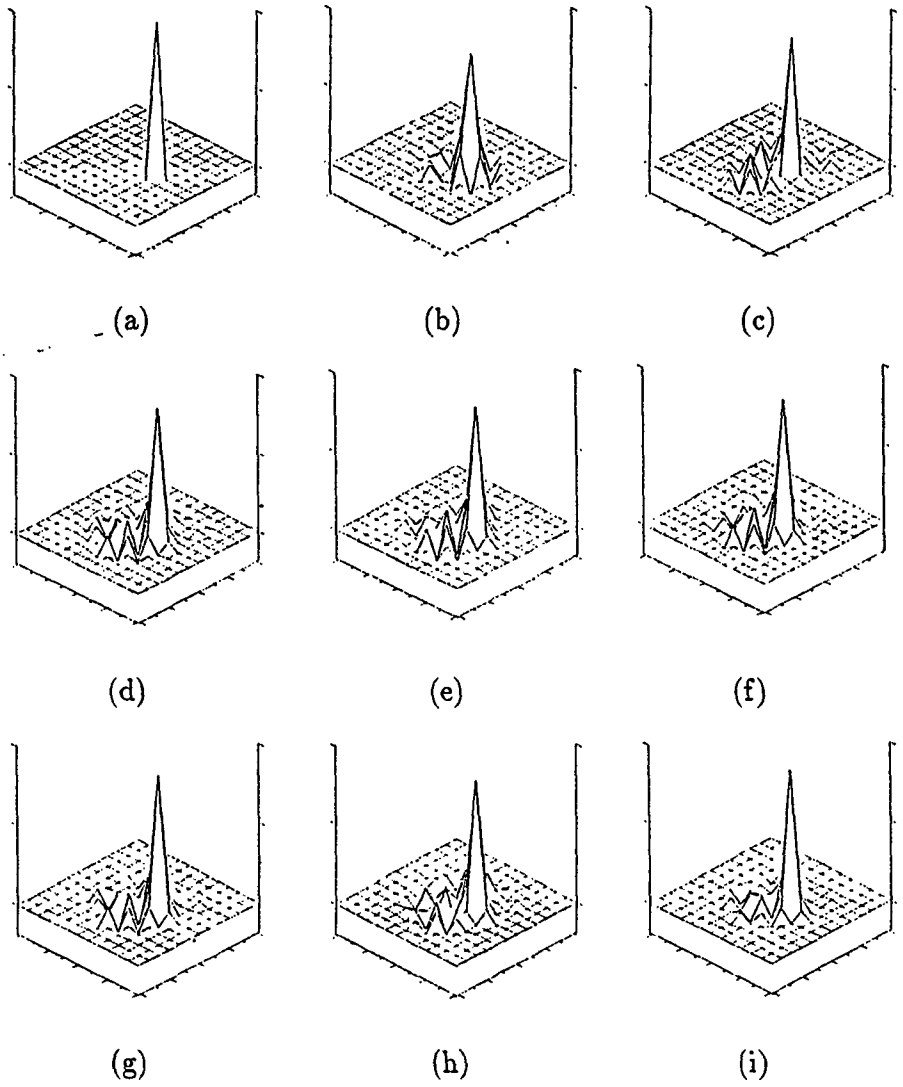

Figure 3.21. Reconstruction of a single-pixel pulse distribution by using the Born iterative method with operating frequency at 100 MHz. The contrast of the relative permittivity is 1:2. The diameter of the reconstructed area is 1.5 meters. (a) is the original distribution. (b) is the result of the first-order approximation. (c) to (h) are the results from the second iteration to the seventh iteration. (i) is the final convergent solution after twenty-five iterations.

3.21(b) is the reconstructed distribution of the first-order Born approximation. Figures 3.21(c)–3.21(h) are the reconstructed distributions from the second to the seventh iterations. Figure 3.21(i) is the final convergent solution after 25 iterations.

This example demonstrates that the distorted Born iterative method possesses much better ability to reconstruct the single-pixel pulse than the Born iterative method. Actually, the final convergent solution of the distorted Born iterative method shown in Figure 3.20(i) is identical to the original distribution shown in Figure 3.20(a). Meanwhile, the final convergent solution of the Born iterative method demonstrates a strong low-pass filter effect which could be recognized easily from the noise of the background in the reconstructed object function. The sharp image obtained by the distorted Born iterative method reveals that generally the distorted Born iterative method possesses better ability to reconstruct the fine-structure of the object function than the Born iterative method. In other word, the distorted Born iterative method should give better resolution of the reconstructed object than the Born iterative method.

As the second example of the reconstruction of the single-pixel pulse function, Figure 3.22 shows the reconstruction of a single-pixel pulse with the height of 11, that is, $\delta\epsilon_r = 11$, by using the distorted Born iterative method. The other configurations and parameters are the same as those in the last example. Figure 3.22(a) is the original distribution. Figure 3.22(b) is the reconstructed distribution of the first-order Born approximation. Figures 3.22(c)–3.22(n) are the reconstructed distributions from the second to the thirteenth iterations. Figure 3.22(o) is the final convergent solution after 20 iterations.

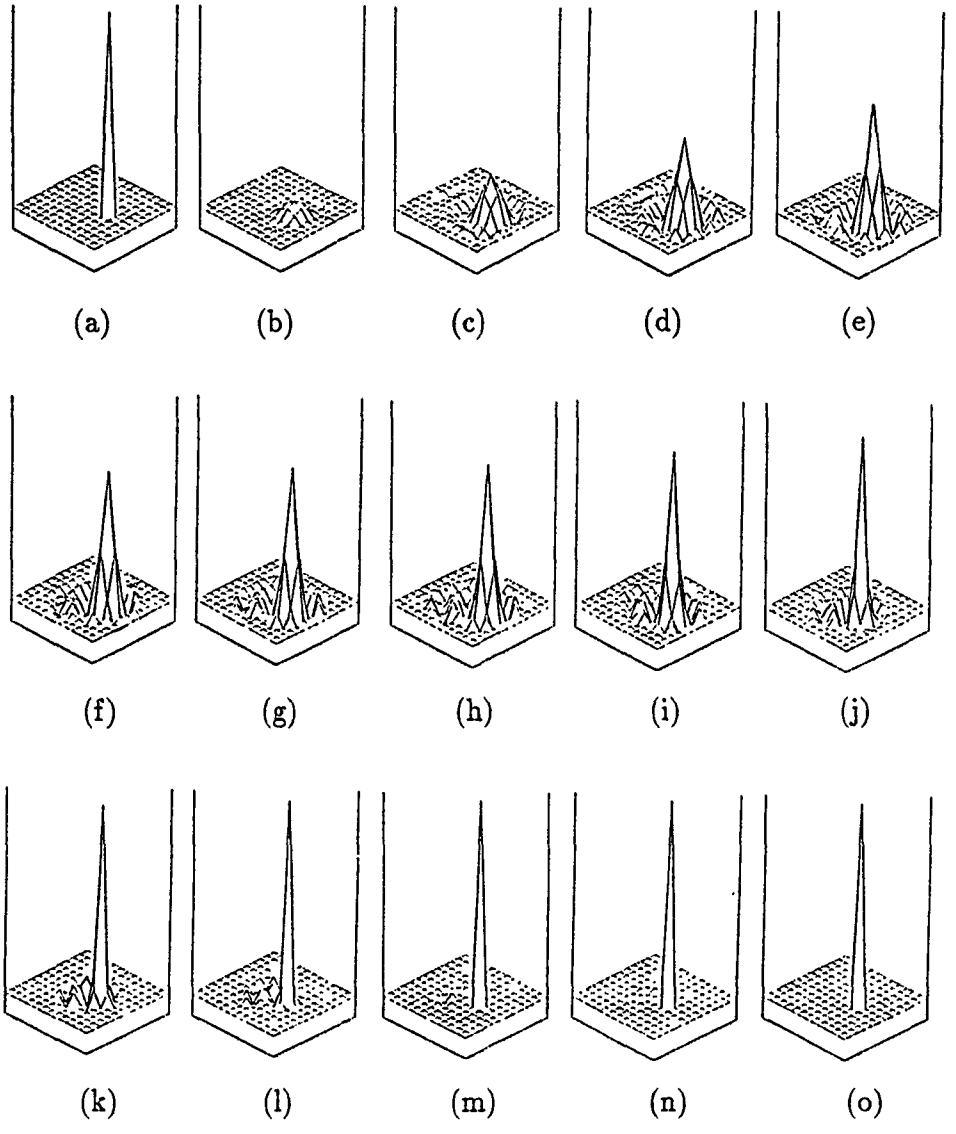

Figure 3.22. Reconstruction of a single-pixel pulse distribution by using the distorted Born iterative method with operating frequency at 100 MHz. The contrast of the relative permittivity is 1:1.1. The diameter of the reconstructed area is 1.5 meters. (a) is the original distribution. (b) is the result of the first-order approximation. (c) to (n) are the results from the second iteration to the thirteenth iteration. (o) is the final convergent solution after twenty iterations.

The last example shows that the distorted Born iterative method works quite well for the reconstruction of very high contrast single-pixel pulse object functions.

In order to investigate the resolution of the algorithm, Figure 3.23 gives the reconstruction of two single-pixel pulses separated by one pixel whose width is about 0.08λ by using the distorted Born iterative method. The height of the two pulses is 1. The other configurations and the parameters are the same as those of the example shown in Figure 3.21. The final result, shown in Figure 3.23, is surprisingly good. The final convergent solution is almost exactly identical to the original object function.

3.3.2.5 Complex permittivity distribution

In this example, the object function is a complex permittivity distribution

$$\epsilon_r(\rho) = \epsilon_r'(\rho) + i\epsilon_r''(\rho),$$

where

$$\epsilon_r'(\rho) = 2.0\cos(\frac{\pi\rho}{2a_0}), \quad \rho \leq a_0,$$

$$\epsilon_r''(\rho) = 0.6\cos(\frac{\pi\rho}{2a_0}), \quad \rho \leq a_0.$$

Figures 3.24 and 3.25 show the reconstruction of the above distribution by the distorted Born iterative method. Shown in Figure 3.24 is the convergent process of the real part of the permittivity distribution. The reconstruction of the imaginary part of the permittivity distribution is given in Figure 3.25. The diameter of the object is 1.5 m. The operating frequency is 100 MHz. In both of the figures, (a) is the original distribution; (b) is the first-order iterative solution or the Born approximation; (c) to (h) are the results from

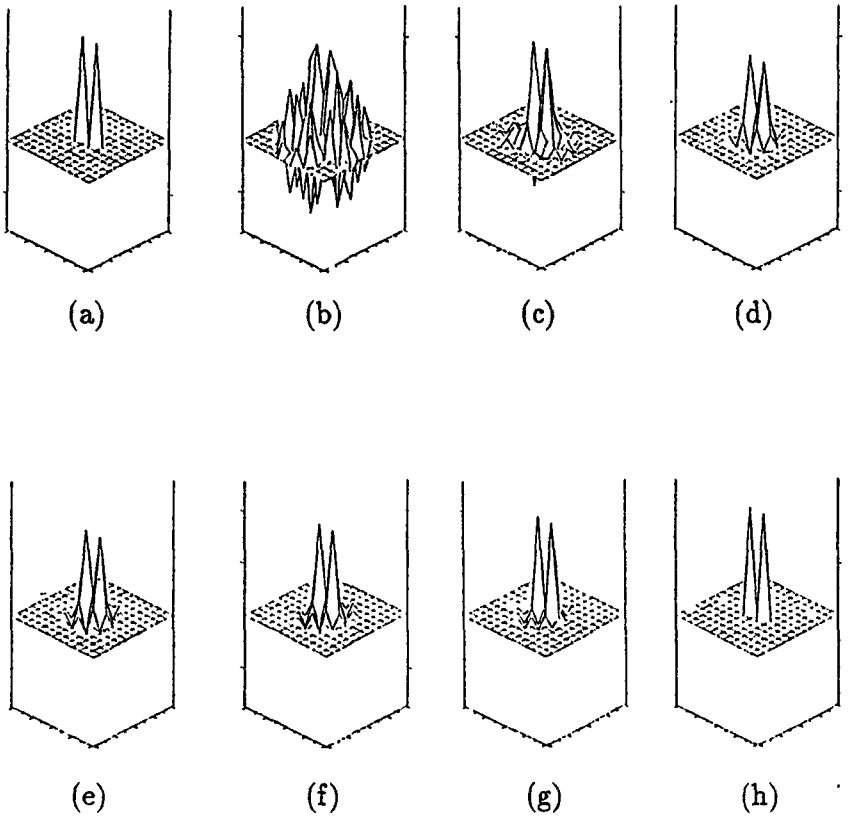

Figure 3.23. Reconstruction of a two single-pixel pulses seperated by one pixel using the distorted Born iterative method with operating frequency at 100 MHz. The contrast of the relative permittivity is 1:2. The diameter of the reconstructed area is 1.5 meters. (a) is the original distribution. (b) is the result of the first-order approximation. (c) to (g) are the results from the second iteration to the seventh iteration. (h) is the final convergent solution after twenty iterations.

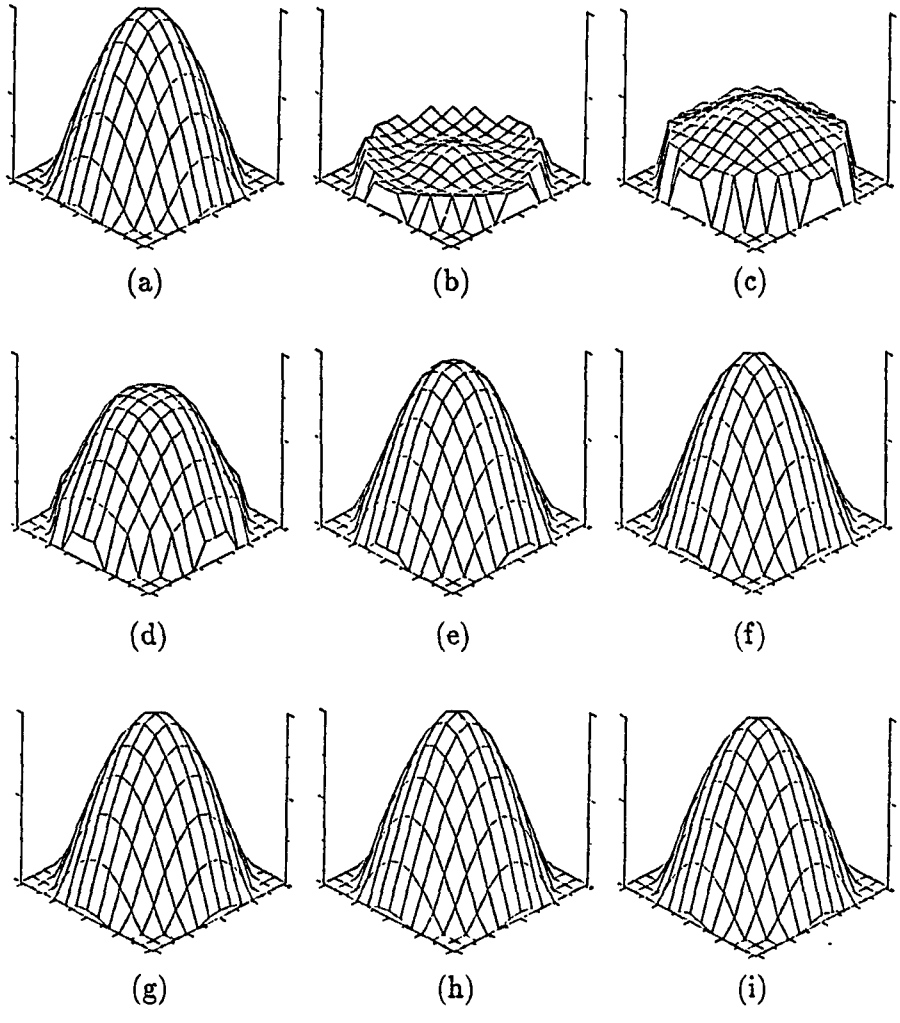

Figure 3.24. Evolution of the convergence of the real part of a complex permittivity distribution reconstructed by using the distorted Born iterative method with operating frequency at 100 MHz. The peak value of the real part of the relative permittivity is 2. The diameter of the object is 1.5 meters. (a) is the original distribution. (b) is the result of the first-order approximation. (c) to (h) are the results from the second iteration to the seventh iteration. (i) is the final convergent solution after twenty iterations.

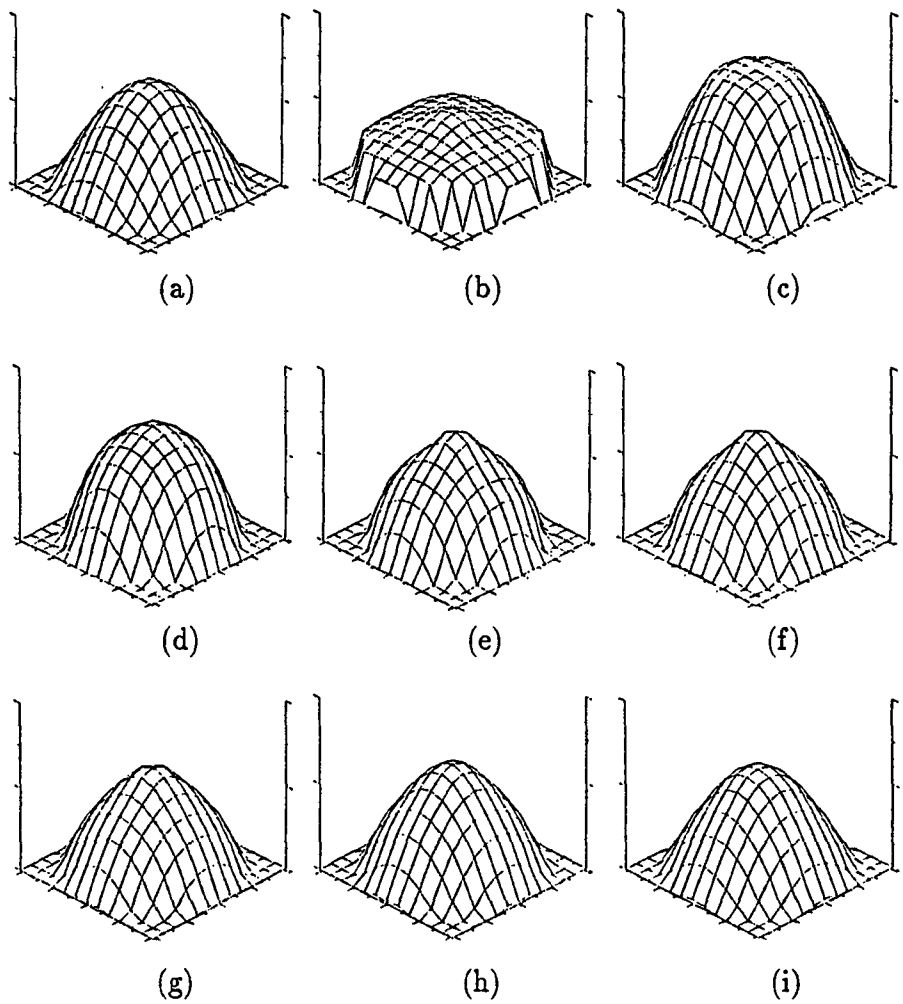

Figure 3.25. Evolution of the convergence of the imaginary part of the reconstructed complex permittivity distribution by using the distorted Born iterative method with operating frequency at 100 MHz. The peak value of the imaginary part of the relative permittivity is 0.6. The diameter of the object is 1.5 meters. (a) is the original distribution. (b) is the result of the first-order approximation. (c) to (h) are the results from the second iteration to the seventh iteration. (i) is the final convergent solution after twenty iterations.

the second iteration to the seventh iteration; and (i) is the final convergent solution after 20 iterations.

Figures 3.26 and 3.27 show the reconstruction of the same distribution as the above by using the Born iterative method. Figure 3.26 gives the result of the reconstruction of the real part of the permittivity distribution, and Figure 3.27 is the result of the reconstruction of the imaginary part of the permittivity distribution. In both of the figures, (a) is the original distribution; (b) is the first-order solution; (c) to (h) are the results from the second iteration to the seventh iteration; and (i) is the final convergent solution after 20 iterations.

Figure 3.28 gives the relative mean square error (MSE) and the relative residual error (RRE) in the reconstruction procedure as a function of the iteration steps for the last example. It is clear that the convergent speed of the distorted Born iterative method is much faster than that of the Born iterative method. Meanwhile, the final convergent solution of the distorted Born iterative method is more accurate than that of the Born iterative method, which could be easily recognized from the MSE and the RRE of the final solution for both methods.

3.4 Discussions and Conclusions

In the above section, the examples are given for both the distorted Born iterative and the Born iterative methods to reconstruct the permittivity profiles. In the noiseless cases, the distorted Born iterative method displays faster convergence than the Born iterative method. However, for the noisy cases, the Born iterative method is more robust than the distorted Born iterative method. The example given in this thesis with the noisy case for the distorted Born iterative method is acceptable because the program is

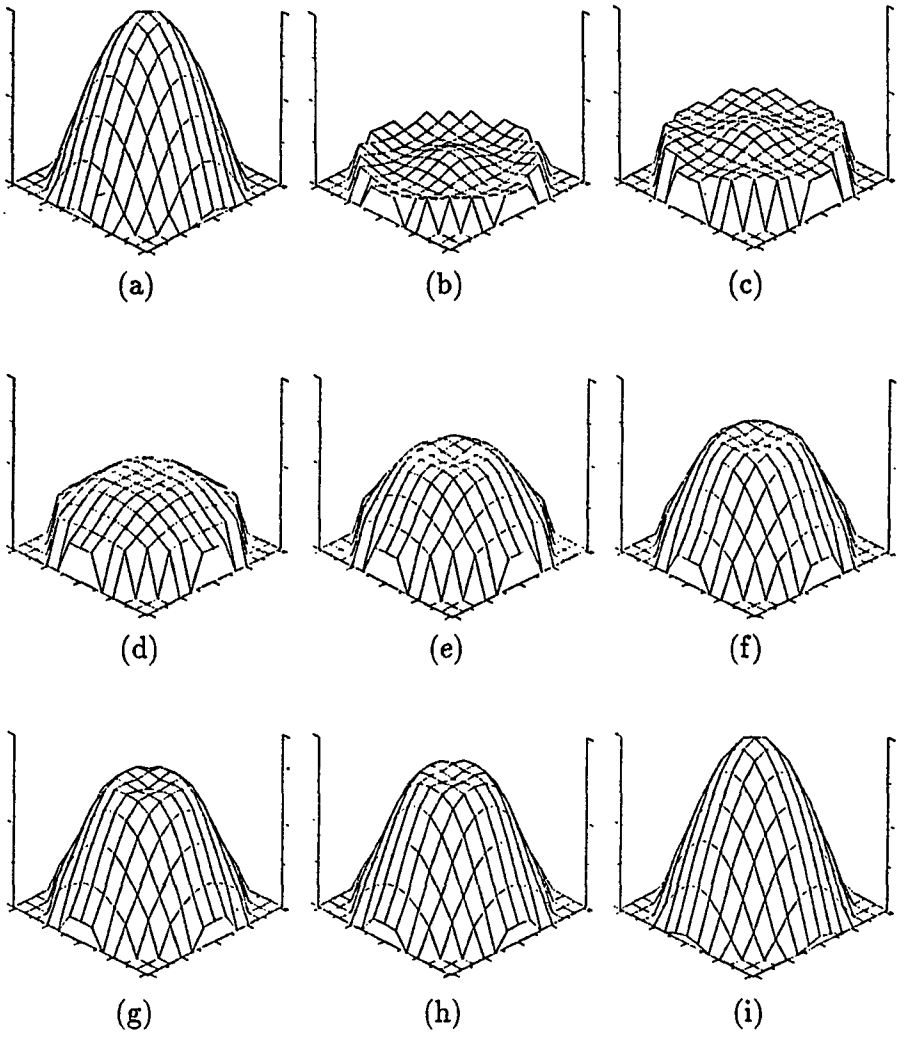

Figure 3.26. Evolution of the convergence of the real part of the reconstructed complex permittivity distribution by using the Born iterative method with operating frequency at 100 MHz. The peak value of the real part of the relative permittivity is 0.6. The diameter of the object is 3.0 meters. (a) is the original distribution. (b) is the result of the first-order approximation. (c) to (h) are the results from the second iteration to the seventh iteration. (i) is the final convergent solution after twenty iterations.

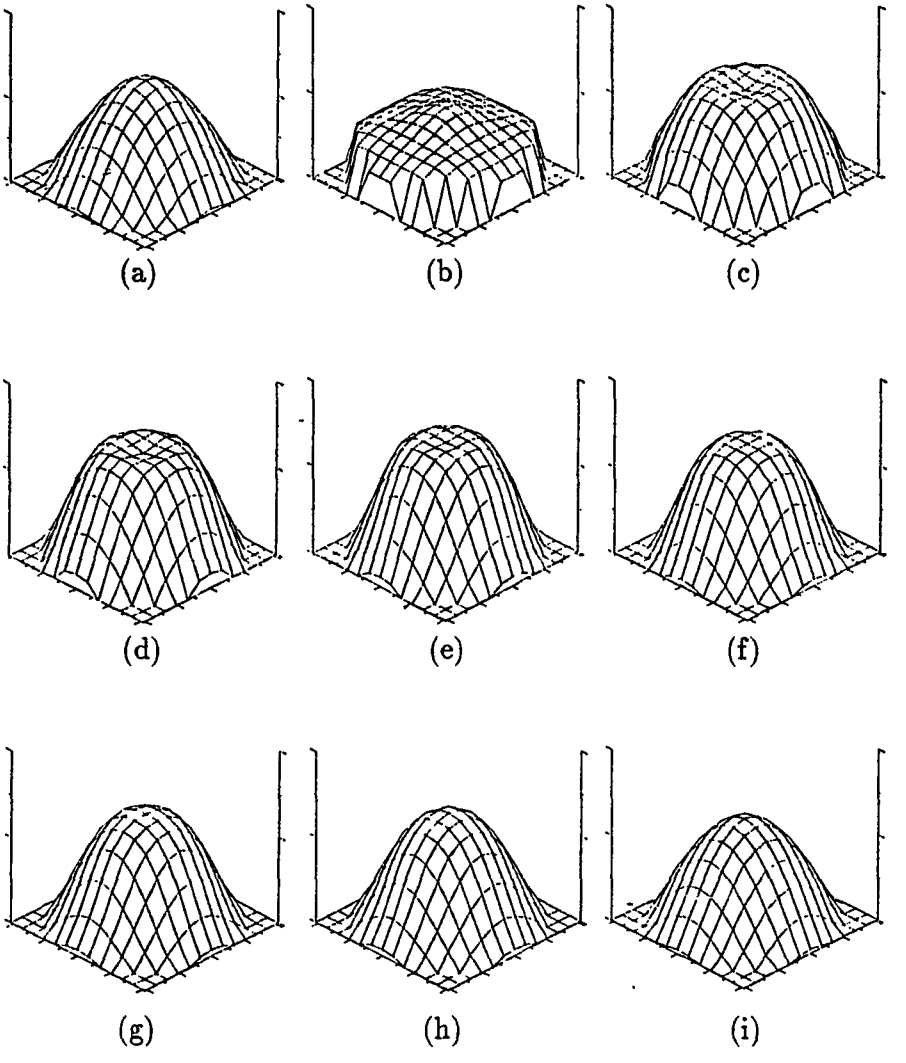

Figure 3.27. Evolution of the convergence of the imaginary part of the reconstructed complex permittivity distribution by using the Born iterative method with operating frequency at 100 MHz. The peak value of the imaginary part of the relative permittivity is 0.6. The diameter of the object is 3.0 meters. (a) is the original distribution. (b) is the result of the first-order approximation. (c) to (h) are the results from the second iteration to the seventh iteration. (i) is the final convergent solution after twenty iterations.

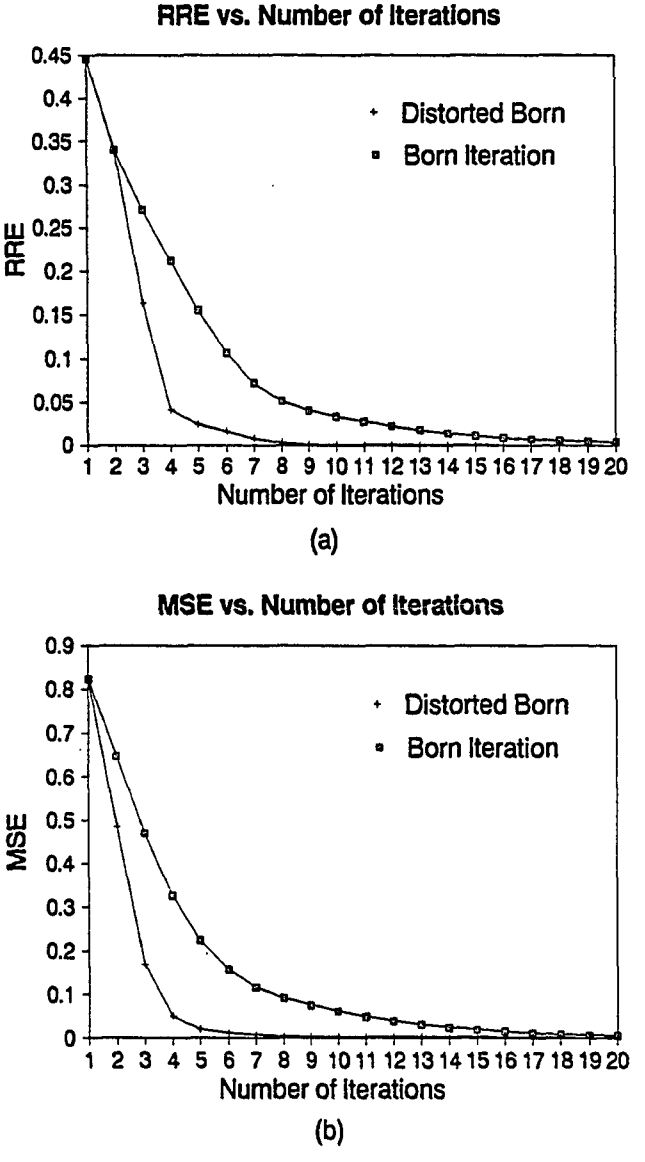

Figure 3.28. (a) is the RRE (Relative Residual Error) in the reconstruction of the complex permittivity distributions in Figures 3.24, 3.25, 3.26, and 3.27 as a function of the iteration steps. (b) is the relative MSE (Mean Square Error) in the reconstruction of the complex permittivity distribution in Figures 3.24, 3.25, 3.26, and 3.27 as a function of the iteration steps.

terminated immediately just after the MSE increases. However, if the MSE and the RRE do not increase at the same step, the final reconstructed profile could be quite noisy. The reason why the distorted Born iterative method is more susceptible to noise contamination is explained in the following paragraph.

The left-hand side of Equation (3.2.4), which is the measured scattered field by the object with the free-space background, is unchanged in the iterative process for the Born iterative method. However, for the distorted Born iterative method, the scattered field from the last reconstructed distribution has to be subtracted from the measurement data on the left-hand side of Equation (3.2.4). If the noise is added in the scattered field at the beginning (in our case, a 25 dB signal-to-noise ratio, which is equivalent to about 5.6% random noise, has been added in the examples given in Figures 10 and 11), then after a few iterations, the noise will dominate the left-hand side of Equation (3.2.4). Consequently, the correction of the distribution after that step contributes only to the noise of the constructed distribution and no more information about the object could be derived.

In conclusion, two algorithms for solving two-dimensional nonlinear electromagnetic inverse scattering problems have been proposed. The algorithms have been successfully applied to the reconstruction of the dielectric distribution functions in a wide range of situations where the Born approximation fails. It turns out, according to the results of the numerical simulations, that the maximum contrast of the dielectric constant can be relaxed by a factor of ten compared to that for the Born approximation. The maximum contrast we can reconstruct using the iterative algorithms is when δka is about 0.8, where a is the diameter of the object if we start our algorithms from a homogeneous background medium. The relaxation of the criteria is important in

many areas of the inverse scattering applications, such as medical imaging, nondestructive testing, and geophysical explorations. Meanwhile, the simulation results demonstrate that each method has its advantages. The distorted Born iterative method shows a faster convergence rate compared to that for the Born iterative method, while the Born iterative method is more robust to noise contamination compared to the distorted Born iterative method.

References

[1] A. J. Devaney, "A computer simulation study of diffraction tomography," *IEEE Trans. Biomed. Eng.*, vol. BME-30, pp. 377–386, 1983.

[2] M. Azimi and A. C. Kak, "Distortion in diffraction tomography caused by multiple scattering," *IEEE Trans. Med. Imaging*, vol. MI-2, pp. 176–195, 1983.

[3] W. Tabbara, B. Duchêne, Ch. Pichot, D. Lesselier, L. Chommeloux and N. Joachimowicz, "Diffraction tomography: contribution to the analysis of applications in microwaves and ultrasonics," *Inverse Problem*, vol. 4, pp. 305–331, 1988.

[4] A. J. Devaney, "A filtered backpropagation algorithm for diffraction tomography," *Ultrasonic Imaging*, vol. 4, pp. 336–360, 1982.

[5] J. B. Keller, "Accuracy and validity of the Born and Rytov approximations," *J. Opt. Soc. Amer.*, vol. 59, pp. 1003–1004, 1969.

[6] M. Slaney, A. C. Kak, and L. E. Larsen, "Limitations of imaging with first-order diffraction tomography," *IEEE Trans. Microwave Theory Tech.*, vol. MTT-32, no. 8, pp. 860–874, 1984.

[7] A. J. Tijhuis, "Iterative determination of permittivity and conductivity profiles of a dielectric slab in time domain," *IEEE Trans. Antennas Propagat.*, vol. AP-29(3), pp. 239–245, 1981.

[8] W. C. Chew and S. L. Chuang, "Profile inversion of a planar medium with a line source or a point source," paper presented at International Geoscience and Remote Sensing Symposium, Inst. of Electr. and Electron. Eng., Strasbourg, France, 1984.

[9] T. M. Habashy, W. C. Chew, and E. Y. Chow, "Simultaneous reconstruction of permittivity and conductivity profiles in a radially inhomogeneous slab," *Radio Sci.*, vol. 21, no. 4, pp. 635–645, 1986.

[10] E. Wolf, "Three-dimensional structure determination of semi-transparent

objects from holographic data," *Opt. Commun.*, vol. 1, pp. 153–169, 1969.

[11] D. K. Ghodgonkar, O. P. Gandhi, and M. J. Hagmann, "Estimation of complex permittivities of three-dimensional inhomogeneous biological bodies," *IEEE Trans. Microwave Theory Tech.*, vol. MTT-31, pp. 442–446, June 1983.

[12] M. M. Ney, A. M. Smith, and S. S. Stuchly, "A solution of electromagnetic imaging using pseudoinverse transformation," *IEEE Trans. Med. Imaging*, vol. MI-3, no. 4, pp. 155–162, Dec. 1984.

[13] N. Bleistein and J. K. Cohen, "Nonuniqueness in the inverse source problem in acoustics and electromagnetics," *J. Math. Phys.*, vol. 18, pp. 194–201, Feb. 1977.

[14] A. J. Devaney and G. C. Sherman, "Nonuniqueness in inverse source and scattering problems," *IEEE Trans. Antennas Propagat.*, vol. 8, pp. 1034–1042, Sept. 1982.

[15] A. J. Devaney and E. Wolf, "Radiating and nonradiating classical current distributions and the fields they generate," *Phys. Rev. D*, vol. 8, pp. 1044–1047, Aug. 1973.

[16] S. A. Johnson and M. L. Tracy, "Inverse scattering solutions by a sinc basis, multiple source, moment method – part I: theory," *Ultrasonic Imaging*, vol. 5, pp. 361–375, 1983.

[17] S. A. Johnson and M. L. Tracy, "Inverse scattering solutions by a sinc basis, multiple source, moment method – part II: numerical evaluations," *Ultrasonic Imaging*, vol. 5, pp. 376–392, 1983.

[18] T. J. Cavicchi, S. A. Johson, and W. D. O'Brien, "Application of the sinc basis moment method to the reconstruction of infinite circular cylinders," *IEEE Trans. Ultrasonics, Ferroelectrics, and Frequency Control*, vol. 35, no. 1, pp. 22–33, 1988.

[19] T. J. Cavicchi and W. D. O'Brien, "Numerical study of high-order diffrac-

tion tomography via the sinc basis moment method," *Ultrasonic Imaging*, vol. 11, pp. 42–74, 1989.

[20] Y. M. Wang and W. C. Chew, "An iterative solution of two-dimensional electromagnetic inverse scattering problem," *Int. J. Imaging Syst. Technol.*, vol. 1, pp. 100–108, 1989.

[21] W. C. Chew and Y. M. Wang, "Reconstruction of two-dimensional permittivity using the distorted Born iterative method", *IEEE Trans. Med. Imaging*, vol. MI-9, no. 2, pp. 218–225, 1990.

[22] J. Richmond, "Scattering by a dielectric cylinder of arbitrary cross-sectional shape," *IEEE Trans. Antennas Propagat.*, vol. AP-13, pp. 334–341, 1965.

[23] R. F. Harrington, *Field Computation by Moment Methods*. Malabar, Florida: Krieger Publishing, 1983.

[24] C. T. H. Baker, *The Numerical Treatment of Integral Equations*. Oxford: Clarendon, 1977.

[25] A. N. Tikhonov, "On the problems with approximately specified information," in *Ill-Posed Problems in the Natural Sciences*, A. N. Tikhonov and A. V. Goncharsky, Eds. Moscow: MIR Publishers, 1987.

[26] A. V. Goncharsky, "Ill-posed problems and their solution methods," in *Ill-Posed Problems in the Natural Sciences*, A. N. Tikhonov and A. V. Goncharsky, Eds. Moscow: MIR Publishers, 1987.

[27] S. Twomey, *Introduction to the Mathematics of Inversion in Remote Sensing and Indirect Measurements*. New York: Elsevier Scientific, 1977.

[28] A. Tarantola, *Inverse Problem Theory - Methods for Data fitting and Model Parameter Estimation*. Amsterdam: Elsevier, 1987.

[29] W. C. Chew, *Waves and Fields in Inhomogeneous Media*. New York: Van Nostrand Reinhold, 1990.

[30] V. B. Glasko, *Inverse Problems of Mathematical Physics*. New York: American Institute of Physics, 1988.

[31] M. Frank and C. A. Balanis, "Method for improving the stability of electromagnetic geophysical inversions," *IEEE Trans. Geosci. Remote Sensing*, vol. 27, no. 3, pp. 339-343, May 1989.

CHAPTER 4

LIMITED ANGLE INVERSE SCATTERING PROBLEMS AND ADDITIONAL RESULTS

4.1 Introduction

Limited angle inverse scattering problems are frequently encountered in many applications. In the limited angle inverse problem, the receivers and transmitters are confined to specific regions enforced by the problem. The effect of the limited view angles is a significant reduction of the information content obtained from the measurement data. As a result, the ill-posedness of the problem is further aggravated. In order to retrieve the maximum amount of information from the limited angle inverse problem, a boosting procedure is introduced in Section 4.2 from a physical point of view. The simulation results given in Section 4.2.3 verified the importance of the boosting procedure in the limited angle inverse scattering problems.

Implementation of the Born and the distorted Born iterative methods discussed in Chapter 3 requires solving the linear system equations in both the direct scattering and inversion parts of the algorithms. By using the Gaussian elimination for the solution of the pertinent linear system equations, the computational complexity of the algorithms will be N^3. The rapid increase of the computer time with the number of unknowns prevents us from applying the algorithm to the solutions of large objects. In order to reduce the computational complexity of the algorithms, the fast recursive operator algorithm discussed in Chapter 2 is applied to the solution of the direct scattering part of the algorithm. The results are presented in

Section 4.3. Meanwhile, the conjugate gradient method is applied to the solution of the inversion part of the iterative algorithm. As a result, the overall computational complexity of the accelerated algorithm is N^2. The result in Section 4.3 shows that significant reduction of the computational time has been achieved by the accelerated algorithm.

4.2 Limited Angle Inverse Scattering Problems

4.2.1 Introduction

Geophysical diffraction tomography has been investigated by several authors [1-5] in the framework of the Born and Rytov approximations for the weak scattering cases. The effects of the limited view angles on the experimental setup result in the further confinement of the image function in the Fourier transform space [5]. Beyond the Born approximation, the inherent nonlinearity of the inverse scattering problem has to be accounted for. For a full-angle problem in which receivers and transmitters are placed in a circle which completely surrounds the object, several methods have been reported for the solution of the problem [6-11]. However, in the limited angle inverse scattering problem, since the receivers and transmitters are restricted to specific regions enforced by the experimental setup for geophysical applications, the information content obtained from the measurement data is significantly limited. Meanwhile, the restriction on the locations of the receivers and transmitters results in further constraints on the experimental setup. The combined effect of the limited information content and the restriction on the locations of receivers and transmitters further aggravates the ill-conditioning of the problem. As a result, part of the valuable information in the measurement data corresponding to the small eigenvalues of the matrix equation will be lost in the regularization procedures.

In principle, there is no difference between the conventional inverse scattering problem and limited angle inverse scattering problem. Both of them reconstruct the image from the remote measurement data by solving a pertinent integral equation. However, the two types of problems differ significantly from a numerical viewpoint. As we know, in the conventional or full angle inverse scattering problem, both receivers and transmitters are located in a full circle which completely surrounds the object to be imaged. In contrast, for the limited angle inverse scattering problem, such as well-to-well tomography, locations of the receivers and transmitters are restricted to the specific regions determined by the specific application at hand, and they do not completely surround the object being reconstructed. The restricted locations of the receivers and transmitters in the limited angle inverse problem make the information contained in the measurement data more incomplete than that in the full-angle inverse scattering problem.

To reconstruct the object function properly, a boosting procedure is proposed in Section 4.2.2 based on a physical viewpoint. In Section 4.2.3, some numerical simulations are given to demonstrate the significance of the boosting procedure for geophysical explorations. The importance of the procedure could be easily recognized from the simulations.

4.2.2 Boosting procedure

The limited angle inverse scattering problem is defined as an inverse scattering problem in which the locations of the receivers and transmitters are restricted in some regions which cannot completely surround the object to be detected. This kind of problem occurs frequently in geophysical explorations because of the restriction on the experimental setup in most applications.

Shown in Figure 4.1 are two typical geometrical configurations of the limited angle problems in geophysical explorations. The effect of the limited angle measurement data results in the reduction of the information content contained in the measurements. The reduction of the information content aggravates the ill-conditioning of the problem further rendering its solution more difficult.

The Born iterative and the distorted Born iterative algorithms summarized in the preceding section have been successfully applied to the solution of the conventional inverse scattering problem in which the receivers and transmitters are located on a circle completely surrounding the object [6,7]. However, in geophysical explorations, because of limited angle measurements, both methods encounter difficulty in obtaining good reconstructions or, sometimes, obtaining any convergent solutions. The difficulty is not from the algorithms used but from the sparsity of the information collected in the limited angle inverse scattering problem. The sparsity of the information content in the measurement data aggravates the ill-conditioning of the linear system matrix in the linearized inversion procedure at each iteration step. After applying the regularization procedure, a considerable amount of information in the measurement data is overwhelmed by the regularization matrix in order to circumvent the ill-conditioning of the linear system equation. Consequently, the amount of information that can be retrieved from the measurement data is further reduced. The reduction of the information content makes it difficult to reconstruct the permittivity distribution in geophysical explorations or in any limited angle inverse scattering problems.

In order to find a remedy, we need to examine the problem more closely. There are two factors which contribute to the above difficulty. One is the reduction of the information content in the limited angle inverse scattering

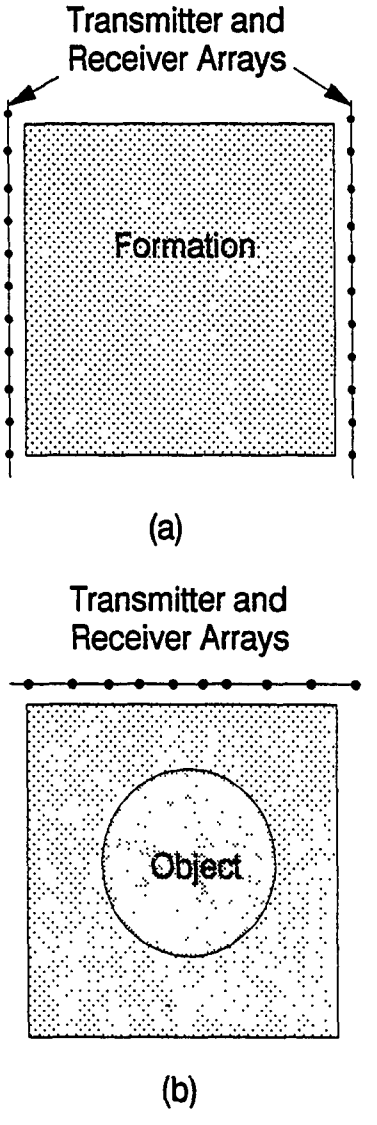

Figure 4.1. (a) is the geometrical configuration for well-to-well tomography. (b) is the geometrical configuration for subsurface detection.

problems. The other is the nonideal arrangement of the experimental setup which comes from the restrictions on the locations of the receivers and the transmitters. The first factor cannot be removed because of the nature of the problem. For instance, in subsurface detection, the transmitters and receivers are restricted to the ground above the object to be detected (see Fig. 4.1(b)). If we suppose that the probed region is finite, then the angle spanned at the center of the object by the transmitter and receiver array will be about 100 degrees for most realistic situations because of the limited length of the transmitter and receiver array. For the second factor, we need to examine more carefully how the locations of the receivers or transmitters contribute to the aggravation of the ill-conditioning problem. Here, only the effect of receiver locations will be investigated. The effect of transmitter locations follows immediately from the reciprocity theorem between the source point and the observation point. To simplify our analysis, we will consider a 2-D case and use the the first-order approximation of Equation (3.2.4) in the following discussion. Under these assumptions, the kernel of the integration in the inverse scattering problem is a product of the Green's function and the incident field. Figure 4.2 gives the locations of two receivers in a limited angle inverse scattering problem. Suppose that receiver A is located at point A and receiver B is located at point B, and $\boldsymbol{\rho}_B > \boldsymbol{\rho}_A$; then, the integral equations corresponding to receivers A and B are

$$E_{sca}(\boldsymbol{\rho}_A) = \iint_S \frac{i}{4} H_0^{(1)}(|\boldsymbol{\rho}_A - \boldsymbol{\rho}'|) k_0^2 \delta\epsilon_r(\boldsymbol{\rho}') E_{inc}(\boldsymbol{\rho}') d\boldsymbol{\rho}', \tag{4.2.1}$$

$$E_{sca}(\boldsymbol{\rho}_B) = \iint_S \frac{i}{4} H_0^{(1)}(|\boldsymbol{\rho}_B - \boldsymbol{\rho}'|) k_0^2 \delta\epsilon_r(\boldsymbol{\rho}) E_{inc}(\boldsymbol{\rho}') d\boldsymbol{\rho}'. \tag{4.2.2}$$

After discretizing the above equations with a set of the subdomain basis functions $\{f_i(\boldsymbol{\rho}), i = 1, 2, \cdots, N\}$, which is defined as

$$f_i(\boldsymbol{\rho}) = \begin{cases} 1, & \text{if} \quad \boldsymbol{\rho} \in S_i \\ 0, & \text{if} \quad \boldsymbol{\rho} \notin S_i, \end{cases} \quad i = 1, 2, ..., N, \tag{4.2.3}$$

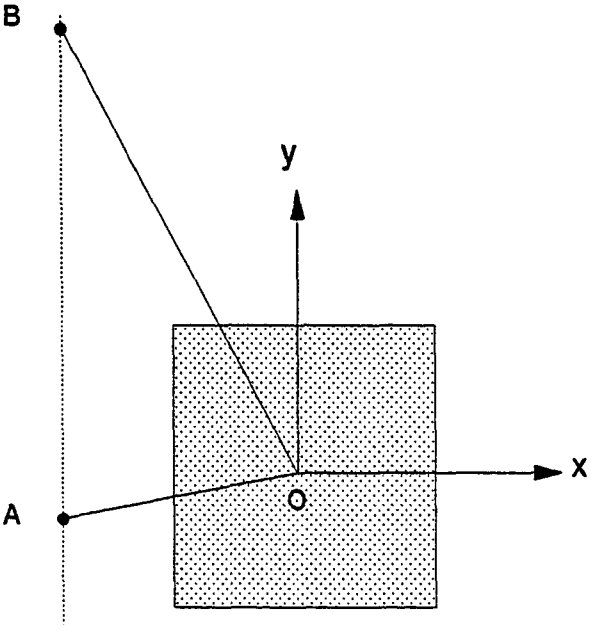

Figure 4.2. Locations of receiver A and receiver B in a limited angle inverse scattering problem.

where S_i is the subdomain of the i-th basis function, the object function could be expanded in terms of the above basis functions as

$$k_0^2 \delta\epsilon_r(\boldsymbol{\rho}) = \sum_{i=1}^{N} a_i f_i(\boldsymbol{\rho}), \tag{4.2.4}$$

where $\{a_i\}$ is the unknown to be sought and is the representation of the object function under the basis $\{f_i(\boldsymbol{\rho}), i = 1, 2, ..., N\}$. Then, (4.2.1) and (4.2.2) become

$$E_{sca}(\boldsymbol{\rho}_A) = \sum_{i=1}^{N} a_i \iint_{S_i} \frac{i}{4} H_0^{(1)}(|\boldsymbol{\rho}_A - \boldsymbol{\rho}'|) f_i(\boldsymbol{\rho}') E_{inc}(\boldsymbol{\rho}') d\boldsymbol{\rho}', \tag{4.2.5}$$

$$E_{sca}(\boldsymbol{\rho}_B) = \sum_{i=1}^{N} a_i \iint_{S_i} \frac{i}{4} H_0^{(1)}(|\boldsymbol{\rho}_B - \boldsymbol{\rho}'|) f_i(\boldsymbol{\rho}') E_{inc}(\boldsymbol{\rho}') d\boldsymbol{\rho}'. \tag{4.2.6}$$

Because receiver B is farther away from the object than receiver A, the signal at receiver B will be weaker than that at receiver A. In the 2-D case, we can roughly estimate that the ratio $|E_{sca}(\boldsymbol{\rho}_B)|/|E_{sca}(\boldsymbol{\rho}_A)|$ is proportional to $(\rho_A/\rho_B)^{\frac{1}{2}}$ by using the asymptotic expansion of Hankel functions for large arguments. Meanwhile, the corresponding entries in the integration for the above two equations are exactly the same except for the variables in the Green's function which are different from each other for the two equations. Hence, the magnitude of the integration on the right-hand side of Equation (4.2.6) should be smaller than that of the corresponding term in Equation (4.2.5) by a factor of $(\rho_A/\rho_B)^{\frac{1}{2}}$. The different scales between the two equations result in the same scale differences between the corresponding rows in the system matrix. For instance, suppose that receiver A corresponds to the i-th receiver and receiver B corresponds to the j-th receiver.

Then generally speaking, the corresponding elements in the j-th row will be approximately scaled down by a factor $(\rho_A/\rho_B)^{\frac{1}{2}}$ compared to the corresponding elements in the i-th row. When solving for the object function using the regularization procedure, the weight of the measurement at receiver B will be automatically scaled down approximately by a factor of $(\rho_A/\rho_B)^{\frac{1}{2}}$ compared to that of receiver A. Hence, after this scaling effect, part of the information contained in the measurement data of receiver B will be lost in the regularization procedures.

In order to make the information measured on receivers A and B equally important, we boost the magnitude of measurement data at receiver B by multiplying Equation (4.2.6) by a constant $(\rho_A/\rho_B)^{\frac{1}{2}}$. By doing so, the new Equations (4.2.5) and (4.2.6) will be of similar magnitude so that information contained in the measurement of receiver B is equally as important as that contained in the measurement of receiver A in the inversion procedure. Consequently, most of the information from the existing experimental setup can be retrieved in this manner. From a mathematical viewpoint, the above boosting procedure results in the decrease of the condition number of the corresponding system matrix. The decrease of the condition number finally results in the alleviation of the ill-conditioning problem of the linear system matrix in the inversion procedure so that a weaker form of the regularization could be adopted. This will consequently enable us to retrieve more information from the measurement data in a predetermined experimental setup.

In order to treat all receivers more systematically, the above procedure can also be achieved by multiplying (4.2.5) and (4.2.6) by $|\boldsymbol{\rho}_A|^{\frac{1}{2}}$ and $|\boldsymbol{\rho}_B|^{\frac{1}{2}}$, respectively. Applying the above boosting procedure to every integral equation corresponding to each receiver i, for $i = 1, 2, \ldots, M$, the weight of the

measurement data from all the receivers will be rescaled to the same degree of importance such that the maximum amount of information could be retrieved in the inversion procedure for a predetermined experimental setup in the limited angle inverse scattering problem. Summary of the above discussions leads us to the following formal description of the boosting procedure:

Boosting Procedure: In the inverse scattering problem described by the integral equation (4.2.1), if the distances from the receivers to the center of the object vary significantly, that is, $\text{Max}(|\boldsymbol{\rho}_{(i)}|; i = 1, ..., M) \gg \text{Min}(|\boldsymbol{\rho}_{(i)}|; i = 1, ..., M)$, where $|\boldsymbol{\rho}_{(i)}|$ is the distance from the i-th receiver to the center of the object, then the ill-conditioning of the system matrix in the inversion procedure will be further aggravated due to the nonuniform distances of the receivers. Therefore, a considerable amount of information contained in the measurement data from the distant receivers will be lost in the regularization procedure. By multiplying every integral equation corresponding to each receiver i, for $i = 1, 2, ..., M$, by a factor $|\boldsymbol{\rho}_{(i)}|^{\frac{1}{2}}$ in the 2-D case and by a factor of $|\mathbf{r}_i|$ in the 3-D case, we can boost the measurement data from all receivers to the same degree of importance so that the maximum amount of information can be retrieved in the inversion procedure for a predetermined experimental setup.

Application of the boosting procedure to the conventional inverse scattering problem is not critically important because the information content obtained in a full angle inverse scattering problem is sufficient to obtain a good reconstruction even if part of the information carried on the distant receivers has been immersed in the regularization procedures. However, in the limited angle inverse scattering problem, e.g., in geophysical exploration, due to the sparsity of the measurement data, the information content becomes critically important. Therefore, we can no longer afford any loss of

the valuable information in the measurement data during the regularization procedures. Then, application of the boosting procedure on the limited angle inverse scattering problems becomes important and will help to boost all of the measurement data to the same degree of importance such that the maximum amount of information can be retrieved in the inversion procedures. The significance of the boosting procedure in the limited angle inverse scattering problems can be verified from the numerical simulations in the following section.

4.2.3 Numerical simulations and results

To verify the importance of the boosting procedure in the limited angle inverse scattering problems, especially in the problems related to geophysical explorations, we devote the following few examples to the comparison between the two algorithms, one without the boosting procedure and the other with the boosting procedure in well-to-well tomography. Configuration of the problem is given in Figure 4.1(a). The length of the receiver and transmitter arrays is about 10 m. The distance between the two holes is 3.6 m. The diameter of the formation object is about 3 m.

As the first example, we reconstruct a sinelike dielectric distribution by using the distorted Born iterative method without the boosting procedure. The peak value of the relative permittivity is 1.8. The operating frequency is 200 MHz; therefore, the relative dimension of the object is about 2λ. The numbers of receivers and transmitters are 36 and 16, respectively.

Figure 4.3 gives the 3-D perspective views of the evolution of the convergence of the iterative solutions. Figure 4.3(a) is the original distribution. Figure 4.3(b) is the first-order Born approximation. Figures 4.3(c)–4.3(k)

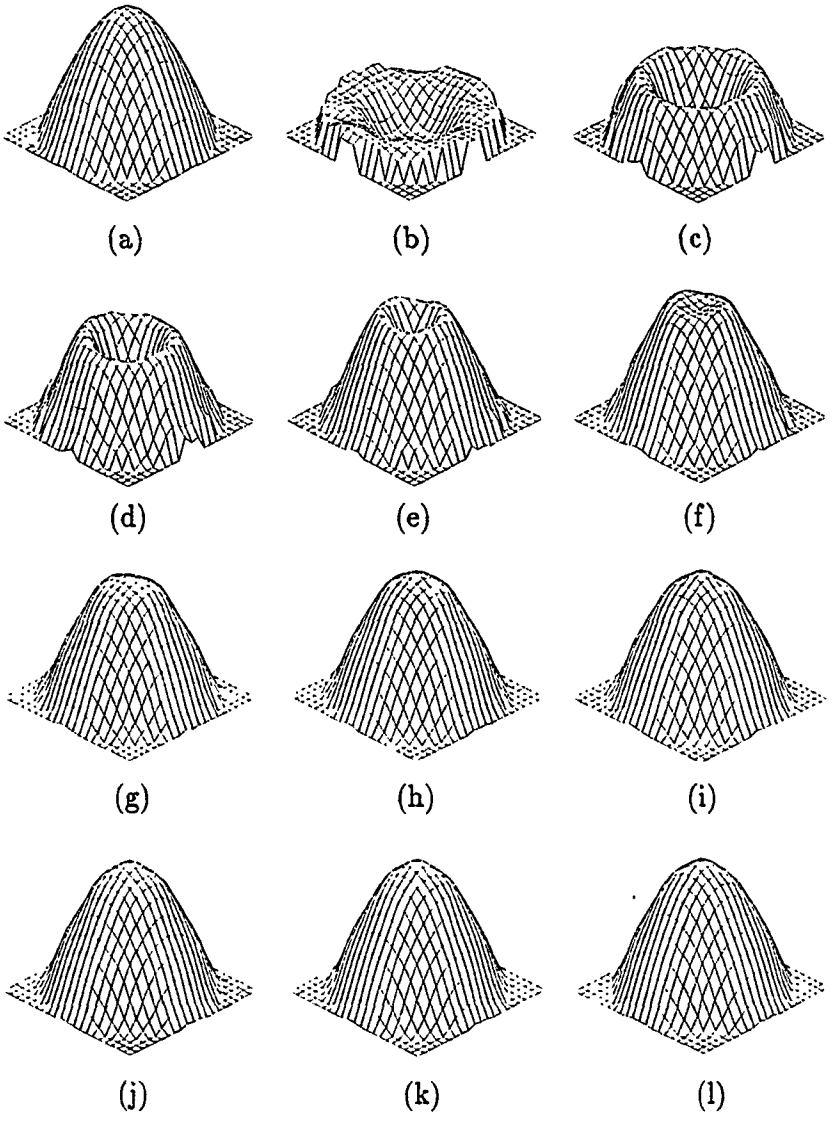

Figure 4.3. Reconstruction of a sinelike permittivity distribution using the distorted Born iterative algorithm without the boosting procedure with operating frequency at 200 MHz. The peak value of the relative permittivity is 1.8. The diameter of the object is about 2λ. (a) is the original distribution. (b) is the result of the first-order Born approximation. (c) to (k) are the results from the second iteration to the tenth iteration. (l) is the final convergent solution after 15 iterations.

are the results from the second iteration to the tenth iteration. Figure 4.3(l) is the final convergent solution after 15 iterations. Figure 4.4 shows the one-dimensional cut of the reconstruction of the problem along the x-axis. Small discrepancies between the final convergent solution and the original distribution can be easily recognized.

Figure 4.5 gives the relative Mean Square Error (MSE) and the Relative Residual Error (RRE) of the reconstructed permittivity distribution in the above example as a function of the iteration steps. Figure 4.5 shows that both the MSE and the RRE stay at around 2% after the tenth iteration, which is consistent with that of Figure 4.4, in which small discrepancies exist between the final convergent solution and the original distribution.

As the second example, we solve the same problem by using the distorted Born iterative algorithm with the boosting procedure. The geometric configuration and the experimental setup are the same as those in the above example. Shown in Figure 4.6 are the 3-D perspective views of the evolution of the iterative solution. Figure 4.6(a) is the original permittivity distribution. Figure 4.6(b) is the first-order Born approximation solution. Figures 4.6(c)–4.6(h) are the results from the second iteration to the seventh iteration. Figure 4.6(i) is the final convergent solution after 15 iterations. On comparing Figure 4.6(g) with Figure 4.3(g), we can see that the result of Figure 4.6(g), which is the 6-th iteratiion solution, is almost as good as the final convergent solution, while the result of Figure 4.3(g) shows obvious discrepancy with the final convergent solution. This proves that the algorithm with the boosting procedure converges faster than the algorithm without the boosting procedure in the limited angle inverse scattering problems.

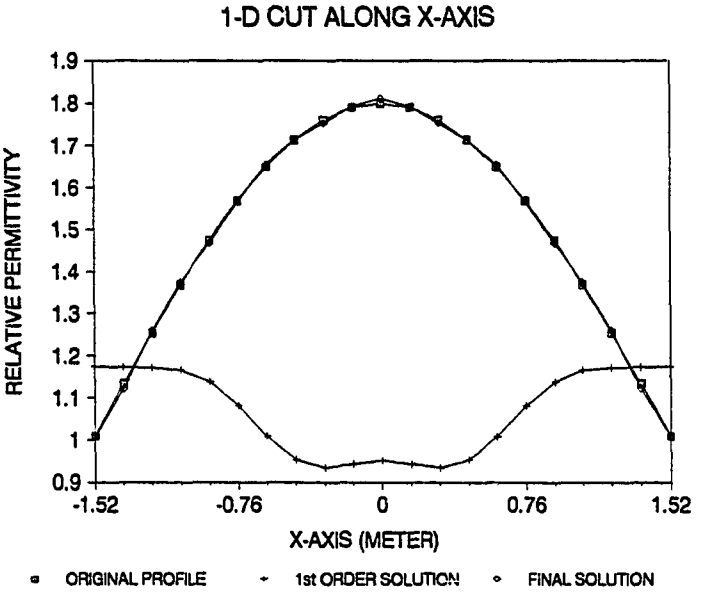

Figure 4.4. 1-D cut of the reconstructed distribution shown in Figure 4.3 along the x-axis. The line with squares is for the original profile. The line with crosses is for the first-order solution, and the line with diamomds is for the final convergent solution.

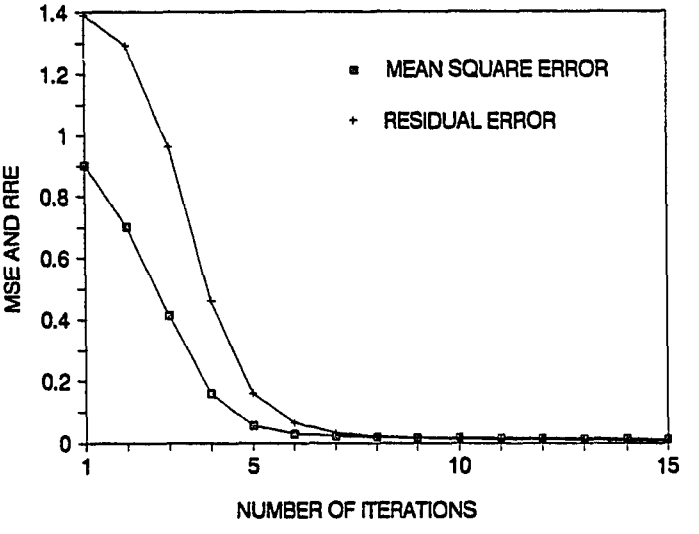

Figure 4.5. The relative MSE (Mean Square Error) and the RRE (Relative Residual Error) of the reconstructed permittivity distribution shown in Figure 4.3 as a function of the iteration steps.

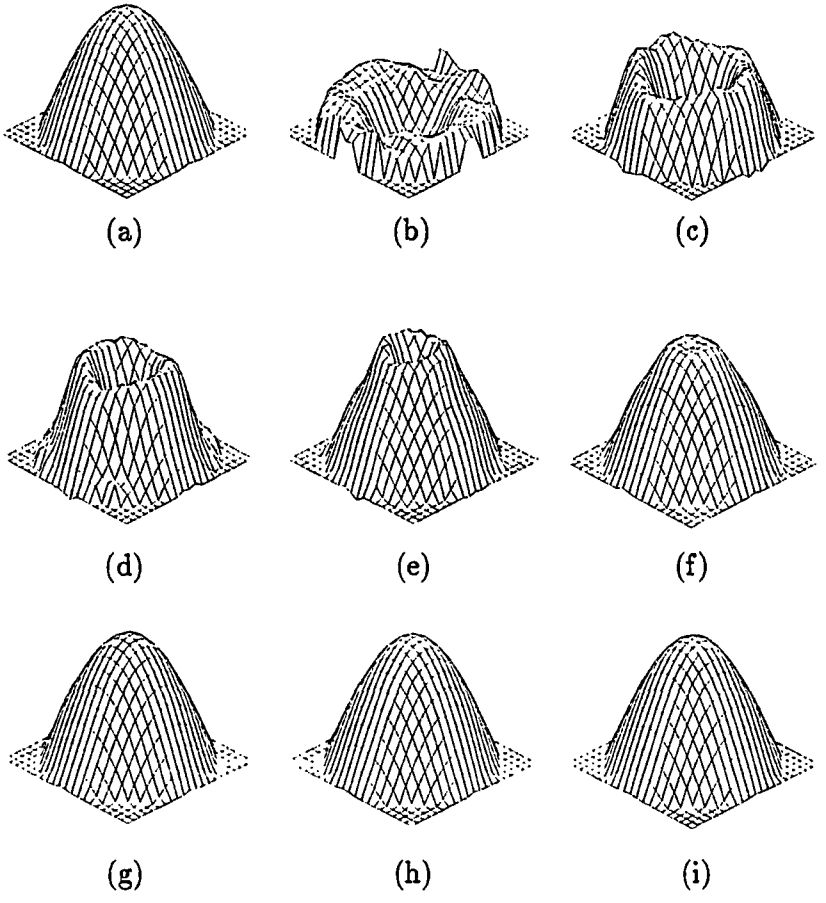

Figure 4.6. Reconstruction of a sinelike permittivity distribution using the distorted Born iterative algorithm with the boosting procedure with operating frequency at 200 MHz. The peak value of the relative permittivity is 1.8. The diameter of the object is about 2λ. (a) is the original distribution. (b) is the result of the first-order Born approximation. (c) to (h) are the results from the second iteration to the seventh iteration. (i) is the final convergent solution after 15 iterations.

Figure 4.7 shows the 1-D cut along the x-axis of the reconstructed relative permittivity distribution shown in Figure 4.6. As we can see, the final convergent solution agrees very well with the original distribution. No observable discrepancy exists between the final convergent solution and the original distribution in Figure 4.7. As we have expected, the first-order Born approximation is far away from the real solution.

Figure 4.8 gives the MSE and the RRE of the reconstructed relative permittivity distribution in the example as a function of the iteration steps. Both the MSE and RRE reach a negligible level after 6 iterations. On comparing Figure 4.8 with Figure 4.5, we can see that the algorithm with the boosting procedure achieves a better final convergent solution as well as faster convergent speed than the algorithm without the boosting procedure.

In order to investigate the effect of the boosting procedure on the limited angle inverse scattering problem in the domain of validity in which a convergent solution can be obtained, we have tested the same problem as the above two examples but reduced the number of transmitters from 16 to 8. In this case, the algorithm with the boosting procedure successfully generated a good convergent solution, which is similar to the result shown in Figure 4.6, although the convergent speed is slower than that in Figure 4.6. Both the MSE and RRE reach a negligible level after about 10 iterations instead of 6 iterations shown in Figure 4.8. However, no convergent solution has been obtained by using the algorithm without the boosting procedure no matter how hard we tried. This test illustrates that the boosting procedure not only improves the quality of the image and the speed of the convergence but also extends the domain of the validity in which the convergent solution can be achieved. In the following examples, all the results are obtained by using the algorithm with the boosting procedure. In the following, we

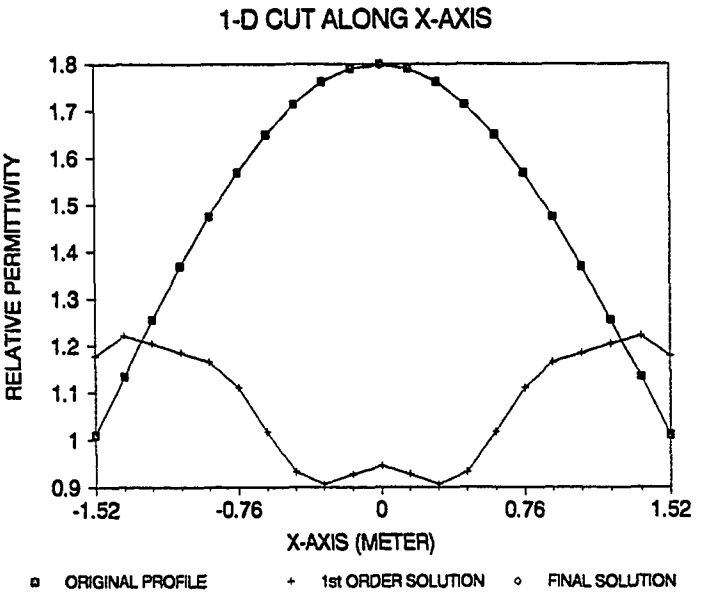

Figure 4.7. 1-D cut of the reconstructed distribution shown in Figure 4.6 along the x-axis. The line with squares is for the original profile. The line with crosses is for the first-order solution, and the line with diamomds is for the final convergent solution.

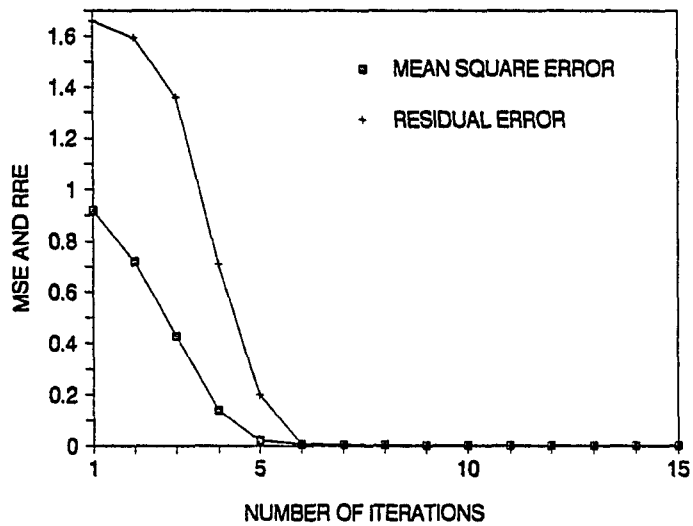

Figure 4.8. The relative MSE (Mean Square Error) and the RRE (Relative Residual Error) of the reconstructed permittivity distribution shown in Figure 4.6 as a function of the iteration steps.

will use the boosting procedure for two cases which come from geophysical explorations. They are well-to-well tomography shown in Figure 4.1(a) and subsurface detection shown in Figure 4.1(b).

4.2.3.1 Well-to-well tomography

Figure 4.9 shows the 3-D perspective views of the reconstruction of an asymmetric permittivity distribution in the well-to-well tomography problem with the geometric configuration and the experimental setup the same as that in the example 1. The frequency of the incident field is 200 MHz. The relative diameter dimension of the formation object is about 2λ. Figure 4.9(a) gives the original distribution. Figure 4.9(b) is the first-order Born approximation solution. Figures 4.9(c)–4.9(k) are the iterative solutions from the second iteration to the tenth iteration. Figure 4.9(l) gives the final convergent solution after 20 iterations.

Figure 4.10 shows the 1-D cut of the reconstructed relative permittivity distribution shown in Figure 4.9 along both the x-axis and y-axis. The final solution matches very well with the original one except in the neighborhood of the origin where the original profile is not smooth.

Figure 4.11 shows the MSE and the RRE of the reconstructed permittivity distribution as a function of the iteration steps. Although the RRE reaches a negligible value after 5 iterations, the MSE stays at around 0.01 until 20 iterations, which is attributed to the nonsmoothness of the original distribution at the origin.

As an example chosen to test the ability of the algorithm to distinguish two nearby objects, Figure 4.12 shows the 3-D perspective views of the reconstruction of a two-pulse permittivity distribution in well-to-well tomography.

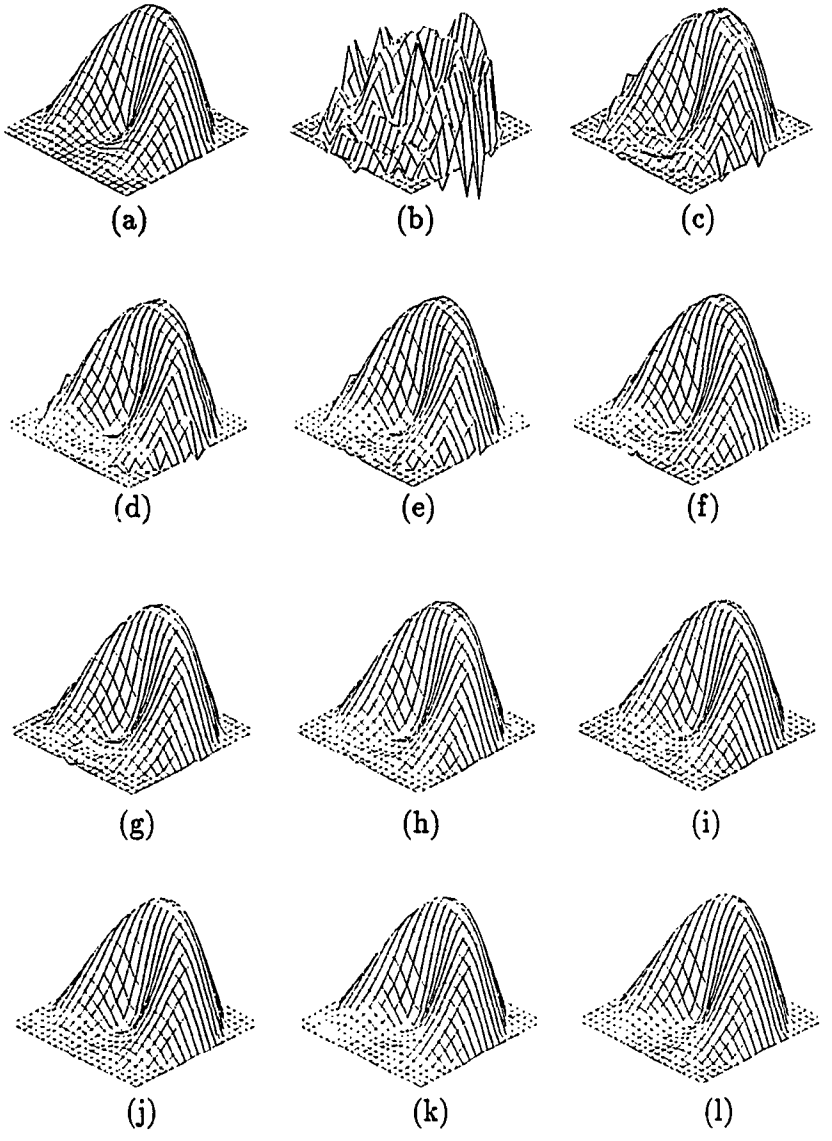

Figure 4.9. Reconstruction of an asymmetric permittivity distribution using the distorted Born iterative algorithm with the boosting procedure with operating frequency at 200 MHz in well-to-well tomography. The peak value of the relative permittivity is 1.4. The diameter of the object is about 2λ. (a) is the original distribution. (b) is the first-order Born solution. (c) to (k) are the results from the second iteration to the tenth iteration. (l) is the final convergent solution after 20 iterations.

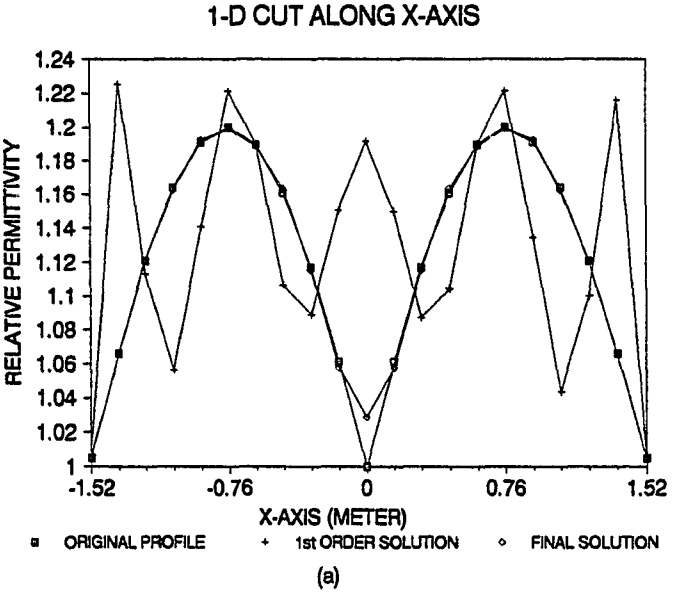

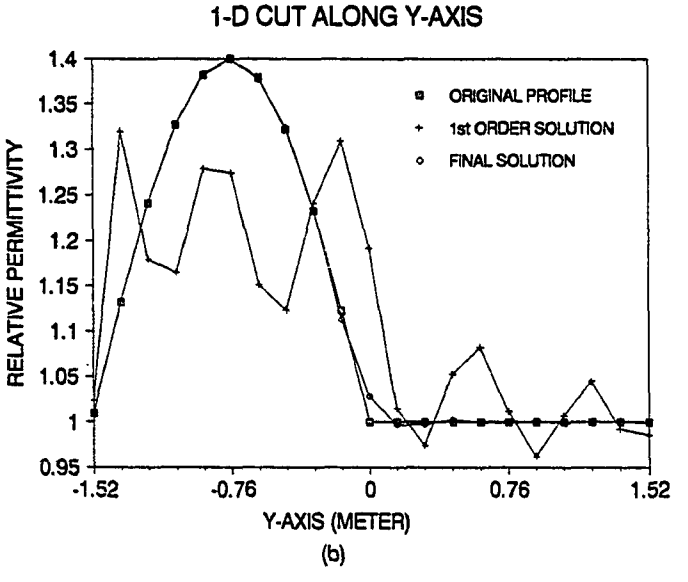

Figure 4.10. (a) is the 1-D cut of the reconstructed distribution shown in Figure 4.9 along the x-axis. (b) is the 1-D cut of the reconstructed distribution along the y-axis. The line with squares is for the original profile. The line with crosses is for the first-order solution, and the line with diamomds is for the final convergent solution.

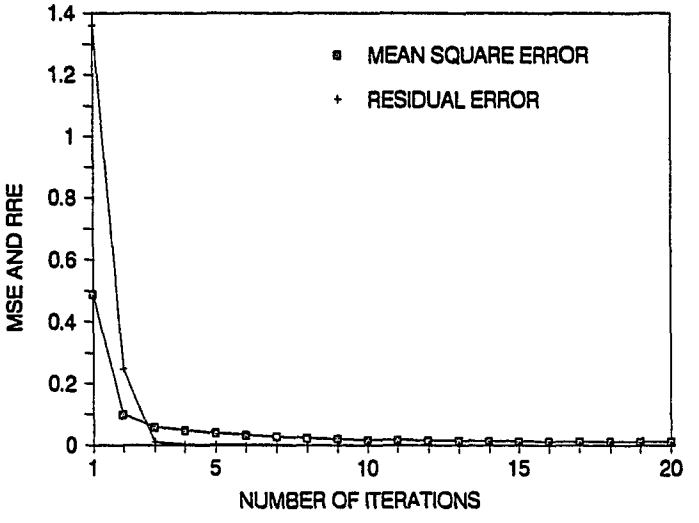

Figure 4.11. The relative MSE (Mean Square Error) and the RRE (Relative Residual Error) of the reconstructed permittivity distribution shown in Figure 4.9 as a function of the iteration steps.

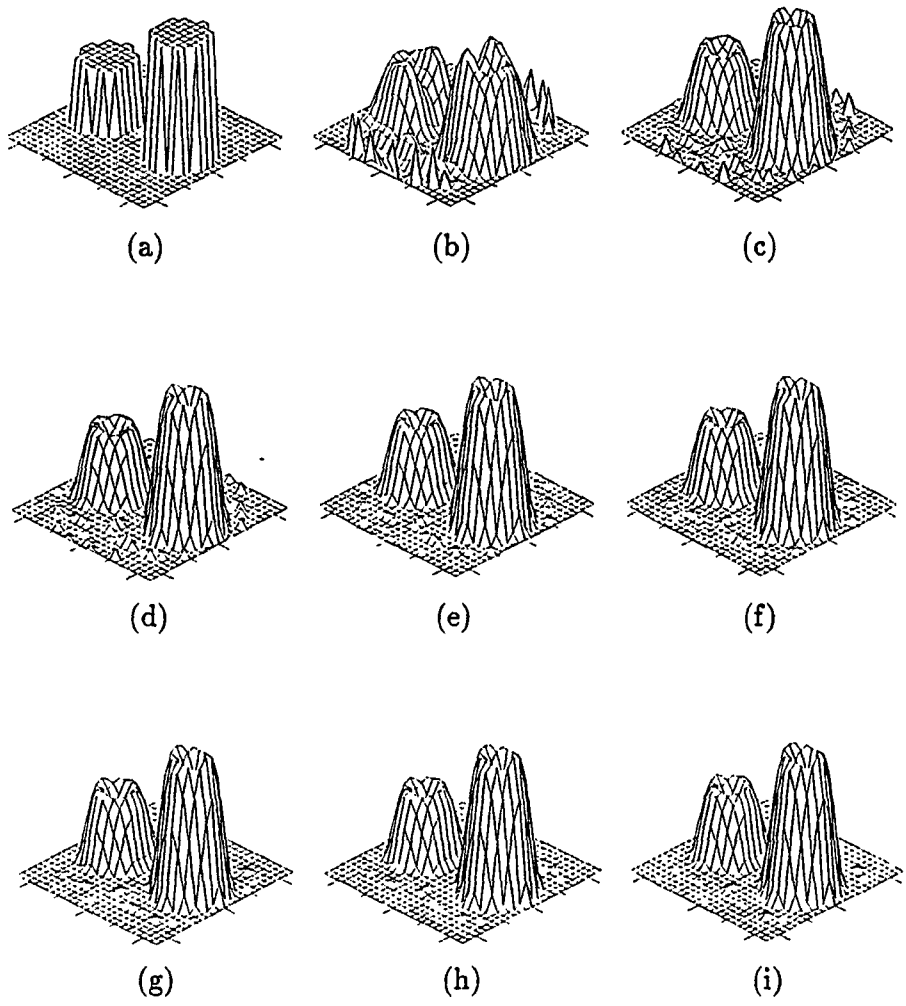

Figure 4.12. Reconstruction of a two-pulse permittivity distribution using the distorted Born iterative algorithm in well-to-well tomography with operating frequency at 200 MHz. The heights of the pulses are 1.2 and 1.4, respectively. The width of the pulses is about 0.65λ. The separation between the two pulses is about 0.42λ. (a) is the original distribution. (b) is the result of the first-order Born approximation. (c) to (k) are the results from the second iteration to the tenth iteration. (l) is the final convergent solution after 20 iterations.

The geometrical configuration and the experimental setup of the problem are the same as that of the last problem. The system operates at 200 MHz. The numbers of receivers and transmitters are 72 and 32, respectively. The width of the pulses is about 0.65λ. The separation between the two pulses is about 0.42λ. The heights of the two pulses are 1.2 and 1.4, respectively. Figure 4.12(a) is the original distribution. Figure 4.12(b) is the first-order Born approximation solution. Figures 4.12(c)–4.12(h) are the iterative solutions from the second iteration to the seventh iteration. Figure 4.12(i) gives the final convergent solution after 9 iterations. The results illustrate the band-limited nature of the algorithm as expected. The final convergent solution is a smoothed version of the original distribution.

In Figure 4.13, we show the 1-D cut of the reconstructed distributions along the x-axis in the above problem. The main characters of the object have been properly reconstructed although there are overshoots at the edges of the pulses, which are attributed to the band-limited nature of the algorithm.

Figure 4.14 illustrates the MSE and RRE of the reconstructed permittivity distribution as a function of the iteration steps. The reason for the relatively large MSE is that the final convergent solution is a smoothed version of the original pulse function.

4.2.3.2 Underground detection

In this subsection, we will examine two examples in subsurface detection tomography. The geometrical configuration of the problem is shown in Figure 4.1(b) where the transmitter and receiver array is confined to the ground surface. The object to be detected is just beneath the transmitter and receiver array. The operating frequency is 200 MHz in both examples.

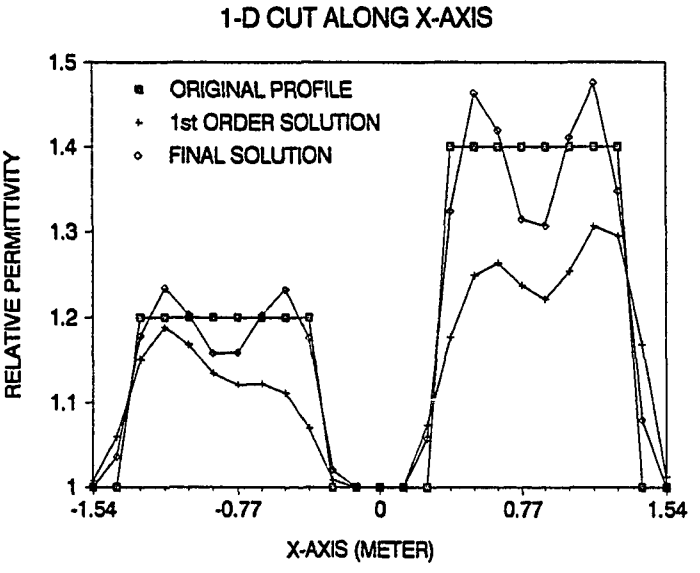

Figure 4.13. 1-D cut of the reconstructed distribution shown in Figure 4.12 along the x-axis. The line with squares is for the original profile. The line with crosses is for the first-order solution, and the line with diamomds is for the final convergent solution.

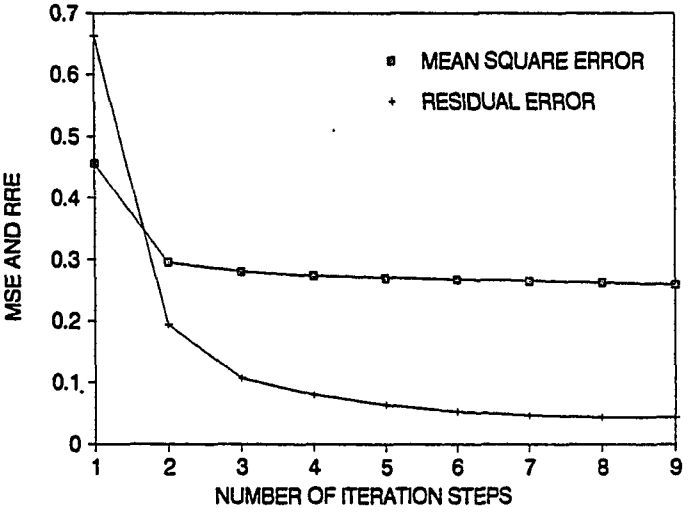

Figure 4.14. The relative MSE (Mean Square Error) and the RRE (Relative Residual Error) of the reconstructed permittivity distribution shown in Figure 4.12 as a function of the iteration steps.

Figure 4.15 shows the 3-D perspective views of the reconstruction of an asymmetric permittivity distribution. The cross dimension of the object is about 3 m which is equivalent to about 2λ. The numbers of the receivers and the transmitters are 36 and 16, respectively. The length of the receiver and transmitter array is about 11 m. Figure 4.15(a) is the original distribution. Figure 4.15(b) is the solution of the first-order Born approximation. Figures 4.15(c)–4.15(k) are the iterative solutions from the second iteration to the tenth iteration. Figure 4.15(l) is the final convergent solution after 20 iterations. Referring to Figure 4.9, we see that for the corresponding iterations, the results in Figure 4.9 demonstrate the faster convergent speed than that in Figure 4.15.

Figure 4.16 shows the 1-D profile of the reconstructed distributions along both the x-axis and y-axis. Figure 4.16(a) gives the 1-D cut along the x-axis and Figure 4.16(b) gives the 1-D cut along the y-axis. The discrepancies between the final solution and the original distribution are negligible except at the neighborhood of the origin where the original distribution is nonsmooth.

Figure 4.17 shows the MSE and RRE of the reconstructed iterative solutions as a function of the iteration steps. The results show that both the MSE and RRE stop at about 2%. On comparing the results with that in the corresponding problem shown in the last subsection, we find that the convergent speed in subsurface detection is much slower than that in well-to-well tomography. The reason is that in subsurface detection, the information content is more sparse than that in well-to-well tomography.

As the last example, we will reconstruct a two-pulse permittivity distribution with different heights. The geometric configuration is the same as that in the example shown in Figure 4.15. The numbers of the receivers

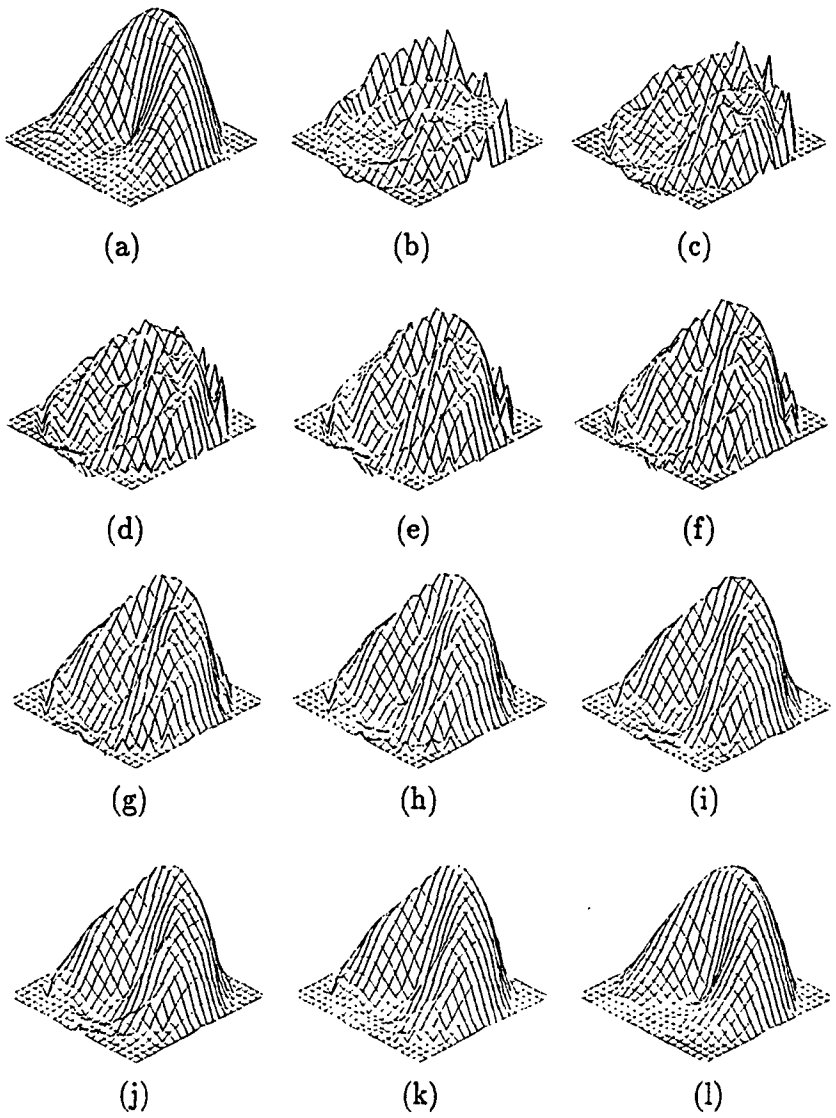

Figure 4.15. Reconstruction of an asymmetric permittivity distribution using the distorted Born iterative algorithm with the boosting procedure with operating frequency at 200 MHz in a subsurface detection problem. The peak value of the relative permittivity is 1.4. The diameter of the object is about 2λ. (a) is the original distribution. (b) is the first-order Born solution. (c) to (k) are the results from the second iteration to the tenth iteration. (l) is the final convergent solution after 20 iterations.

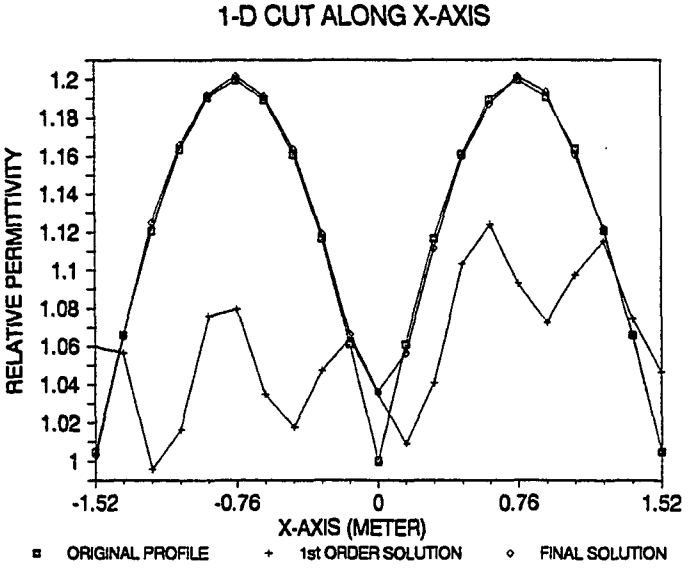

(a)

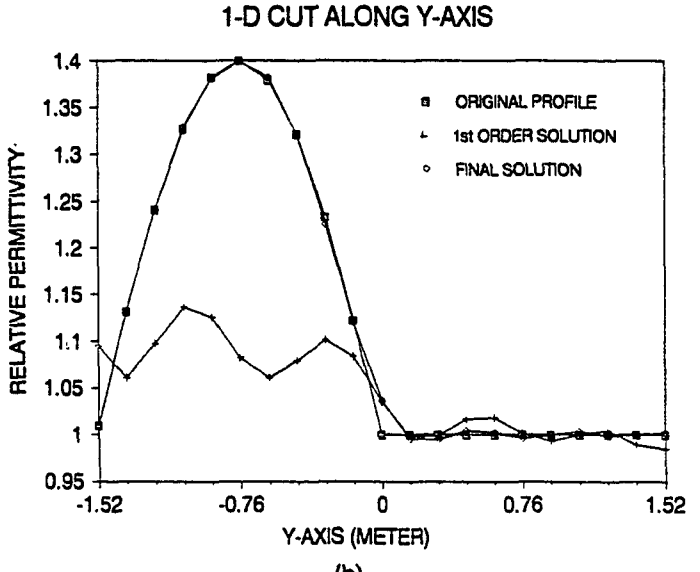

(b)

Figure 4.16. (a) is the 1-D cut of the reconstructed distribution shown in Figure 4.15 along the x-axis. (b) is the 1-D cut of the reconstructed distribution along the y-axis. The line with squares is for the original profile. The line with crosses is for the first-order solution, and the line with diamomds is for the final convergent solution.

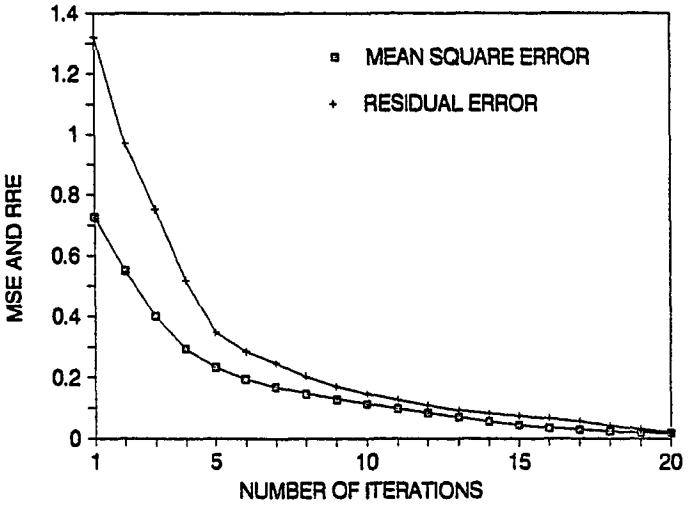

Figure 4.17. The relative MSE (Mean Square Error) and the RRE (Relative Residual Error) of the reconstructed permittivity distribution shown in Figure 4.15 as a function of the iteration steps.

and the transmitters are 72 and 32, respectively. Figure 4.18 shows the 3-D perspective views of the evolution of the convergent solution. Figure 4.18(a) is the original distribution. Figure 4.18(b) is the solution of the first-order Born approximation. Figures 4.18(c)–4.18(h) are the iterative solutions from the second iteration to the seventh iteration. Figure 4.18(i) is the final convergent solution after 14 iterations. Figure 4.19 gives the 1-D cut of the reconstructed distribution along the x-axis. The results show an obvious band-limited nature of the algorithm. Figure 4.20 gives the MSE and RRE of the reconstructed distributions as a function of iteration steps. Comparing Figure 4.20 with Figure 4.13 in the last subsection for well-to-well tomography, we can see that the convergent speed for subsurface detection is slower than that for well-to-well tomography.

4.2.4 Conclusions

In this section, the boosting procedure has been introduced to retrieve the maximum amount of information from the measurement data in the limited angle inverse scattering problem. The validity of the boosting procedure has been asserted by the results of the numerical simulations although the rigorous proof of the boosting procedure is still open for further investigations. The numerical simulations demonstrate that the boosting procedure not only improves the quality of the reconstruction and the speed of the convergence but also extends the domain of the validity in which the convergent solution can be obtained. By using the boosting procedure, we have successfully reconstructed the images for both well-to-well tomography and subsurface detection beyond the Born approximation.

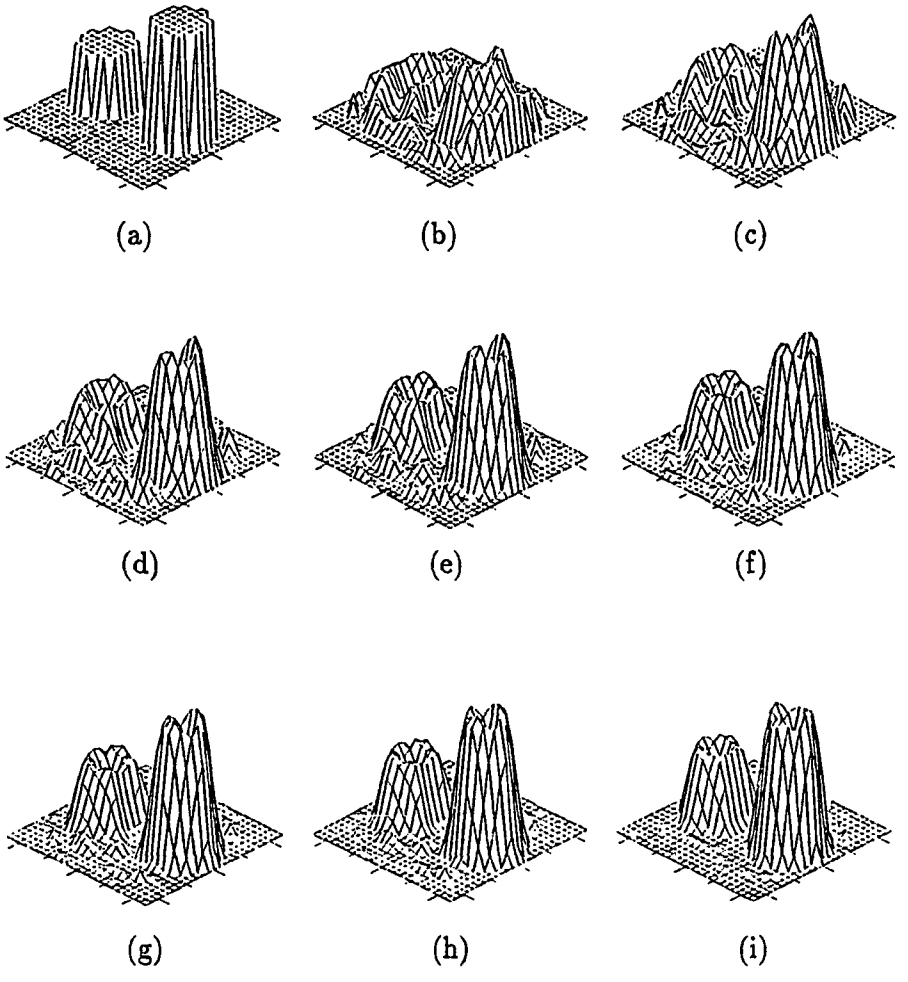

Figure 4.18. Reconstruction of a two-pulse permittivity distribution using the distorted Born iterative algorithm in subsurface detection with operating frequency at 200 MHz. The heights of the pulses are 1.2 and 1.4, respectively. The width of the pulses is about 0.65λ. The separation between the two pulses is about 0.42λ. (a) is the original distribution. (b) is the result of the first-order Born approximation. (c) to (h) are the results from the second iteration to the seventh iteration. (i) is the final convergent solution after 20 iterations.

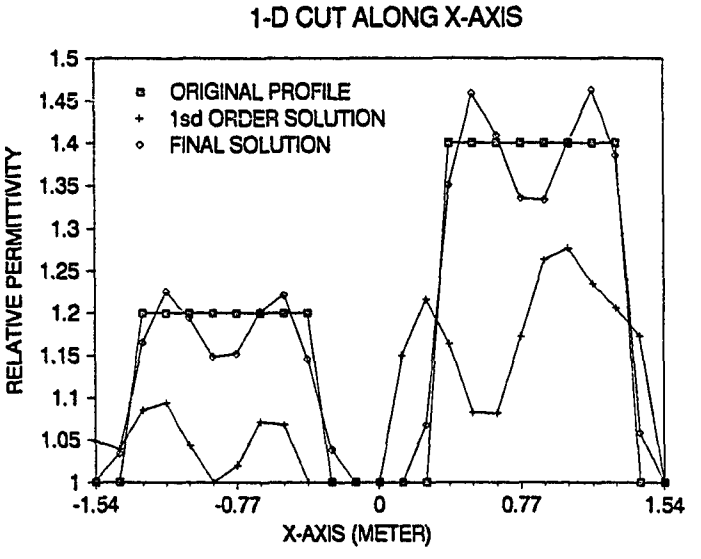

Figure 4.19. 1-D cut of the reconstructed distribution shown in Figure 4.18 along the x-axis. The line with squares is for the original profile. The line with crosses is for the first-order solution, and the line with diamomds is for the final convergent solution.

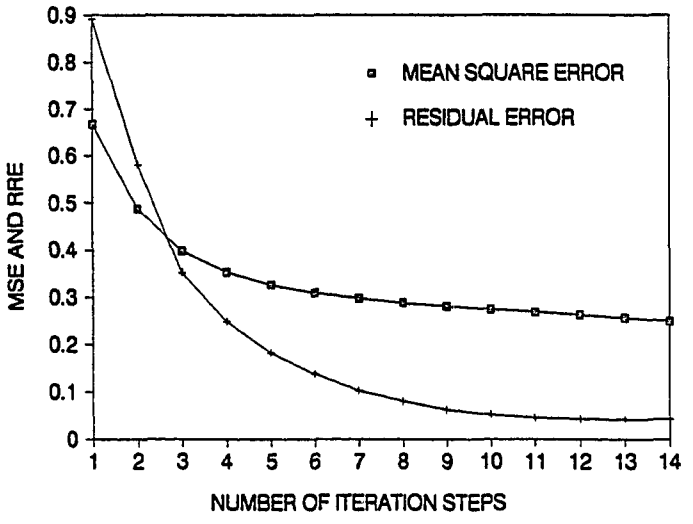

Figure 4.20. The relative MSE (Mean Square Error) and the RRE (Relative Residual Error) of the reconstructed permittivity distribution shown in Figure 4.18 as a function of the iteration steps.

4.3. Accelerated Inverse Scattering Algorithms

One problem of the nonlinear inverse scattering algorithms discussed in Chapter 3 of this thesis is the intensive computation time involved. In both the direct and inverse solutions in the iteration procedure, matrix inversions are required. By using the standard Gaussian elimination algorithm, computational time for the matrix inversion is proportional to N^3. Therefore, the computational complexity of the algorithms discussed in Chapter 3 is N^3, where N is the number of meshes in the object.

One way to reduce the computational complexity of the algorithms is to apply the conjugate gradient method to both the direct and inverse solutions of the algorithms. However, the conjugate gradient method provides a solution for only one incident wave at a time. If M, the number of the incident fields (or transmitters) is large, overall computation time, which is proportional to MN^2, can be quite computationally intensive for a large object.

In order to significantly accelerate the algorithm, we applied the fast recursive operator algorithm discussed in Chapter 2 to the solution of the direct scattering problem in each iteration step. Since the fast algorithm gives a full solution of the direct scattering problem, the computational time will be independent of the number of the transmitters (or incident fields) in the experimental configuration of the inverse scattering problem. The computational complexity of the fast algorithm discussed in Section 2.4 is N^2 in high frequency cases. Therefore, if the conjugate gradient method is applied to the inversion part of the algorithm, overall computational time will be roughly proportional to N^2. This is a significant reduction of the computational time.

Shown in Figure 4.21 is a comparison of the computer time as a function of the number of unknowns between the standard iterative algorithm and the algorithm accelerated by using the fast direct scattering solver. The results show that a significant reduction of the computer time has been achieved by the accelerated algorithm.

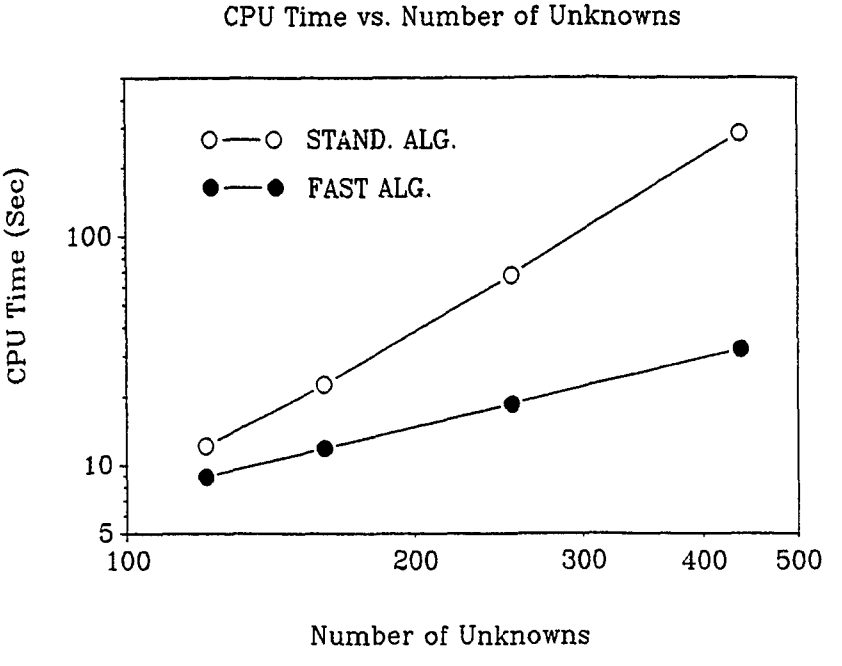

Figure 4.21. Comparison of the computer time as a function of the number of unknowns for the standard iterative inverse scattering algorithm and the algorithm accelerated by using the fast direct scattering solver on a CRAY-2 supercomputer. The conjugate gradient method has been applied to the solution of the inversion in the accelerated algorithm.

References

[1] S. K. Kenue and J. F. Greenleaf, "Limited angle multifrequency diffraction tomography," *IEEE Trans. Sonics Ultrason.*, vol. SU-29, pp. 213–217, July 1982.

[2] A. J. Devaney, "Geophysical diffraction tomography," *IEEE Trans. Geosci. Remote Sensing*, vol. GE-22, pp. 3–13, January 1984.

[3] K. A. Dines and R. J. Lytle, "Computerized geophysical tomography," *Proc. IEEE*, vol. 67, pp. 471–418, 1979.

[4] S. Ivansson, "Seismic borehole tomography —Theory and computational results," *Proc. IEEE*, vol. 74, pp. 328–338, 1986.

[5] J. H. Justice, A. A. Vassiliou, and D. T. Nguyen, "Geophysical diffraction tomography," *Sig. Process.*, vol. 15, pp. 227–235, 1988.

[6] Y. M. Wang and W. C. Chew, "An iterative solution of two-dimensional electromagnetic inverse scattering problem," *Int. J. Imaging Syst. Technol.*, vol. 1, pp. 100–108, 1989.

[7] W. C. Chew and Y. M. Wang, "Reconstruction of two-dimensional permittivity using the distorted Born iterative method," *IEEE Trans. Med Imaging*, vol. MI-9, no. 2, pp. 218–225, 1990.

[8] M. M. Ney, A. M. Smith, S. S. Stuchly, "A solution of electromagnetic imaging using pseudoinverse transformation," *IEEE Trans. Med. Imaging*, vol. MI-3, no. 4, pp. 155–162, Dec. 1984.

[9] S. J. Johnson and M. L. Tracy, "Inverse scattering solutions by a sinc basis, multiple source, moment method - part I: theory," *Ultrasonic Imaging*, vol. 5, pp. 361–375, 1983.

[10] S. J. Johnson and M. L. Tracy, "Inverse scattering solutions by a sinc basis, multiple source, moment method - part II: numerical evaluations," *Ultrasonic Imaging*, vol. 5, pp. 376–392, 1983.

[11] T. J. Cavicchi and W. D. O'Brien, Jr., "Numerical study of higher-order diffraction tomography via the sinc basis moment method," *Ultrasonic Imaging*, vol. 11, pp. 42–74, 1989.

[12] W. C. Chew, *Waves and Fields in Inhomogeneous Media*. New York: Van Nostrand Reinhold, 1990.

[13] N. Bleistein and J. K. Cohen, "Nonuniqueness in inverse source problem in acoustics and electromagnetics," *J. Math. Phys.*, vol. 18, pp. 194–201, Feb. 1977.

[14] A. J. Devaney and G. C. Sherman, "Nonuniqueness in inverse source and scattering problems," *IEEE Trans. Antennas Propagat.*, vol. 30, pp. 1034–1042, Sept. 1982.

[15] A. J. Devaney and E. Wolf, "Radiating and nonradiating classical current distributions and the fields they generate," *Phys. Rev. D*, vol. 8, pp. 1044–1047, Aug. 1973.

[16] J. Richmond, "Scattering by a dielectric cylinder of arbitrary cross--sectional shape," *IEEE Trans. Antennas Propagat.*, vol. AP-13, pp. 334–341, 1965.

[17] R. F. Harrington, *Field Computation by Moment Methods*. Malabar, Florida: Krieger Publishing, 1983.

[18] S. Twomey, *Introduction to the Mathematics of Inversion in Remote Sensing and Indirect Measurements*. New York: Elsevier Scientific, 1977.

[19] C. T. H. Baker, *The Numerical Treatment of Integral Equations*. Oxford: Clarendon, 1977.

[20] A. Tarantola, *Inverse Problem Theory - Methods for Data fitting and Model Parameter Estimation*. Amsterdam: Elsevier, 1987.

CHAPTER 5

CONCLUSIONS AND FUTURE WORK

In this thesis, several solution methods for the direct and inverse electromagnetic scattering problems have been discussed. The recursive operator algorithms for the solution of electromagnetic scattering problems have been implemented in the two-dimensional cases. The algorithm has been successfully applied to the solution of large 2-D inhomogeneous scatterers for TM waves. Application of the recursive algorithm to TE waves is an important topic for future studies. Meanwhile, (A.1), (A.2) and (A.3) in Appendix A, which are the translation relations for the harmonic functions at two different locations, are actually the convolution of two discrete series. Thus, the computational complexity of the algorithm could be further reduced by using the FFT in the translation relations.

For the inverse scattering problems, the Born and the distorted Born iterative methods have been discussed in this thesis. The algorithms have been implemented in the two-dimensional case for the reconstruction of the permittivity distribution of the object. The simulations reveal that the maximum contrast of the dielectric constant can be relaxed by a factor of ten compared to that for the Born approximation. The relaxation of the criteria is important in many areas of the inverse scattering applications, such as medical imaging, nondestructive evaluation, and geophysical explorations. Meanwhile, the maximum contrast we could reconstruct by using the iterative algorithms is at δka being about 0.8, where a is the diameter of the object. Here we start the iteration from a homogeneous background. To

reconstruct higher contrast objects, we have made some test runs by using multiple frequencies. This does make some successful reconstructions for the contrast δka higher than one, if we calculate this criterion according to the highest frequency in the multiple frequencies applied. But, generally, application of the multiple frequencies in the inverse scattering system will slow down the convergent speed of the algorithms. The other approach to reconstruct a higher contrast object is to use the frequency increasing method. In this method, we start from a relative low frequency at which δka is smaller than 0.8 to find a good initial guess for the high frequency reconstruct. Then we jump to another frequency which is higher than the first one to improve our initial guess by using the reconstructed profile from the last frequency as the initial guess. The number of this step depends on the contrast of the object. Finally, we apply the desired frequency to reconstruct the final imaging by using the reconstructed distribution from the last frequency as the initial guess. Using this technique, we have reconstructed the object whose contrast δka could be as high as 3 according to the final frequency applied. The iterative algorithms developed in this thesis have the ability to reconstruct any object, if the initial guess is close to the original distribution. Therefore, the above method is a good candidate to reconstruct a high contrast object.

Reconstruction of the permittivity distribution in a limited angle inverse scattering problem has been achieved by applying the boosting procedure. The domain of validity can also be further relaxed by the frequency increasing method discussed in the last paragraph. Moreover, the further reduction of the algorithmic complexity of the iterative algorithms for the solution of the nonlinear inverse scattering problems is much desired. If this goal could be achieved, the algorithm can be immediately applied to the solution of inverse scattering problem for large scatterers. Finally, it is also important to apply the iterative algorithm to the electromagnetic inverse scattering problem with TE polarization.

APPENDIX A

TRANSLATION MATRICES FOR CYLINDRICAL HARMONICS

The translation matrices used in Chapter 2 are obtained by Graf's addition theorem and its generalizations (Ref. 36 of Chapter 2). Let (r,φ), (a,ψ), and (R,ϕ) be the cylindrical coordinates of $\mathbf{r}$, $\mathbf{a}$, and $\mathbf{R}$, respectively (Figure A.1). Then for the regular cylindrical harmonics $J_m(kr)e^{im\varphi}$, we have

$$J_m(kr)e^{im\varphi} = \sum_{m'=-\infty}^{\infty} J_{m'}(kR)e^{im'\phi}\{\beta_{ij}(ka,\psi)\}_{m'm}, \tag{A.1}$$

where

$$\{\beta_{ij}(ka,\psi)\}_{m'm} = J_{m-m'}(ka)e^{i(m-m')\psi}. \tag{A.2}$$

The subscripts ij of β mean that (A.2) translates the cylindrical harmonic basis from the coordinates O_j to the coordinates O_i (Figure A.1). For $a < R$, we have the analogous relation for the Hankel functions (Ref. 36 of Chapter 2)

$$H_m(kr)e^{im\varphi} = \sum_{m'=-\infty}^{\infty} H_{m'}(kR)e^{im'\phi}\{\beta_{ij}(ka,\psi)\}_{m'm}, \tag{A.3}$$

where $H_m(x)$ can be a Hankel function of the first or second kind. For $a > R$, the relation becomes

$$H_m(kr)e^{im\varphi} = \sum_{m'=-\infty}^{\infty} J_{m'}(kR)e^{im'\phi}\{\alpha_{ij}(ka,\psi)\}_{m'm}, \tag{A.4}$$

where $\{\alpha_{ij}(ka,\psi)\}_{m'm}$ is obtained from $\{\beta_{ij}(ka,\psi)\}_{m'm}$ by replacing $J_{m-m'}$ by $H_{m-m'}$. Since all elements in β and α are also cylindrical harmonics, they are also related by the same relations as (A.1) and (A.3). For all $\mathbf{a}$, $\mathbf{a}_1$, and $\mathbf{a}_2$ with $\mathbf{a} = \mathbf{a}_1 + \mathbf{a}_2$, we have

$$\{\beta(\mathbf{a})\}_{m'm} = \sum_{m''} \{\beta(\mathbf{a}_1)\}_{m'm''} \{\beta(\mathbf{a}_2)\}_{m''m}, \tag{A.5}$$

and if furthermore $a_1 < a_2$,

$$\{\alpha(\mathbf{a})\}_{m'm} = \sum_{m''} \{\beta(\mathbf{a}_1)\}_{m'm''} \{\alpha(\mathbf{a}_2)\}_{m''m}. \tag{A.6}$$

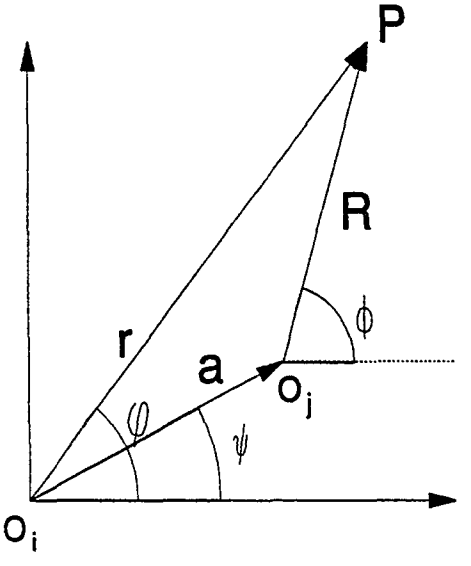

Figure A.1. Translation in the cylindrical coordinate systems.

VITA

Yi-Ming Wang was born in Henan, China, on March 30, 1957. He received the B.S. degree from Beijin University, Beijin, China, in January 1982 and the M.S. degree from the University of Illnois at Urbana-Champaign in May 1988.

From 1982 to 1986, he worked at the China Reseach Institute of Radio Wave Propagation, Xinxiang, Henan, China. In January 1986, he enrolled at the University of Illinois at Urbana-Champaign to pursue his graduate education in the Department of Electrical and Computer Engineering. While he was a graduate student, he worked as both a research assistant and a teaching assistant. During the summers of 1988 and 1989, he worked at the Schlumberger Well Services, Houston, Texas, developing software for the induction logging tool.

Mr. Wang is a member of Phi Kappa Phi and IEEE.